PROCESSING AND PROPERTIES EVALUATION OF CNFs DISPERSED SIC BASED COMPOSITES

A

THESIS

SUBMITTED IN PARTIAL FULFILLMENT OF THE REQUIREMENT FOR THE AWARD OF THE DEGREE OF

DOCTOR OF PHILOSOPHY

IN

METALLURGICAL AND MATERIALS ENGINEERING

BY

MUBINA SHAIK

(ROLL NO: 716157)

UNDER SUPERVISION OF

Dr. ASIT KUMAR KHANRA

Dr. BHASKAR PRASAD SAHA

Department of Metallurgy & Materials Engineering

National Institute of Technology Warangal

Telangana, India.

FEBRUARY 2021

CERTIFICATE

This is to certify that the thesis entitled **"Processing and Properties Evaluation of CNFs Dispersed SiC based Composites"** is being submitted by Miss. Mubina Shaik (Roll no. 716157), is a bonafide work submitted to National Institute of Technology, Warangal in partial fulfillment for the award of the degree of **Doctor of Philosophy** in **Metallurgical and Materials Engineering**. The results embodied in this thesis have not been submitted to any other University or Institute for the award of any degree or diploma.

Dr. Asit Kumar Khanra
Associate Professor and HOD
Department of Metallurgical and Materials Engineering
NIT- Warangal

Dr. Bhaskar Prasad Saha
Scientist and Team Leader,
Centre for Non-Oxide Ceramics,
ARCI- Hyderabad

Thesis Approval for Ph.D

The thesis, entitled **"Processing and Properties Evaluation of CNFs Dispersed SiC-based Composites "**, which is submitted by **Ms. Mubina Shaik (Roll no. 716157)** in partial fulfillment for the award of **Doctor of Philosophy (Ph.D.)** in the Department of Metallurgical and Materials Engineering, National Institute of Technology, Warangal, is approved by

Examiner

_____

Supervisors

_____ _____

Chairman

_____

Date: _____

ACKNOWLEDGEMENTS

I would like to express my sincere and heartfelt gratitude to my research supervisors, **Dr. Asit Kumar Khanra**, Associate Professor & HOD, Department of Metallurgy and Materials Engineering (MME), NIT-Warangal and **Dr. Bhaskar Prasad Saha**, Scientist-F & Team Leader at Centre for Non-Oxide Ceramics (CNOC), ARCI-Hyderabad, for their constructive guidance and relentless encouragement. Their dedication towards research motivated me throughout the duration of my research study. Their expertise, availability to discuss ideas and willingness to share their knowledge were instrumental in motivating me. It is indeed a great honor and privilege to work under their supervision.

I would like to express my deepest gratitude to the Director ARCI, **Dr. G Padmanabham**, and Director of NITW, **Prof. N.V. Ramana Rao**, for giving me the opportunity to carry out my PhD work and for providing me with the necessary infrastructure.

I register my gratitude and sincere thanks to Associate Directors of ARCI, **Dr. Roy Johnson** and **Dr. Tata Narsinga Rao**, for their continuous support and guidance.

I express my thanks to **Dr. Prasenjit Baric**, Scientist-D and **Dr. Dulal Chandra Jana**, Scientist-E, CNOC, ARCI for their unconditional support and guidance throughout my research work.

I express my sincere thanks to Former Heads of Department of MME, NITW, for their valuable help and support. I sincerely thank the members of the Doctoral Scrutiny Committee, **Prof. A. Kumar**, Department of Mechanical Engineering, **Dr. Arockia Kumar** (Asst. Prof), **Dr. Brahma Raju Golla** (Asst. Prof), and **Dr. Sukla Mondol** (Asst. Prof), Department of MME, NITW for their valuable suggestions at every stage of my research work.

I sincerely thank the following Scientists of ARCI, **Dr. P. Sudharshan Phani,** Scientist-E, Centre for Engineered Coatings (CEC), **Dr. Y. Srinivasa Rao**, Scientist-F, Centre for Ceramic Processing (CCP), **Dr. G. Ravi Chandra,** Scientist-G, **Mr. M. Ramakrishna**, Scientist-D, Centre for Materials Characterization and Testing (CMCT), **Dr. P. K Jain**, Scientist-G, Center for Carbon Materials (CCM), **Dr. Ravi Nathuram Bathe**, Scientist-F, Centre for Laser Processing of Materials (CLPM) for their valuable support and time for testing my samples. I would like to thank my annual ARCI review committee members for their constant motivation, suggestions and positive critical comments that acted as the much needed guiding light and route map for my PhD journey.

My special and sincere thanks to all the technical staff of Centre for Non-Oxide Ceramics, **Mr. M. Ilaiyaraja, Mr. R. Anbarasu, Mr. M. Srihari, Ms. B. V. Shalini, Mr. A. Jagan, Mr. Praveen Kumar, Mr. M. Srinivas,** and **Mr. P. K. Mukhopadhyay** for their great support and help during my research work and I also thank Technical officers **Ms. Ramya** from NITW and **Mr. G. Venkata Ramana Reddy** from ARCI, for their help in characterization of samples.

I also wish to thank all my friends **Ms. Yamini Ananthan, Mr. Sravan, Mr. Raju Vemoori**, **Mr. Katti Bharath, Mr. K. Venkata Ashish Srivatsav, Mr. Shiva Bejugama, Ms. Keerthi Sanghamitra, Ms. Madhavi Yarlagadda, Ms. Lalitha, Ms. Chandrakala** for their constant support and motivation.

My sincere thanks to my grandparents and my father **Sri**. **Raheem Shaik**, mother **Smt**. **Beebjan**, brother **Mr. Hamraj** and other family members for providing me all the unstinted support, love, affection and patience, which made this work possible.

Place:

Date:

Signature: _____

(MUBINA SHAIK)

Dedicated to

My Family, Friends and Teachers

LIST OF SYMBOLS & ABBREVIATIONS

SYMBOLS	ABBREVIATIONS
α-SiC	Hexagonal silicon carbide
β-SiC	Cubic silicon carbide
CNFs	Carbon nanofibers
C_f	Long or continuous carbon fiber filaments
SiC_f	Long or continuous silicon carbide fiber filaments
ASTM	American Society for Testing Materials
ANOVA	Analysis of Variance
DOF	Degrees of Freedom
S/N	Signal to Noise
IR	Infra-Red
FT-IR	Fourier Transform Infra-Red spectroscopy
KBr	Potassium bromide
SEM	Scanning Electron Microscope
EDX	Energy Dispersive X-ray
EDS	Energy dispersive Spectroscopy analysis
EBSD	Electron Backscatter diffraction
XRD	X-ray Diffraction
H.V	Vickers Hardness
TEM	Transmission Electron Microscopy
HR-TEM	High Resolution Transmission Electron Microscopy
TGA	Thermo gravimetric analysis
DTA	Differential thermal analysis
SDS	Sodium docecyl sulphate
BN	Boron nitride
HNO_3	Nitric acid
H_2SO_4	Sulfuric acid
CIP	Cold isostaitc pressing
MAM	Methylacrylamide

MBAA	N,N′-methylenebisacrylamide
APS	Ammonium persulfate
MTS	Methyl trichlorosilane
CVD	Chemical vapour deposition
LSI	Liquid silicon infiltration
OM	Optical metallography
RS	Raman spectroscopy
UV/VIS	Ultraviolet/visible absorption spectroscopy
µm	Micrometer
mm	Millimeter
cm	Centimeter
nm	Nanometer
M	Meters
k	1000
g/cc	Grams per Centimeter ^{3}
g	Grams
cc	cm^3
M	Molarity
N	Newton
mV	Millivolts
MPa	Mega Pascal
GPa	Giga Pascal
Wt %	Weight percent
Vol %	Volume percent
2Ɵ	Diffraction angle
D	Interplanar spacing
Å	Angstrom
λ	Wave length
FT	Fracture toughness
K	Thermal conductivity
E	Elastic modulus

c	Indentation crack length
P	Applied load
^{o}C	Degree Celsius
ρ	Density
RD	Relative density

LIST OF FIGURES

LIST OF TABLES

ABSTRACT

Silicon carbide (SiC) is a covalently bonded refractory semiconductor with unique combinations of thermal, mechanical, and chemical properties. Hence, it has been widely used as a structural part and as a sensor material in various applications like high-pressure chemical pumps, space propulsion systems, aerospace industry, etc. The performance of monolithic SiC can be further enhanced in terms of its thermal conductivity and fracture toughness by using it in the form of composites. Common reinforcements used in the SiC matrix are carbon nanofibers, carbon fibers, silicon carbide fibers, nano SiC particles (SiC_p) etc. Carbon fiber reinforced SiC-based composites show an excellent combination of physical, mechanical and thermal properties. The combination of these properties makes SiC composites a material of choice for high-temperature load-bearing applications.

The main aim of the present work is the fabrication of SiC-based composites with optimized physical, thermo-mechanical, oxidation resistance properties etc. The effects of powder processing routes such as conventional drying and advanced spray freeze granulation were also studied. The surface modification and dispersion stability studied of different types of secondary phase materials were tested. The effect of different types of secondary phase incorporation and their combined effect on the properties of SiC composites were also studied.

SiC and its composite powders dispersed with 1 to 3 wt % CNFs were spray freeze granulated to produce spherical granules with uniform composition. Powders were shaped to thin dense tubes for use in a harsh environment by cold isostatic pressing followed by pressureless sintering according to Taguchi experimental design array. The optimization of sintering parameters and the properties of SiC-CNFs composites with respect to the CNFs amount were designed and measured by Taguchi statistical analysis. The material properties of the composite tubes were optimized through the design of experiments to optimize the parameters like sintering temperature, heating rate, holding time and at different CNFs compositions by using Taguchi experimental design method with an L_9 (3^4) orthogonal array. The effect of variables on the properties of the composites was studied from the signal to noise ratio (S/N), analysis of variance (ANOVA), and interaction plots. The thin SiC-CNFs composite tubes of 1-2 mm wall thickness

were fabricated and sintered at optimized conditions obtained from the Taguchi analysis83. The subsequent post sintering techniques such as chemical vapour deposition (CVD) was carried out on the thin tubes. The physical, microstructural and thermo-mechanical properties of the CVD SiC coated thin composite tubes were evaluated and compared with bare SiC tubes.

Further, the sintered SiC-CNFs composite tubes were braided with long carbon fabric (C_f) of different braiding patterns and subsequently, liquid silicon infiltrated and CVD SiC coated to study the high temperatures oxidation resistance. The oxidation behaviour of LSI composite and CVD-SiC coated samples were examined separately from room temperature to 1450 ^{o}C in the air using thermogravimetric analysis (TGA).

The SiC-based hybrid composite tubes (BN-C_f/SiC-CNFs) with 10-12 mm wall thickness were also fabricated by systematically laying of boron nitride coated continuous carbon fiber (BN-C_f) in the SiC-CNFs composite powder matrix. The fractographic analysis of the hybrid composite tubes was carried out to understand the influence of long fibers on the improvement of fracture toughness of the nanofibers containing a hybrid composite matrix.

An advanced high-speed nanoindentation technique is employed to analyze the combined benefit of the particulate and continuous fiber's reinforcing effect of carbon fibers in the SiC matrix. The CVD SiC coated thin tubes (1-2 mm) of SiC, SiC-CNFs and SiC-based hybrid composite tubes (10-12 mm) properties were evaluated using conventional processes as well as the nanoindentation technique and compared at different length scales. Attempts have been made to correlate the structure-property relations of complex multi-phase of SiC composites employing high-speed nanoindentation mapping as well as XRD, Digital optical, SEM, and TEM analysis.

The objective of the research work is to optimize the properties of SiC-based composites using various powder processing routes with the incorporation of different types of secondary phase materials and adopting post sintering processes. This thesis provides the purpose of the research, experimental methods, results, discussions and conclusions with the future scope.

CONTENTS

CHAPTER 1

General Introduction

1.0 General Introduction

In recent years structural ceramic materials, in particular, non-oxide ceramics have gained a lot of attention in various high temperatures and corrosive atmosphere related applications in different fields such as solar, chemical industry, defence, nuclear, space, etc [1]. SiC is known to be one of the most suitable non-oxide ceramic materials for its vast applications due to high-temperature properties [2]. Hence, in considering the importance of SiC, the thesis has mainly focused on optimization of processing methods and properties of SiC-based composites. SiC is a covalently bonded refractory semiconductor with unique combinations of optical, thermal, electrical, mechanical and chemical properties [3]. Hence, it has been widely used as a structural part for various applications like high-pressure chemical pumps, space propulsion systems, aerospace industry, as a sensor material etc [4]. SiC has the capability to withstand high-temperature of up to 2500 °C, and shows exceptionally low oxidation rates up to 1700 °C [5]. The oxidation behavior of SiC which is lower (2 to 3 order magnitude) than that of zirconium-based alloys makes SiC a potential candidate for nuclear fuel cladding to avoid accidents by significant reduction in hydrogen generation [6].

In the present chapter, classification of structural ceramics, basic introduction to the SiC, structure, properties, and various applications, are discussed. Different types of SiC-based composites in various fields of applications are also discussed here.

1.1 Structural ceramic materials

Ceramic materials have strong bond strength which enables them to be used in many structural applications. Many advanced structural ceramics have the potential to be used in various structural applications as load-bearing members [1]. The advanced structural ceramics possess extraordinary properties such as high strength, load-bearing capacity, hardness, oxidation resistance, thermal shock resistance, high young's modulus even at high temperatures. The combined properties of advanced structural ceramics i.e. traditional ceramic properties and high-temperature properties attributed them to be used in various fields such as aerospace, nuclear, chemical, manufacturing industries, medical applications, etc [7]. The demand for advanced structural ceramic composite materials for high-temperature and harsh environment applications are tremendously increasing due to their exceptional thermo-mechanical properties and good

dimensional stability. The advanced structural ceramics can be classified into three distinct categories based on the chemical bonding between the elements such as [8]:

1) ***Oxide-based ceramics*** are inorganic and non-metallic compounds, where the metallic or metalloid elements bond with oxygen and have a high proportion of electrovalent bonds. Oxide ceramics with their superior properties like low density, extreme hardness, friction resistance, oxidation resistance, electrical insulating properties etc., find applications in various fields. Some of the applications listed are furnace construction, manufacture of high-pressure pistons and pumps for the chemical industry, electrical industry, food industry, pharmaceutical sectors etc. The most commonly used advanced oxide ceramics for structural applications are Al_2O_3, MgO, ZrO_2, TiO_2, SiO_2, etc. Some of the oxide ceramics like Al_2O_3 and ZrO_2 have been used for orthopedic and dental applications, due to similar chemical composition with the tissues [9,10]. The polycrystalline oxide ceramics fibres offer significant improvement in application temperature limit with its superior modulus and tensile strength. The self-oxidic nature of the oxide ceramics has been acting as a protective shield for the structural design from high-temperature oxidation [11].

2) ***Non-oxide based ceramics*** is a category of ceramics classified as inorganic, non-metallic materials that are bonded to form silicides, borids, nitrides or oxynitrides, carbides, etc [12]. They are covalently bonded and based on the element of the bonding, it exhibits conductive (carbides) or non-conductive (nitrides) nature. Non-oxide ceramics are characterized by their unusual properties like very high hardness, excellent resistance to wear, high strength, resistance to oxidation even at very high temperatures, good thermal shock resistance, low thermal expansion, very high thermal conductivity, good tribological properties, high semi-conductivity, etc [13,14]. Few of the most important advanced non-oxide structural ceramics are $MoSi_2$, TiB_2, Si_3N_4, B_4C, BN, SiAlON, SiC, etc [12]. The non-oxide ceramics with its superior properties have been used in applications such as cutting tools, ball bearings, car brake disc, heat exchanger, rocket nozzles, armors, LEDs, etc [15]. The non-oxide ceramics fibers also have demand in the market for many high-temperature applications. The crystal structure and composition of

the non-oxide ceramic fibres contribute to high tensile strength, elastic modulus, and lower creep rate even at high temperatures compared to the oxide fibers. The commercially available non-oxide ceramics in the market are SiC, TiB_2 and SiC (N) O based ceramic materials [16,17].

3) ***Composites*** are the substances made up of a combination of two or more oxide and non-oxide ceramics compounds [18]. One compound acts as a matrix which is binding and holds the second compounds which are called the secondary phase materials or reinforcements. Structural ceramics are generally brittle in nature, in order to obtain better reliability of ceramics for various applications, the reinforcement of secondary phase or composite formation is the best solution. The produced composites materials obtained from the initial (raw) materials possess superior properties on combining, thereby making up for its drawbacks. The requirement of composite for a particular application can be processed with an appropriate selection of matrix and reinforcement materials. The well known natural composites are plant wood, human or animal bones etc [19]. The modern or synthetic ceramic composite classification is based on the type of reinforcement or secondary phase material. Further sub-classification of these composites based on the nature of reinforcement also given in the form of flow chart in Figure 1.1 [20,21]. Many composites also provide design flexibility due to which complex shaped components can be fabricated. Ceramic matrix composites (CMC) have superior physical, thermo-mechanical and electrical properties compared to monolithic materials, such as being lightweight, having high flexural modulus to bear heavy loads, excellent strength, improved fracture toughness, high damping capacity, corrosion resistance, high impact strength, creep resistance and superior thermal stability [22].

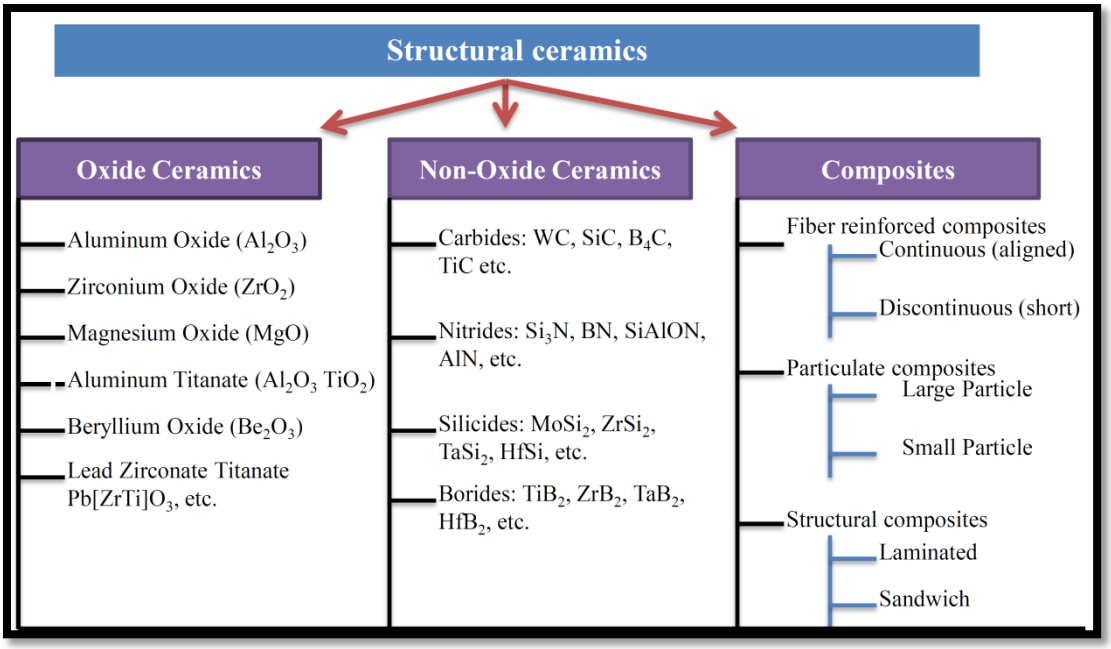

Figure 1.1: Classification of structural ceramics [20, 21].

1.2 Introduction to silicon carbide

SiC is also called as carborundum and is considered one of the lightest and hardest ceramic materials for many structural applications. The natural mineral of SiC is only found in meteors, but the synthetic SiC powder was first processed by Cowless in 1885 and has been mass produced on an industrial scale since 1893 by Acheson [15]. The reactions involved between SiO_2 and SiO with C, while processing of SiC is clear from the phase diagram of the SiO_2-C system as given in Figure 1.2. From the phase diagram its seen that theformation of SiC is favourable at a temperature above 1515 ^oC, represented as stoichiometric composition. At temperatures below the stoichiometric composition, the SiC forms a mixture of SiO_2. The gaseous product is formed at above 1515 ^oC with respect to the mole ratio between raw materials i.e C and SiO_2 [23].

The formation of large number of crystal structure i.e polytypism is known to be one of the salient features of SiC. However, the polytypes have a tendency to remain constant compositionally, even though there is structural transformation and modification in the material properties at different working temperatures [24]. SiC comprises polytyes (more than 200) and each one possesses its own significant optical, thermo-mechanical and electrical properties with respect to stacking sequence. Most common forms of SiC polytypes are cubic (C), hexagonal (H)

and rhombohedral (R).

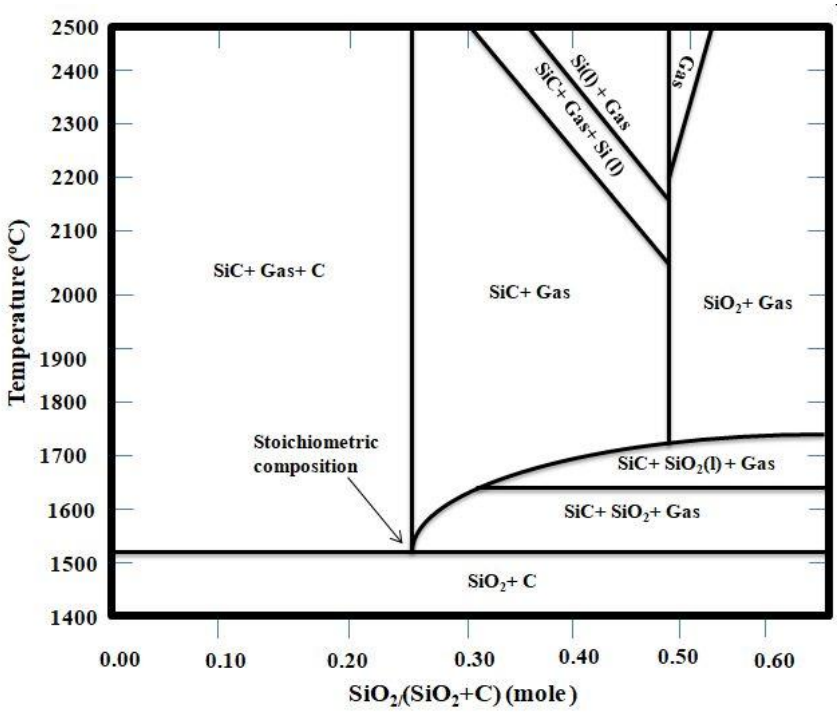

Figure 1.2: Phase diagram of SiO_2-C system [23].

1.2.1 Structure of SiC

The crystal structure of SiC consists of a double layered, close packed stacking of Silicon and carbon atoms as shown in Figure 1.3 (a). Ramsdell notation was used to denote the SiC polytypes based on Si and C layers in the unit cell, where the number denotes the number of layers and the letter denotes the types of crystal structure [25]. The stacking sequence follows one of three possible relative positions; hence the layers were arbitrarily labelled A, B and C as shown in Figure 1.3. The most common forms of stacking sequences shown by SiC are 3C, 2H, 4H, 6H, and 15R respectively as shown in Figure 1.3 (b-f) [26]. The only cubic form of SiC i.e 3C, also called beta SiC (β-SiC) has a three layered stacking sequence i.e ABCABCABC. For the non-cubic polytypes or alpha forms (α-SiC) are 4H, 2H, 15R, 6H, the detailed stacking sequence and lattice parameters are shown in Table 1.1 [24,27]. As in the case of hexagonal structured SiC the double layers are adjoined in the same position [28]. All the SiC polytypes crystal structures correspond to either zinc blend or wurzite or a mixture of both, such as bi-layered 2H polytye (ABAB…) with hexagonal or wurtzite structure; 3C is referred to as zinc

blende structure, whereas 4H, 6H and 15R polytyes have mixed cubic and hexagonal bonds, but the overall symmetry is known to be hexagonal and rhombohedral respectively.

Much of the literature on the stability of SiC polytypes reveals that the polytypes were strongly dependent on the temperature and growth rates. Most of the polytyes, except 2H, are meta-stable. At a temperature beyond 1600 ^{o}C, the cubic structured SiC is transformed to hexagonal structure as a result of recrystallization and growth process [29].

Table 1.1: SiC polytypes stacking sequence and lattice parameters [23, 25].

Polytypes	**Lattice spacing (Å)**		**Stacking sequence**	**Symmetry**
	A	**C**		
3C	4.36	N.A	ABC	Cubic
2H	3.07	5.05	AB	Hexagonal
4H	3.08	15.12	ABCB	Hexagonal
6H	3.08	10.05	ABCACB	Hexagonal
15R	3.07	37.5	ABCACBCABACABCB	Rhombohedral

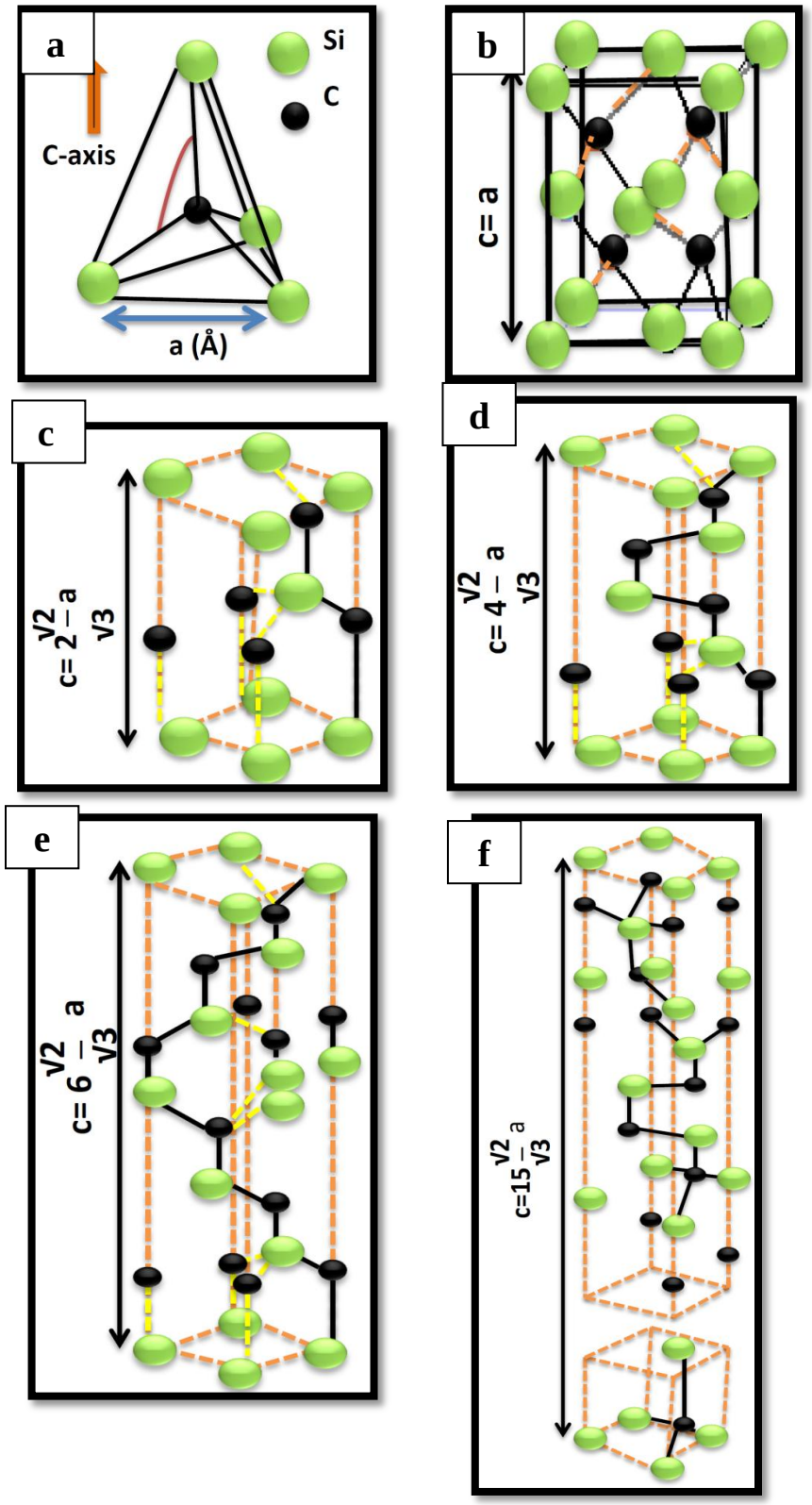

Figure 1.3: Crystal structure of SiC a) basic tetrahedral formation Si and C atoms in SiC b) 3C c) 2H d) 4H e) 6H f) 15R [25, 26].

1.2.2 Properties of SiC

1.2.2.1 ***Physical and chemical properties*:** SiC is considered to be a significant light weight ceramic material for its low density, which is in the range of 3.166 - 3.25g/cc based on the polytype as shown in Table 1.2 [28]. Inter atomic distance and bonding between Si and C is 1.89 Å, which is 88 % covalent and 12 % ionic respectively. SiC has been organized in a tetrahedral arrangement of Si and C atoms with sp^3 hybridization. The occurrence of polytpes of SiC crystal was also identified based on the change in colour i.e 6H polytype shows green crystal and yellow for 15R and dark black for 4H [30,31]. SiC has excellent chemical stability and very high decomposition temperature (~ 2800 ^{o}C under ambient atmosphere), which can be varied with different atmosphere pressures (low and high) [32-34].

1.2.2.2 ***Thermal and mechanical properties*:** SiC is one of the prominent materials for many high temperature and energy-related applications due to its chemical inertness, superior thermo-mechanical properties, such as high thermal conductivity, high temperature oxidation resistance, high hardness, high compressive strength and moderate toughness as shown in Table 1.2 [28]. In addition to the aforementioned properties, the low induced radioactivity and quick decay of activity, high-temperature resistance to high-energy neutron irradiation make these composites promising materials for nuclear fuel cladding as they help to avert a sudden built up of accidental hydrogen gas when hot steam comes in contact with overheated nuclear fuel rods. The 3C polytype of SiC crystal has isotropic properties, whereas hexagonal polytypes are observed to have variation in several material properties with respect to *C* axis, which is called anisotropy.

Table 1.2: Mechanical and thermal properties of SiC [28].

Attribute	Properties
Light weight	Density: 3.21g/cc
High temperature stability	It does not melt, but decomposition as high as $2830 \pm 40°C$
Excellent mechanical properties	High hardness: 28 GPa (only 3 materials e.g. diamond, cubical boron nitride, boron carbide exhibit higher hardness than SiC) Young's modulus: 430 GPa Compressive strength: 3.3 GPa
High thermal shock resistance	High thermal conductivity: 146 W/m.K Low coefficient of thermal expansion: $4\times10^{-6}/^{o}C$
Corrosion and oxidation resistance	Does not react with HNO_3, HF etc., oxidation resistance of sintered SiC up to 1400 ^{o}C
Application temperature	As high as 1400 ^{o}C

1.2.2.3 ***Optical and Electrical properties:*** SiC crystal lattice has different arrangement of Si and C atoms, each polytype exhibiting unique electrical and optical properties [35]. The most common polytypes of SiC used for electronic applications are 3C, 4H, and 6H. Since, the crystallographic direction strongly influences the direction of current flow at an applied electric field, the non-isotropic nature of polytypes is considered to be one of the important aspects for some of the electrical application. SiC with it low density, high dimensional stability under cyclic thermal and mechanical stress and high elastic modulus is considered to be ideal material for high level optical mirror applications in developing high resolution telescopes. The cubic form of SiC is also extensively used in wear resistance coatings, infrared windows etc [36]. Owing to the wide band gap and semiconducting nature, SiC is also used in various electronic and optoelectronic devices. Few important electrical and optical properties are provided in Table 1.3 [37,38].

Table 1.3: Standard optical and electrical parameters for SiC [37–39].

Optical parameters	Dielectric constant 6.5 - 10	Reflectivity 4 - 25 eV	Absorption coefficient 6H: 4.9-5.8 eV	Infrared refractive index 2.55	Reflection spectra 3-13 eV
Electrical parameters	Band gap energy E_g 2.4 - 3.33 eV	Relative dielectric constant 9.7	Electro reflectance spectra (4H, 6H & 3C) 1-5.6 eV		

1.2.3 Various applications

There are many uses of SiC in different industries. Its physical hardness makes it ideal to be used in abrasive machining processes like grinding, horning, sand blasting, water jet cutting, etc [40]. The ability of SiC to withstand very high temperatures without breaking or getting distorted enables its use in the manufacture of ceramic brake discs for sports cars [41]. It is also used in bulletproof vests as an armour material and as seal ring material for pump shaft sealing where the machine frequently runs at high speed and comes in contact with similar SiC seal. One of the major advantages in these applications is high thermal conductivity of SiC which enables it to dissipate frictional heat generated at the rubbing interface [42,43].

The high surface hardness of SiC enables its use in many engineering applications where a high degree of sliding, erosive and corrosive wear resistance is required [44]. Typically this can be in components used in pumps or for example as valves in oilfield applications where conventional metal components would display excessive wear rates that would lead to rapid failures [45].

The unique electrical properties of SiC such as its application in semiconducting devices and wide band gap make it ideal for manufacturing high voltage and ultra-fast light emitting diodes, transistors, U.V photodiodes, thyristors for high power switching, solar cells etc [46].
The light weight, high hardness, high thermal conductivity, and low coefficient of thermal expansion makes it an ideal material for astronomical telescope mirrors [47,48]. In optical pyrometer, SiC fibers are used to measure gas temperatures [49].

SiC is also used in heating elements where extremely high temperatures need to be accommodated. It is even used in nuclear power plants to provide structural supports in high temperature gas cooled reactors [50]. Porous SiC foam has been used for molten metal filtration due to its high temperature thermal stability and chemical inertness and functionalized silicon carbide nanosheet (SiCNS) membranes are used for water desalination applications [51].

SiC with its excellent biocompatibility, chemical stability and superior mechanical properties is an ideal material for long-term, implantable biomedical devices such as brain-machine interface applications [52,53].

1.3 Characteristic features of SiC based composites and its applications

SiC is considered to be a desirable ceramic material for its low density, high hardness and high modulus. SiC also exhibits excellent high temperature properties like high thermal shock and creep resistance in addition to high temperature withstanding capability of temperatures as high as 2500 °C because of its very high sublimation temperature of ~2700 °C [5]. Further, the exceptionally low oxidation rates of SiC up to a temperature of 1700 °C and cost effectiveness make it a promising choice for various applications such as rocket nozzles, engine flaps, leading edges of aircrafts, etc [4]. Recent studies on monolithic SiC have shown that oxidation rates can be minimized to the tune of two to three orders of magnitude lower than that of zirconium-based alloys commonly used in nuclear industries [6]. Despite having superior properties at room and high temperatures, it has one severe shortcoming: low fracture toughness, which restricts its use in many high energy-related applications. Also, due to the strong covalent bonding between silicon and carbon atoms of SiC and the poor diffusivity of reactant species, the densification of SiC is a challenging task, whether it is in solid state or liquid phase. The shortcoming of low fracture toughness can be overcome by the incorporation of fiber in the matrix to produce composites for use in applications like, gas turbines, heat exchangers, aerospace, etc.

In addition to the aforementioned properties, the low induced radioactivity and high-temperature resistance to high-energy neutron irradiation make the composites promising materials for nuclear fuel cladding to avoid the sudden built up of accidental hydrogen gas in case of hot steam coming in contact with overheated nuclear fuel rods [54–59].

Considering salient features of SiC such as high temperature capability, low activation, relatively low neutron absorption and resistance to radiation, a continuous research has been on going on development of SiC composite tubes technologies for fusion applications [60]. Many studies have been reported on short or long fibers reinforced SiC based composites. However, CNTs/CNFs, SiC_f and C_f have received an enormous degree of attention in recent years, due to the remarkable physical, thermo-mechanical properties and compatibility with the matrix [61-63]. The incorporating second phase like CNTs or CNFs is not only improving the mechanical, thermal and electrical properties of SiC, also improves the fracture toughness.

The continuous C_f or SiC_f reinforced SiC based composites are having wide range of applications as structural component for high temperature fusion reactors, gas turbines and aircrafts etc. The continuous fibers reinforcement improves the load bearing capacity SiC matrix and also aids pseudo-ductile fracture behavior and high fracture energy which improves the reliability SiC components for various structural applications. Continuous fiber systems exhibit considerable anisotropy. This anisotropy can be very beneficial in certain applications. In the continuous fiber-reinforced ceramic composites, the fibers need to be masked with an interfacial coating to avoid reaction with the matrix and allow them to withstand high temperatures. The interfacial bonding improves fracture toughness of SiC with the interfacial debonding along with other fracture toughening mechanism, i.e., fiber bridging, fiber pullouts, and fiber fracture etc [64].

However, fabrication of composites using these conventional processes has been a challenging task due to the presence of residual porosity, inclusions, and microscale defects which especially influence the properties of the SiC composites. In order to overcome the shortcomings encountered in the aforementioned processes, a relatively easy and marginal route has been conceived for the fabrication of dense SiC hybrid composite tubes. The novel route was attempted in the present study to achieve superior mechanical and thermal properties. Amongst various routes of powder processing, spray freeze granulation is considered to be a superior technique for producing high-quality composite spherical granules as it offers uniform dispersion of the second phase in the matrix maintaining sphericity of the powder. The new approach was adopted for the fabrication of continuous C_f reinforced SiC-based hybrid composite to assess the combined effect of matrix nanofibers and weaved long fibers on the hybrid composite properties.

1.4 Objective and scope of the thesis

The main aim of the present work is fabrication of dense SiC based composites with improved fracture toughness and oxidation resistance properties along with other optimized thermo-mechanical properties.

The scope of the present work can be listed as follows

1. Studying the effects of powder processing routes such as conventional drying and advanced spray freeze granulation on SiC based composites.
2. Studying the influence of large number of variables such as powder particle size, sintering parameters and secondary phase on the properties of SiC-CNFs composite using Taguchi statistical design of experiments and analysis.
3. Analyzing the physical, thermal and mechanical properties of spray freeze granulated surface modified CNFs dispersed and pressureless sintered SiC-CNFs composites.
4. Exploring the effect of different types of secondary phase incorporation and their combined effect on the properties of SiC composites.
5. Carrying out post sintering techniques such as CVD, LSI and studying the oxidation kinetics of LSI based C_f/SiC composites.
6. Investigating micro meter length properties of the monolithic SiC and CVD SiC coated SiC-CNFs composites using high speed nanoindentation maps.
7. Studying the influence of combined effect secondary phases such as CNFs and nano SiC on the properties of SiC matrix.

1.5 Layout of the thesis

The research work present in the thesis is presented in eight chapters, with the outline of each chapter given below.

CHAPTER 1: Introduction

This chapter comprises the general introduction, scope and objectives of the present work. The classification of structural ceramics and its applications are discussed in detail. In particular, SiC ceramic structure, properties and its applications in various fields have been discussed thoroughly.

CHAPTER 2: Literature review

This chapter presents a detailed description of the methods used for powder processing and fabrication of SiC based composites. Various types of secondary phase materials and their surface treatment methods are analyzed. It highlights the literature associated with SiC based composites, using different secondary phase material. The literature study on the experiments design and analysis using Taguchi statistical analysis are also discussed. The details of the shaping and sintering techniques for processing SiC based composite components are given.

The influence of different types of reinforcement on the mechanical properties, namely, processes that improve fracture toughness and different types of toughening mechanisms involved have been studied. In the end, the common challenges faced while fabricating the SiC based composites have been addressed.

CHAPTER 3: Experimental design

The experimental techniques employed for the characterization of SiC composites such as XRD, DSC-TGA, SEM-EDS, TEM, HR-TEM, FTIR, Raman, UV-Vis studies were discussed in detail. The description of the apparatus used and the detailed procedure of the experimental measurements have also been included.

CHAPTER 4: Optimization of processing parameters and fabrication of CVD coated SiC-CNFs thin composite tubes using Taguchi statistical analysis

This chapter deals with the optimization of material properties of the CNFs composite tubes through Taguchi experimental design. The experimental results i.e. performance parameters were analyzed by Taguchi optimization method and microstructure analysis. The fabrication and characterization of CVD coated CNFs thin composite tubes at

optimized conditions of processing parameters received by Taguchi analysis is also discussed. The influences of surface treatment of CNFs and CVD SiC coating on the properties of SiC composite tubes are analyzed.

CHAPTER 5: Fabrication of BN coated long carbon and carbon nanofibers reinforced SiC based hybrid tubes through CIP and pressureless sintering

Boron nitride coated continuous carbon fiber (BN-C_f) reinforced SiC-CNFs hybrid composite tubes were fabricated by adopting a novel approach: cold isostatic pressing (CIP) combined with pressureless sintering. The effect of BN coating to maintain the stability of C_f were studied using XRD phase analysis, selected area electron diffraction and microstructure analysis. The quantitative phase analysis using Rietveld's refinement using MAUD software is discussed.

CHAPTER 6: Enhancement of oxidation resistance of CVD SiC coated C_f/SiC-SiC(CNFs) hybrid composites processed through Si-infiltration

Fabrication of three different types of C_f/SiC-SiC(CNFs) hybrid composite tubes by liquid silicon infiltration process is discussed. The oxidation behavior of bare C_f, C_f/SiC composite and CVD-SiC coated C_f/SiC composite is examined separately using TGA under air atmosphere from room temperature to 1350 ^oC. The influence of individual phases on the oxidation resistance of the hybrid tube was studied thoroughly using XRD, and SEM-EDS analysis.

CHAPTER 7: Surface properties evaluation of SiC based composites using high speed nanoindentation technique

The surface properties of CVD SiC coated SiC-CNFs based composite tubes were studied by employing conventional as well as advanced high speed nanoindentation mapping technique at different loading and holding times under ambient conditions. Microstructure and mechanical properties were studied to analyze the influence of CVD coating on composite properties. Further, XRD, SEM and TEM analysis were employed to characterize the microstructure of individual composite constituents and its CVD coating.

CHAPTER 8: Summary, Future plan of the work, Implication and List of publications

1.6 References:

[1] Bikramjit Basu and Kantesh Balani: *Am. Ceram.Soc*, Wiley, 2011, pp. 257–285.

[2] R. Naslain: *Compos. Sci. Technol.*, 2004, vol. 64, pp. 155–70.

[3] Brian Bertram and Rosario Gerhardt: *Intech. Open*, 2011, pp. 1–36.

[4] Roman Pampuch: *An Introduction to Cramics. Eur. Ceram. Soc.*, 1998, vol. 18, pp. 993–1000.

[5] S. Somiya: *Silicon Carbide Ceramics -1*, Springer, 1991.

[6] Zhengang Duan, Huilong Yang, Yuhki Satoh, Kenta Murakami, Sho Kano, Zishou Zhao, Jingjie Shen, and Hiroaki Abe: *Nucl. Eng. Des.*, 2017, vol. 316, pp. 131–50.

[7] Kotoji Ando, Koji Takahashi, and Toshio Osada: in *Handbook on Smart Coatings Mater. Prot.*, Elsevier Inc., 2014, pp. 586–605.

[8] Improving Test Quality and Reducing Escapes: *Process Technol.*, 2014, vol. 10, pp. 1–2.

[9] Tanya J Levingstone: *Head Start : In Materials Engineering. Issue 1 : Ceramics for Medical Applications*, 2008.

[10] Frederik Böke, Norina Labude, Ines Lauria, Sabrina Ernst, Gerhard Müller-Newen, Sabine Neuss, and Horst Fischer: *ACS Appl. Mater. Interfaces*, 2018, vol. 10, pp. 38669–80.

[11] Junzi Sun: *Open Aircraft Performance Modeling Based on an Analysis of Aircraft Surveillance Data*, PhD thesis, Delft University of Technology, 2019.

[12] Jacobson, N S Opila, E J: *Reference Module in Materials Science and Materials Engineering*, Elsevier, 2016, pp 6285–6287.

[13] A Bellosi: in *Mater. Sci. Carbides, Nitrides Borides*, Y G Gogotsi and R A Andrievski, eds., Springer Netherlands, Dordrecht, 1999, pp. 285–304.

[14] Schubert C. Klemm H.: *J. Eng. Gas Turbines Power*, 2000, vol. 122, pp. 13–18.

[15] Makuteswara Srinivasan and William Rafaniello: in *Carbide, Nitride Boride Mater. Synth. Process.*, Alan W Weimer, ed., Springer Netherlands, Dordrecht, 1997, pp. 3–42.

[16] James DiCarlo and Hee-Mann Yun: in 2005, pp. 33–52.

[17] D. Agrawal: *Trans. Indi. Ceram. Soc.*,Taylor & Francis,vol 65, 2006, pp. 1–16.

[18] Randall Allemang, James De Clerck, Christopher Niezrecki, and Alfred Wicks: *Conf. Proc. Soc. Exp. Mech. Ser.*, 2014, vol. 45, pp. 577–617.

[19] Murr L.E: *Handbook of Materials Structures, Properties, Processing and Performance*, Springer, 2015, pp. 451–464.

[20] Idowu D Ibrahim, Tamba Jamiru, Rotimi E Sadiku, Williams K Kupolati, Stephen C Agwuncha, and Gbenga Ekundayo: *J. Reinf. Plast. Compos.*, 2015, vol. 34, pp. 1347–56.

[21] Sumit Pramanik, Ayan Manna, Ashis Tripathy, and Kamal K. Kar: in *Compos. Mater. Process. Appl. Charact.*, Kamal K Kar, ed., Springer Berlin Heidelberg, Berlin, Heidelberg, 2016, pp. 457–96.

[22] Aljaz Ivekovi´, Sasa Novaka, Goran Drazic, Darina Blagoeva, and Sehila Gonzalez de Vicente: *J. Eur. Ceram. Soc.*, 2013, vol. 33, pp. 1577–89.

[23] Matizamhuka WR: *Heliyon*., Elsevier, 2019, vol. 5 (4), pp. 1–12.

[24] V. A. Izhevskyi, L. A. Genova, J. C. Bressiani, and A. H. A. Bressiani: *Cerâmica*, 2000, vol. 46, pp. 4–13.

[25] L S Ramsdell and J A Kohn: *Acta Crystallogr.*, 1952, vol. 5, pp. 215–24.

[26] Patrice Mélinon: *IntechOpen*, 2011, pp. 1–33.

[27] S. Nakashlma and M. Hangyo: *Solid State Commun.*, 1991, vol. 80, pp. 21–24.

[28] Gary Lynn Harris : *Handbook on Properties of Silicon Carbide*, IEE, INSPEC, 1995.

[29] P. A. Kistler-De Coppi and W. Richarz: *Int. J. High Technol. Ceram.*, 1986, vol. 2, pp. 99–113.

[30] Ajit Ram Verma, P. Krishna, and H. M. Otte: *Phys. Today*, 1967, vol. 20, pp. 111–15.

[31] Cary Y. Yang, M. Mahmudur Rahman, and Gary L. Harris, eds.: *Amorphous and Crystalline Silicon Carbide IV*, Springer Berlin Heidelberg, Berlin, Heidelberg, 1992.

[32] R.T Dolloff: *WADD-TR-60–143*, N.S.A., 1960, vol.15, pp. 1–28.

[33] Kierstin Daviau and Kanani K.M. Lee: *Crystals*, 2018, vol. 8, 1–18.

[34] P. S. Sokolov, V. A. Mukhanov, T. Chauveau, and V. L. Solozhenko: *J. Superhard Mater.*, 2012, vol. 34, pp. 339–41.

[35] Gury Timofeevic Petrovsky, Michael N Tolstoy, Sergey V Ljubarsky, Yuri P Khimitch, and Paul N Robb: in *Adv. Technol. Opt. Telesc. V*, Larry M Stepp, ed., SPIE, 1994, pp. 263–70.

[36] Xinchang Wang, Chengchuan Wang, Xiaotian Shen, and Fanghong Sun: *Appl. Opt.*, 2017, vol. 56, pp. 4113–22.

[37] Yukina Taki, Mettaya Kitiwan, Hirokazu Katsui & Takashi Goto: *J. Asian Ceram. Soci.*, 6:1, 95–101.

[38] C. Tablero : *Phys. Chem. C*, 117, 42, 2013, 21949–21954.

[39] T. Ayalew: in *SiC Semicond. Devices Technol. Model. Simul.*, n.d., pp. 8–11.

[40] Ahsan Ali Khan: in Mohammad Yeakub Ali ED1 - Moumita Mukherjee, ed., IntechOpen, Rijeka, 2011, p. Ch. 18, 1–25 .

[41] Walter Krenkel and Nico Langhof: *Proc. IV Adv. Ceram. Appl. Conf.*, 2017.

[42] R Azarafza, Ali Arab, and A Mehdipoor: *Int J Adv. Des. Manuf. Technol.*, 2013, vol. 5, pp. 83–87.

[43] William Charles Hoskins: *Silicon Carbide Materials Properties Selection for Mechanical Seal Faces, Chancellor's Honors Program Projects,* 2017, pp. 1–128.

[44] Mamtha Ramachandra and K Radhakrishna: *Mater. Sci.*, 2006, vol. 24, pp. 332–349.

[45] Eugene Medvedovski: *Adv. Appl. Ceram.*, 2012, vol. 111, pp. 311–22.

[46] Przybylko, S. J: *AIAA/SAE/ASME/ASEE 29th Joint Propulsion Conference and Exhibit*, American Institute of Aeronautics and Astronautics, Washington DC, 1993, pp. 93–2581.

[47] Noboru Ebizuka, Hiroaki Eto, Yutang Dai, Toru Suzuki, Weimin Lin, Hitoshi Omori, Toshikazu Ebisuzaki, and Hideki Takami: *Proc. SPIE - Int. Soc. Opt. Eng.*, 2004.

[48] Longxiang Li, Zhenyu Liu, Donglin Xue, Weijie Deng, Ruigang Li, Yang Bai, Xuefeng Zeng, and Xuejun Zhang: *Results Phys.*, 2018, vol. 10.

[49] Nasa Glenn: *AeroSpace Frontiers*,2020, vol. 22, pp. 20–22.

[50] H Grübmeier, A Naoumidis, and B A Thiele: *Nucl. Technol.*, 1977, vol. 35, pp. 413–27.

[51] Roghayeh Jafarzadeh, Jafar Azamat, and Hamid Erfan-Niya: *Struct. Chem.*, 2019.

[52] C L Frewin, C Coletti, J J Register, M Nezafati, S Thomas, and S E Saddow: in *Carbon Sens. Devices*, Danilo Demarchi and Alberto Tagliaferro, eds., Springer International Publishing, Cham, 2015, pp. 153–207.

[53] S E Saddow, Christopher Frewin, Fabiola Araujo, Marioa Gazziro, Evans Bernadin, and Sylvia Thomas: *Mater. Sci. Forum*, 2016, vol. 858, pp. 1010–14.

[54] Svante prochazka and Ronald M. scanlan: *J. Am. Ceram. Soc.*, 1975.

[55] Xin Jing, Xiaoguang Yang, Duoqi Shi, and Hongwei Niu: *Ceram. Int.*, 2017, vol. 43, pp. 6721–29.

[56] Jixiang Dai, Jianjun Sha, Junqi Shao, Yufei Zu, Mingkai Lei, Stefan Flauder, Nico Langhof, and Walter Krenkel: *Corros. Sci.*, 2017, vol. 124, pp. 71–79.

[57] Akira Kohyama and Hirotatsu Kishimoto: *Int. Electron. J. Nucl. Saf. Simul.*, 2013, vol. 4, pp. 72–79.

[58] Gyanender Singh, Kurt Terrani, and Yutai Katoh: *J. Nucl. Mater.*, 2018, vol. 499, pp. 126–43.

[59] M. L. Wu, C. Z. Ren, H. Z. Xu, and C. L. Zhou: *Mater. Chem. Phys.*, 2017, vol. 201, pp. 251–61.

[60] Yutai Katoh, Lance L Snead: *J. Nucl. Mater.*, 2019, vol. 526, pp. 1–24 .

[61] Xin Jing, Xiaoguang Yang, Duoqi Shi, and Hongwei Niu: *Ceram. Int.*, 2017, vol. 43, pp. 6721–29.

[62] Dusan Bucevac and Vladimir Krstic: *Mater. Chem. Phys.*, 2012, vol. 133, pp. 197–204.

[63] Kazuya Shimoda, Tatsuya Hinoki, and Akira Kohyama: *Compos. Sci. Technol.*, 2010, vol. 70, pp. 387–92.

[64] Katsumi Yoshida: *J. Ceram. Soc. Japan.*, 2010, vol. 118, pp.82-90.

CHAPTER 2

Literature Review

2.0 Introduction

In the present chapter, the literature review of SiC-based composites using various powder processing routes, such as conventional drying, spray drying, and advanced spray freeze granulation techniques have been outlined and the differences are compared. Various types of secondary phase materials and their prior surface treatment processes have been introduced. The study of the influence of processing and sintering parameters on the properties of SiC composites using Taguchi statistical analysis has been discussed. The effects of different types of green shaping, sintering and post sintering processes on the properties of the composites have been described. The fracture studies and the toughening mechanism of SiC composites with respect to the type of reinforcement have been explained. Challenges encountered in process of SiC based composites have been addressed.

2.1 Various types of secondary phase materials and their surface treatment

Reinforcement highly influences the structural properties and fracture behavior of CMCs. Secondary phase materials in a different form are used to enhance the properties of the original material by holding it together. The reinforcement not only provides internal support to the fiber but also a new identity to the material with superior properties. Hence, selection reinforcement is considered an important aspect in the fabrication of composites. The specific applications or specific structural properties requirements, shape and size of the final product, processing routes, temperature, etc., are the factors to be considered before selecting the secondary phase material for the fabrication of CMCs. Particulates, fibers, tubes, plates, whiskers, etc., are commonly used reinforcement for the composites [1]. The final properties of the composites depend on the size, shape, concentration, orientation, and distribution of secondary phase material.

i) Whiskers: Whiskers are known to be single crystals with preferred growth in specific crystal direction and exhibit extraordinary strength (6-30 GPa) and modulus (400-600 GPa) based on the material type due to the defect-free structure. Typically, whiskers measure micron (0.5-10 μm) in diameter, few micrometers to centimeter (3-55 mm), in length and very high strength in specific direction [2]. Whereas, aluminium oxide, graphite, silicon carbide, hydroxylapatite, cellulose, etc., are commonly known materials to produce whiskers based on the requirement [3-4]. Mostly, whiskers of the same material or different are used as reinforcement in the processing of

the different types of composites such as alumina, iron, graphite, silicon, silicon carbide, etc., for various applications [5-8]. Due to the high strength and unique specific properties, whisker reinforced ceramic matrix composites can be used in high-temperature structural applications like energy conversion systems, advanced heat engines etc. Whiskers are randomly oriented in the matrix as shown in Figure 2.1(a). However, they can be easily damaged during the fabrication process, which can lead to unwanted anisotropy in the composite structure. Whiskers are very expensive due to their processing method and it is also difficult to handle them.

ii) Particulates: Particulates are the most widely used reinforcement type due to their availability and affordability. The fabrication process of particulate reinforced ceramic matrix composites involves an easy mixing of dispersed phase with matrix, whether in wet condition or a dry state (based on the size of the particles) as shown in Figure 2.1(b). The properties of particulate dispersed ceramic matrix composites mainly depend on the size, shape and arrangement of the dispersed particles. The particle size of lower than 0.2 μm, strengthens the composite by impeding the motion of dislocations and deformations in the material at the atomic scale. Similar to the precipitation hardening, the small ceramic particles diapers in the matrix of particulate composite are stable even for high-temperature applications.

The most commonly used ceramic particles used as dispersants are Titania (TiO_2), Silicon carbide, Thoria (ThO_2), Titanium diboride (TiB_2), Alumina (Al_2O_3), etc [2,9]. The large size particulate (1-50 μm) reinforced composites are designed to produce an unusual combination of properties rather than improving the strength alone. Moreover, these particulates optimize the toughness of the ceramic matrix by diverting the crack initiated in the ceramic matrix and energy dissipation mechanisms [10]. Tungsten carbide (WC), titanium carbide (TiC), SiC are the most commonly dispersed particulates in the ceramic matrix [11]. The particulate reinforcement is less effective in optimizing the properties including strength when compared with the fiber reinforcement. In general, particulate reinforced ceramic composites find applications where a high level of wear resistance is required [12].

iii) Fibers: Fibers are the most widely used class of reinforcement, as they help to achieve the desirable enhancements in properties like load-bearing capacity and fracture toughness of the

ceramic matrix. The classification of fibers is given as a flow chart in Figure 2.2 [13]. Oxide-based ceramic fibers most frequently used are alumina (Al_2O_3), silica (SiO_2), zirconia (ZrO_2), and alumina and silica mixture i.e. Mullite ($3Al_2O_3$. $2SiO_2$), etc [14]. The commonly reinforced non-oxide ceramic fibers are SiC, titanium diboride (TiB_2), boron nitride (BN), Si-C-O (N), Si-C-B-N, etc [15]. The fiber-reinforced composite strength is mainly dependent on the orientation, length, shape, and composition of the fibers and mechanical properties of the matrix material. The fiber incorporation in the ceramic matrix composites not only provides improved strength and other mechanical properties but also optimizes the strength to weight ratio. The matrix transfers the applied loads to the fibers and also protects the fibers from adverse atmospheric conditions. The fibers contribute to fracture toughness to the ceramic matrix by mechanisms like crack bridging, crack deflection, debonding of the fiber-matrix interface, etc., as shown in Figure 2.3 [16]. Even at the critical conditions such as crack initiation or propagation, fiber inhibits such a process by absorbing energy at the interface of the failure [17]. Although fibers are brittle, in the case of ceramic fiber reinforced ceramic matrix composites, the overall composites are tough due to the effective design of the fiber-matrix interface, which deflects or arrests the cracks and also prevents the failure of the reinforcement.

The ceramic matrix composites are mainly classified into two types based on the type of reinforcement i.e.

- ***Discontinuous fiber reinforcement:*** short fibers (micron to nanoscale in length) are distributed randomly in the ceramic matrix as shown in Figure 2.1(c). Fabrication techniques like slip casting, injection molding, and powder metallurgy routes are used to produce this type of composites. Uniformly distributed discontinuous fiber-reinforced ceramic composites are being used in abrasive and mining industries, high-pressure heat exchangers and high wear applications [18–21].
- ***Continuous fiber reinforcement:*** Preformed long fibers are reinforced in the ceramic matrix as shown in Figure 2.1(d). The typical process employed in the formation of fiber performs and the fabrications of the composites are chemical vapor deposition (CVD) or chemical vapor infiltration (CVI) or electrophoretic deposition. The excellent combined properties of continuous fiber-reinforced SiC composites such as being lightweight, low

thermal expansion, high thermal conductivity, good corrosion resistance and wear resistance, etc., are desirable in many high temperatures industrial applications [22–25].

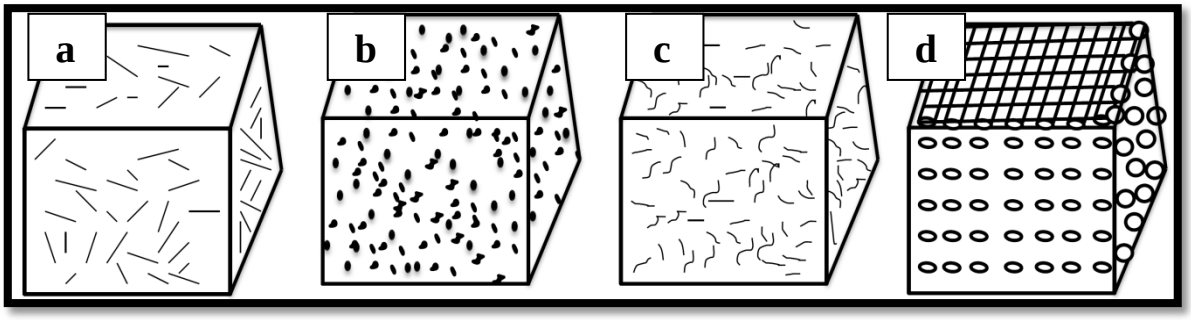

Figure 2.1: Pictorial representation of ceramic matrix, distributed with a) whiskers b) particulates c) discontinuous or short fibers
d) continuous fibers [2,4,25-26].

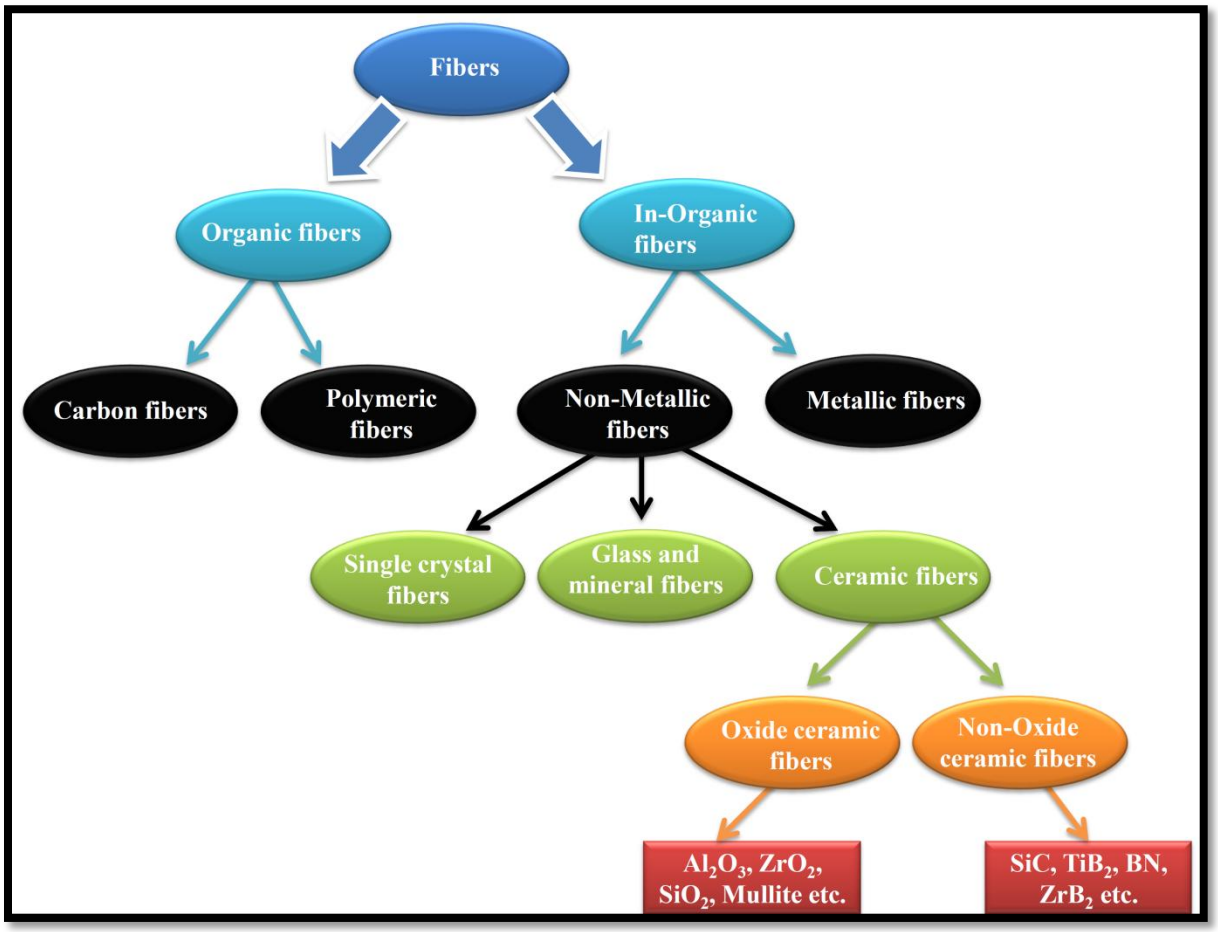

Figure 2.2: Classification of the fibers used as reinforcements [13].

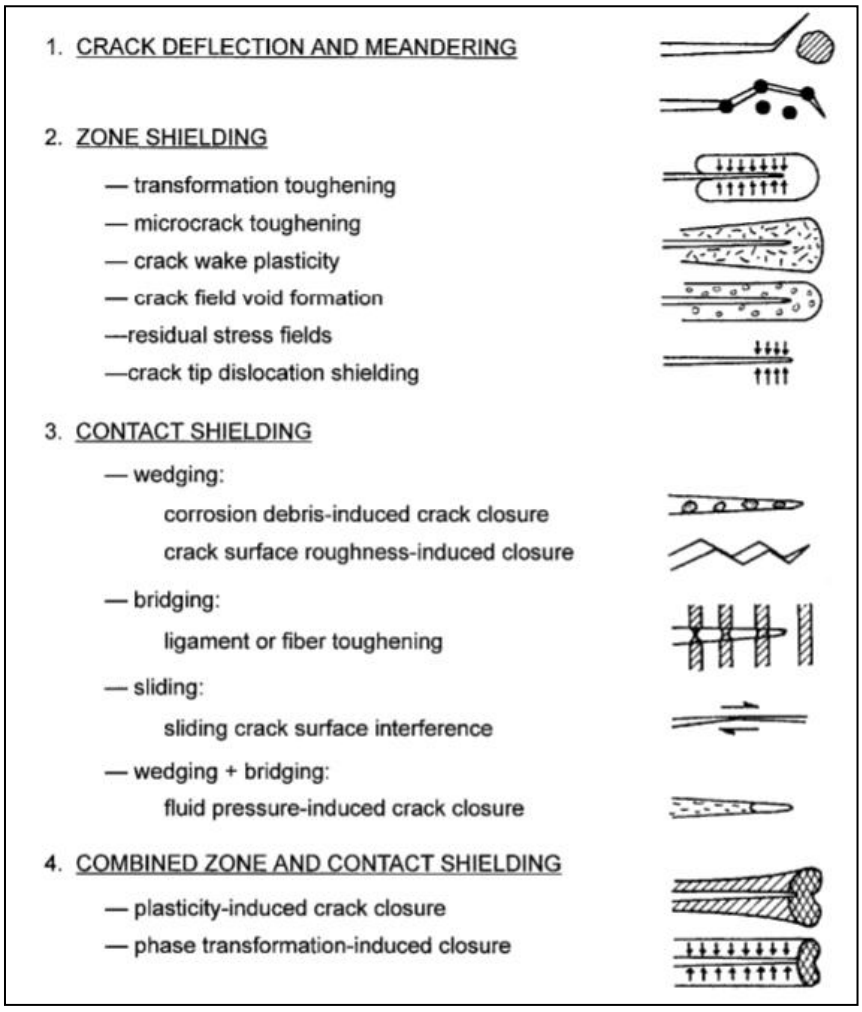

Figure 2.3: Extrinsic toughening mechanisms of ceramic matrix composites [27].

The fibers which are most frequently used in the ceramic matrix and used in the current research are listed below.

i. ***Carbon fibers:*** They are composed of carbon atoms and fiber filament dimensions have diameter ranging from 5-10 μm to several meters in length. These are commercially available in the form of nanotubes, nanofibers, fiber tow (with ~8000 filaments), fabric, woven perform, etc. The extensive advantage of using carbon fibers in different types of the matrix includes light weight (density: 1.7-1.9 g/cc), high tensile strength (2-4.5 GPa), high stiffness, good chemical resistance and temperature stability, etc [27]. These excellent properties of different types of carbon fibers are given in Figure 2.4 [13, 28–30]. Carbon fibers are used as

reinforcement in different types of matrix materials such as metallic (Al/CNF, Ti/CNF, Cu/CNF etc.,) [29], polymeric (PI/CNF, PEEK/CNF, PEI/CNF) [28], ceramic (C/SiC, C/B_4C) and non-metallic (C/C composites) [31-32], etc. Based on the precursor material involved the fabrication process of carbon fibers are classified as 1) Polyacrylonitrile (PAN) 2) Pitch 3) Rayon 4) Gas-phase grown carbon fibers [27]. On the other hand, while considering the mechanical performance, carbon fibers are classified as low modulus, medium modulus, high modulus and ultra-high modulus and the respective modulus vs tensile strength of these fibers are as given in Figure 2.4 [31].

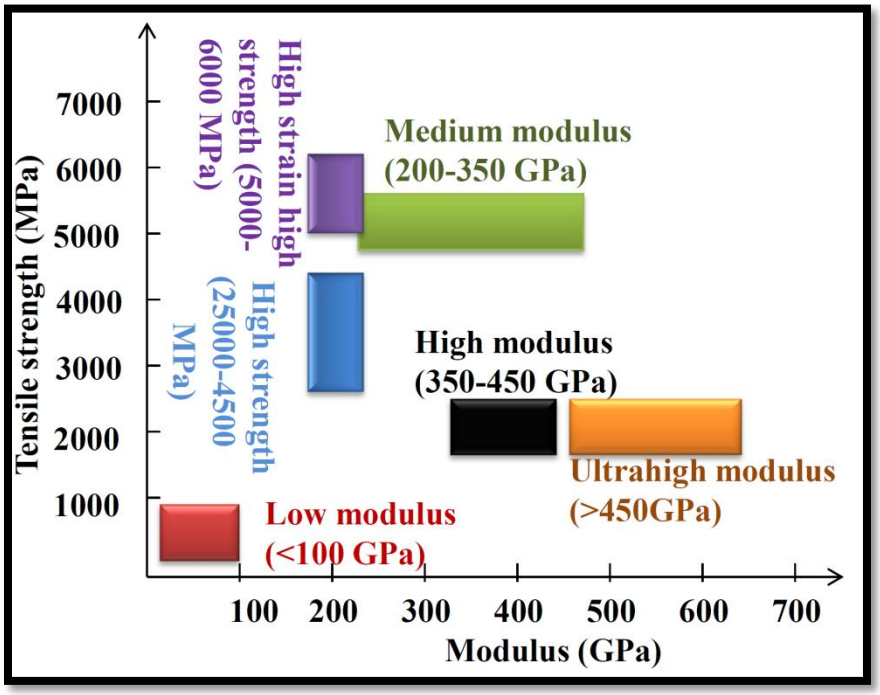

Figure 2.4: Classification of carbon fibers based on the mechanical performance [13, 29-31].

Carbon fiber (short or long) is considered to be potential high-temperature secondary phase reinforcement in the SiC matrix which not only improves the fracture toughness and other mechanical properties but also aids the thermal conductivity of newly formed SiC composite. The mechanical properties of various types of carbon fibers are given in the Table 2.1 below.

Table 2.1: Commercially available carbon fibers and their specifications [33–35].

Trade name and Company	**Specifications**	**Tensile Strength (MPa)**	**Tensile Modulus (GPa)**	**Coefficient of thermal expansion (CTE) (m/ m ^{o}C)**	**Thermal conductivity (Cal/ cm s ^{o}C)**
PX30, Zoltek^{TM}, U.S.	Filament dia: 7 µm, Density:1.75 g/cc		242		
T300, Toray. Inc., USA.	Filament dia: 7 µm, Density:1.76 g/cc	3530	230	-0.41×10^{-6}	0.0250
NCF W300C, SHIMTEQ, Japan.	Filament dia: 6 µm, Density:1.80 g/cc				
T700S, Toray. Inc., USA.	Filament dia: 7 µm, Density:1.80 g/cc	4900	230	-0.30×10^{-6}	0.0224
T800S, Toray. Inc., USA.	Filament dia: 5 µm, Density:1.80 g/cc	5880	294	-0.56×10^{-6}	0.0839
T100, Toray. Inc., USA.0G	Filament dia: 5 µm, Density:1.80 g/cc	6370	294	-0.55×10^{-6}	0.0765
M40J, Toray. Inc., USA.	Filament dia: 5 µm, Density:1.77 g/cc	4410	377	-0.83×10^{-6}	0.1640
M50J, Toray. Inc., USA.	Filament dia: 5 µm, Density:1.88 g/cc	4120	475	-1.10×10^{-6}	0.3720
M60J, Toray. Inc., USA.	Filament dia: 5 µm, Density:1.93 g/cc	3920	588		

ii. ***Silicon carbide fibers:*** The excellent combination of thermo-mechanical properties of SiC fibers such as high modulus, high strength, thermal stability, superior creep, better resistance to chemicals and oxidation even at high-temperatures, are considered ideal for high-temperature reinforcement for ceramic matrix composites. SiC fiber-reinforced SiC-based composites are mostly used for high temperatures, for applications under harsh conditions such as heat exchangers, nuclear fuel cladding, gas turbines, water reactors, etc. Commercially available SiC fiber dimensions range from 5-150 μm diameter and a few hundreds of mm to cm in length [32–36]. SiC fibers are generally reinforced as continuous fibers in the ceramic matrix (due to chemical compatibility and low thermal gradient). SiC fibers are composed of silicon and carbon as the primary molecules. Based on the manufacturing process they also possess a small amount of oxygen, boron, nitrogen, etc. The commercial processing methods used for the fabrication of SiC fibers are 1) melt spinning of polymer precursor and subsequent heat treatment, 2) chemical vapour deposition of Si based precursor on the carbon filaments. The variation in the thermal stability of various types of SiC fibers depending on the composition and specifications are given in Table 2.2.

Table 2.2: Different types of SiC fibers along with their specifications [36-37].

Fiber type	Nicalon CG	Hi-Nicalon	Hi-Nicalon type S	Sylramic	Tyrano	HPZ
Manufacturer	Nippon Carbon Ltd., Japan	Nippon Carbon Ltd., Japan	Nippon Carbon Ltd., Japan	Dow Corning	Ube Industries Ltd., Japan	Dow Corning-ATK COI Ceramics Inc., USA
Fiber diameter	14	12	11	10	10	10
Composition wt % **Si** **C** **O**	 56.6 31.7 11.7	 62.4 37.1 0.5	 68.9 30.9 0.2	 67 29 0.8	Si-Ti-C-O	Si-C-N
Crystallization of SiC	Low	Moderate	High	Near-stoichiometric β-SiC with a large grain size	Near-stoichiometric β-SiC with a large grain size	
Thermal stability (^{o}C)	1110	1230	1450	1420	1300	
Tensile strength (GPa)	3.0	3.4	2.6	3.1	2.76	
Tensile modulus (GPa)	190	270	420	400	193	

2.2 Surface treatment of secondary phase materials

Most of the available secondary phase materials such as fibers, tubes and particles etc., (μm to nm range) contain a small percentage of impurities due to the processing methods involved. As already explained in the above section, the main role of secondary phase material in many composites is to enable the acquisition of unique properties by the composite to avoid the catastrophic failure and to improve the load bearing capacity of the brittle matrix. Moreover the unique properties of these nanophases can be transferred only through good adhesion. However, the presence of impurities and their structure made them hydrophobic or inert, and therefore not miscible with many solvents and forms agglomerates. In order to form a good adhesion with the matrix, the reinforcement needs to be homogeneously dispersed in the matrix. Hence, before the reinforcement, the material needs to be purified and functional groups embedded on its surface as per requirement, a process known as surface treatment or functionalization. Based on the type

of the secondary phase material, process involved and the required outcomes as per the applications, surface treatments are varied [37-39].

The different purification methods are classified based on mode of separation. Such as, 1) The physical separation which can be further classified as arc method [40], photo-oxidation [41], gas phase treatment [46-47], 2) The chemical separation method further differentiated as acid oxidation treatment, liquid-phase oxidation treatment [48-49], and finally 3) physical and chemical separation method that are bifurcated into microwave heating of nitric acid [50-51], and coating: sol-gel dip coating [48].

With regard to interfacial adhesion of CNFs or SiC nano particles with SiC matrix for the current work, incorporation of oxygen containing functional groups (mainly carboxyl and hydroxyl) on its surface is a very crucial step. The exfoliation of nano particles or fibers aided by these oxygen functional groups helps in enhancing its dispersion stability in the matrix. In the present study, chemical oxidation routes were adopted for the surface treatment of nano particles or fibers and sol-gel dip coating method was employed for the coating of continuous or long carbon and SiC fiber filaments with suitable interface material. In the present study, boron nitride (BN) was used as interface material [53-54]. The fiber-matrix interface plays an important role to protect the fiber from cracks and deflects the cracks by transferring the loads between the fiber and matrix [55-56]. The main purpose of interface is to maintain the fiber intact and optimize the fracture toughness of the composite. The ability of the fiber to remain intact even with the initial cracking of the matrix can be assessed by the frictional sliding of fiber-matrix interface. The BN has a layered crystal structure, is light weight, has high temperature stability, enjoys high thermal shock resistance, and has excellent oxidation resistance and good thermal conductivity. Hence, the BN material with its structure, low shear modulus and superior thermo-mechanical properties, is considered to be an effective interface material for various continuous fibers reinforced ceramic matrix composites [53–57].

2.3 Various processing methods to fabricate SiC based composites

Majority of polycrystalline ceramic parts are fabricated via powder consolidation followed by pressureless sintering. The advantages of these methods such as easy processing of complicated shapes over a considerable range, better control of the component size, shape and properties, moderate processing costs, etc., are reasons for them to be employed in many industrial applications. Processing of polycrystalline ceramic components generally involves three basic steps: a. slurry preparation (mixing the powders with the additives), b. powder processing (granulation or drying, crushing, grinding), c. shaping and firing. Some of the processes like slip casting and injection molding etc., have only two step processes such as mixing of raw powders with the additives and shaping (casting or molding) followed by firing [58]. In general, ceramic powders are processed either by mechanical route or chemical route [59]. Mechanical route involves processes like screening, ball milling, elutriation, vibratory milling, roll crushing etc. The chemical processes involve precipitation, sol-gel, decomposition, freeze drying, liquid mix, hydro thermal, laser, plasma etc [60].

Many studies in the literature reveal that SiC based composites have been fabricated with reinforcement such as the ones mentioned in previous section (2.2) : carbon fibers (nano or micron), SiC fibers (nano or micron) and nano powders of cubic SiC are most commonly incorporated for high temperature and high corrosion resistance applications [18,61,62]. There have been many attempts to fabricate SiC based composites, using various processes, some of which are given below :

i) ***Polymer infiltration and pyrolysis (PIP)*** process is known to be one of the most preferred processes to fabricate SiC composites with complex shapes and large sizes. Preform fabrication (C_f/C preform), infiltration of polymer (silicon-based polymer) and pyrolysis are the steps involved in PIP [63].

ii) ***Chemical vapour infiltration (CVI)*** process offers distinct advantages in obtaining highly pure SiC matrix with minimal damage to the fibers (C_f) with the use of simple processing equipment. A major shortcoming of the CVI process is the formation of occasional large pores in the matrix leading to inferior mechanical performance in an oxidizing atmosphere [64–66].

iii) ***Liquid silicon infiltration (LSI)*** process also called reactive melt infiltration (RMI), where the C_f is coated with a polymeric precursor to produce porous C_f/C preform. Liquid silicon (Si) is then infiltrated in the porous carbon perform, due to the capillary action of molten Si at a temperature of more than 1450 ^oC (exceeding the melting point of Si) which rises into the pores of carbon perform and simultaneously reacts with carbon, resulting in the formation of C_f/C-SiC composite, where SiC acts as matrix [67–69].

iv) ***Electrophoretic deposition (EPD)*** process in which a thick film of the matrix is deposited on tightly woven fiber preform. EPD is known as a simple and easy process involving two steps. Firstly, the charged particles are dispersed in a suitable liquid medium move towards an oppositely charged electrode in an applied electric field called electrophoresis. The second step involves the deposition of accumulated charged particles on to the electrode as a thick film [70–72].

v) ***Ceramic route or nano powder infiltration and transient eutectic phase method (NITE)*** method comprises nano matrix slurry impregnation on the coated fibers followed by drying and sintering of stacked fabric layers under pressure. In this process, an interface is formed between fibers and matrix with a transient eutectic phase which solidifies before cooling of the composite [73]. However, fabrication of composites using these processes has been a challenging task due to the presence of residual porosity, inclusions, and microscale defects which especially influence the properties of the C_f/SiC composites.

vi) ***Powder processing and sintering***: Among the various afore-cited processes the fabrication of SiC composites by powder metallurgy route is known to be very common as well as cost-effective. In powder processing route, composite powder is normally produced by initial mixing of SiC powder and appropriate binders, sintering aids and secondary phase (micron to nano range fibers or particles) materials in a suitable solvent media. Hence, the suspension or slurry generated is dried and sieved. The three different types of powder processing routes used in the thesis have been discussed here.

Conventional drying of ceramic composite slurries by air or rotary evaporator is an old, well-known old and easy technique for powder processing. Even though it is time taking (for drying), it is suited for monolithic powder processing and also economically viable for large scale powder production. However, obtaining the homogeneous dispersion of the reinforcement in processing

of composite powders through conventional process is difficult, due to the easy agglomeration of nano sized reinforcement. Some of the drawback of the conventional process such as non-uniform shape and sizes, inhomogeneous composition and non-favorable flow properties of the powders etc., are highly influencing the compaction process, macrostructure characteristics and sintered properties of the final components.

However, powder in the form of granules has made the fabrication process easy. Since, the free flowablity of granules is helping in filling the pressing die evenly and can easily get disintegrated at pressing. In this regard, to improve the powder properties which further optimize the final product properties of SiC based composites, advanced powder processing routes have been initiated. There are few literatures mentioning the improvement of the properties of SiC by adopting combinations of various advanced powder processing techniques like spray drying, spray freeze granulation are given brief here.

Spray drying is comparatively advanced and a well-practiced process compared to conventional process. In spray drying process, composite powder slurry is sprayed through a nozzle of required dimensions and spherical granules are produced after the drying process. However, the draw backs of spray granulation technique are its non-uniform flow properties, non-homogeneous and hard granules, with cavity inside due to the thermal gradient effect during slow drying process [74].

The density of the final product depends largely on the nature of the powders which in turn depends on the processing routes. Among the various routes of powder processing, spray freeze granulation is considered a superior technique for producing high-quality composite spherical granules as it offers uniform dispersion of the second phase in the matrix maintaining sphericity of the powder [75,76]. A recent study by our group has revealed that the spray freeze granulated nano SiC spherical powder has shown superior green and sintered properties [77]. Nyberg et al. carried out a study where micron size SiC powder was used for producing low-temperature liquid phase sintered SiC with yttrium oxide (Y_2O_3) and aluminium oxide (Al_2O_3) as sintering additives showing improved properties [78].

In freeze granulation process, powdered slurry is prepared in an aqueous media using suitable dispersants and sintering aids. Hence, produced well mixed slurry is sprayed through a spherical nozzle into a liquid nitrogen chamber using nitrogen gas as a carrier. The sprayed granules are instantaneously frozen in liquid nitrogen like spherical ice balls, which are further dried through the sublimation process, using freeze drier under low pressure and negative temperatures, as shown in Figure 2.5(a). The spray dried powders have internal void or dried shell due to the formation of large thermal gradient. However, due to the negligible or low thermal gradient, the spray freeze granulation process produces spherical, homogeneous and free flowing granules, as shown in Figure 2.5(b). Hence, with these advantages, the spray freeze granulation process has been adopted to produce powder of different materials for various applications [79,81-82].

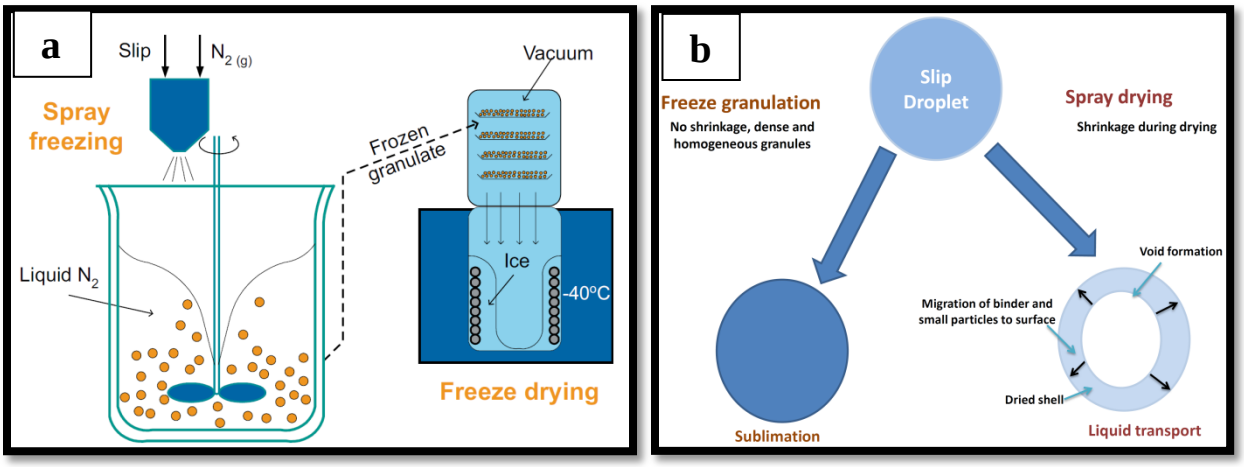

Figure 2.5: Illustration of a) spray freeze granulation process b) comparison of spray granulation and spray freeze granulation processes [83].

2.4 Shaping or compaction process

Shaping or powder compaction is one of the most important steps in producing ceramic components in powder metallurgy route, where powders are densified in a die under high pressure. Along with the green density, compaction provides handling strength and desired final shape to powders. The green product properties after the compaction are mainly influenced by the powder properties such as size, shape, flowability, porosity, homogeneity, etc., and in turn green properties influence the final microstructure and sintered properties of the components [80]. While considering various factors such as component shape, size, productivity, surface,

microstructure characteristic, shaping process or compaction etc., can be selected. Various types of shaping process are summarized in Table 2.3. Die pressing is known to be most widely employed compaction process in many large scale production industries.

Table 2.3: Major compaction techniques used for ceramic components fabrication [85].

Techniques	Sub-category
Pressing	Uniaxial Isostatic (cold and hot isostatic pressing) Hot pressing
Slip casting	Gel casting Pressure casting Vacuum casting Drain casting Centrifugal casting Electrophoretic deposition Fugitive-mold casting
Tape casting	Doctor blade Waterfall
Plastic forming	Extrusion Compression molding Roll forming Injection molding
Additive manufacturing	3D printing Inkjet printing Robocasting

In the present study, only pressing technique has been adopted for fabrication green components of SiC based composite. Pressing is accomplished by compaction of free flowing powder into die under pressure. Some commonly employed pressing techniques are 1) uniaxial and 2) isostatic pressing.

1. ***Uniaxial pressing:*** It involves the compaction of powders by applying pressure along a single axis direction through rigid punch and piston, as shown in Figure 2.6. Pressure can be applied either i) mechanically i.e. by applying cyclic loads either manually or through automation, or ii) hydraulically where pressure media is fluid which transmits the pressure via fluid against piston. Based on the moisture content present in the powders, the pressing is classified as dry

pressing (0-5 %) and wet pressing (10-15 %). In dry pressing, compaction occurs by crushing of the powder granules and the crushed particles are redistributed into a close-packed array.

2. ***Wet pressing*** on the other hand is mainly carried out on clay based composites to achieve plasticity. Even though the pressing process is easy, quick, and economic for many applications, there are a few drawbacks of using this process such as non-uniform density, die wearing, surface cracks etc., which can severely affect the final sintered product properties. Maximum theoretical green density achieved through the uniaxial pressing for ceramic powder is around 55-58 % [81]

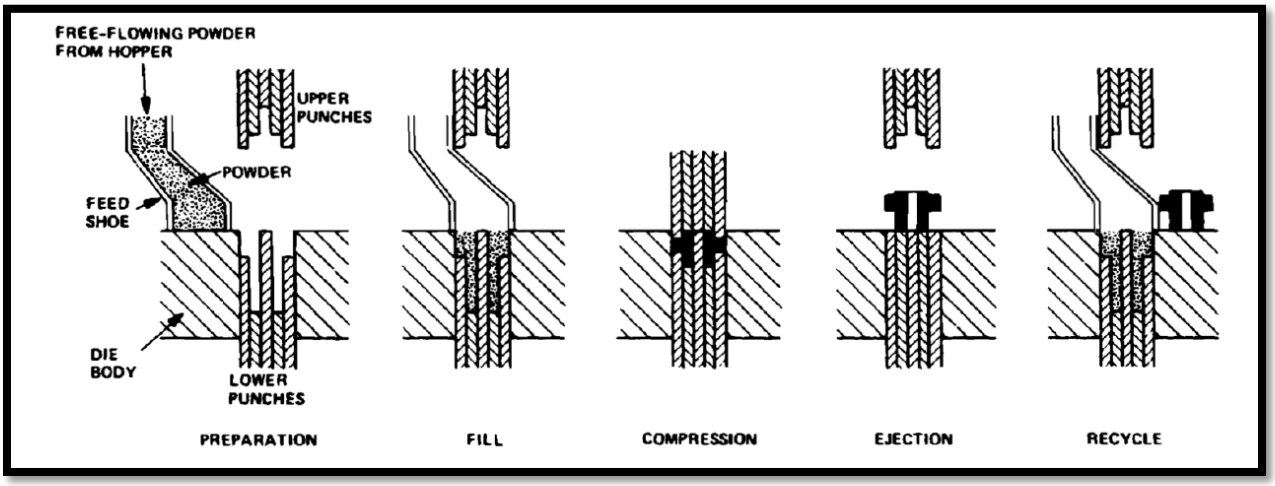

Figure 2.6: Schematic of automated uniaxial pressing [86].

3. ***Isostatic pressing:*** It is also called cold isostatic pressing (CIP), where compaction is attained by applying pressure from all directions [82]. Applying pressure from multiple directions has a great influence in attaining great uniformity of green body properties. Along with uniform green density, some of the advantages of CIP are reduced surface flaws and improved shape capabilities. CIP is the most preferred process for the consolidation of metal and ceramic powders. In this process granulated powders are isostatically pressed using a cold isostatic press where liquid media was used as a pressuring media and the powders are sealed in a mold. Mold is equipped with the mandrel, core set-up for internal shape and the seal plates, which preserves the shape of the components and protects it from liquid pressure media. Commonly employed liquid media for the CIP process are water, oil or glycol mixed

water mixture. Through Trough CIP process, maximum theoretical green density of around 95-100 % can be achieved (for metallic and ceramic powders) [83].

Based on the type of mold used for the pressing, the CIP process is classified as [84]

a) ***Wet-bag isostatic pressing*:** powders are sealed in the mold and placed in the liquid containing high-pressure chamber and the pressure of the liquid media has been increased by hydraulic pump. The uniform green properties are achieved by the distribution of pressure isostatically to the mold. Advantages of adopting the wet-bag isostatic pressing are uniform density, wide verity of complex shapes and various sized components etc.

b) ***Dry-bag isostatic pressing:*** In the process, the mold is not immersed in the fluid media and the set-up has a separate internal channel to pump the high pressure liquid media. Advantages of this process are close dimensional tolerance and quicker process compared to wet-bag isostatic pressing and high production rate etc.

The schematic of the CIP process, i.e., wet bag and dry bag processes are as illustrated in Figure 2.7.

Common applications for CIP include the consolidation of metallic and ceramic powders for various applications such as electrical insulators, spacecraft parts, automotives, refractories, dental parts, etc., [82, 85–87].

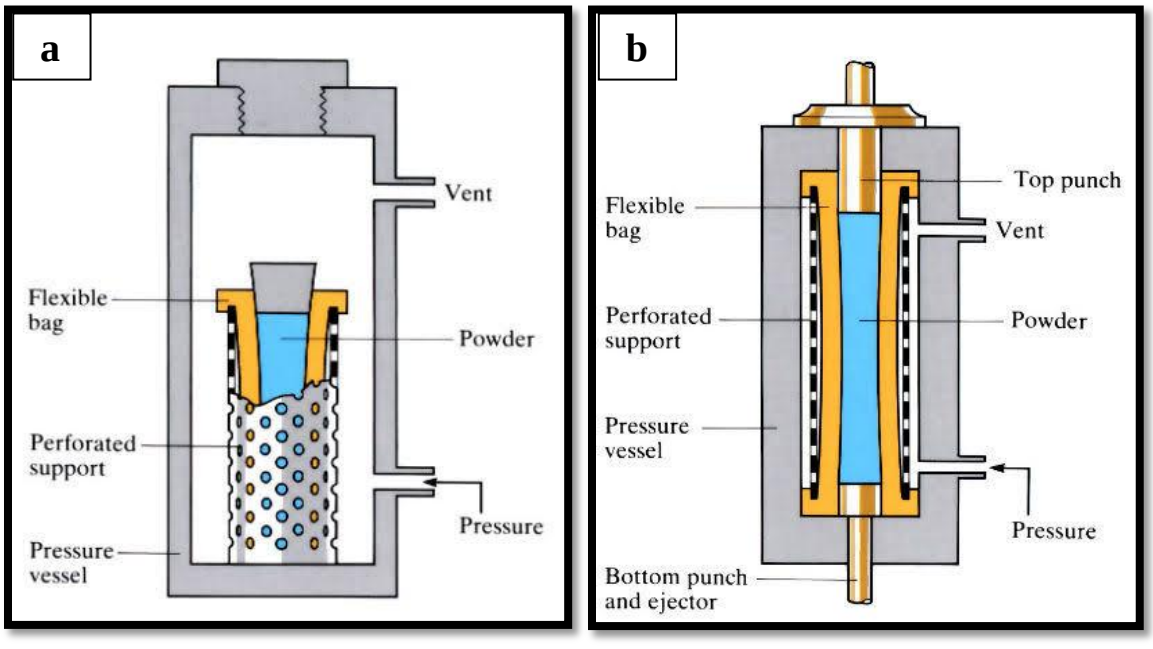

Figure 2.7: Schematic illustration of a) wet-bag and b) dry-bag CIP processes [89].

2.5 Taguchi Modeling techniques for process optimization of SiC composites

Taguchi method is a well-known modeling technique employed in various fields of research enabling one to obtain high quality products economically through optimization of properties by reducing the number of experiments. A lot of time and resources are therefore saved by adopting this process [88–91]. It is known that the powder properties, processing techniques, sintering conditions like temperature, holding time and rate of heating play an important role in densification process of SiC based ceramic composites. Amongst the various controlling variables, sintering parameters command fundamental importance in dictating the final properties [92]. The individual and combined effects of parameters on the properties of the composites are even more complicated when the number of controlling variables are more. These require more number of experiments using all combinations of response variables. Hence, to obtain optimized condition and a set of variables with the well balanced experiments, the Taguchi method of design of experiments and analysis is employed in the present study [93–95]. In this method, a set of control parameters were arranged in an orthogonal array to give the optimum number of experiments with the best combination of parameters. A L_a (b^c) orthogonal array was used in the present study where, 'a' represents the number of experimental runs, 'b' is the number of levels of each factor, and 'c' is the number of variables. The acquired experimental results were analyzed with respect to signal to noise ratio (S/N) and analysis of variance (ANOVA) to understand the effect of variables on the properties of the composites [95–97].

2.6 Sintering techniques

Densification of green compact under heat or pressure or both is known as sintering or firing process. Sintering process is primarily influenced by parameters like sintering temperature, average particle size, atmosphere, applied pressure, packing efficiency, green body properties etc. Decrease in free energy of the system initiates the sintering process. The driving force and material transport mechanisms play a vital role in achieving the required microstructure characteristics and final sintered properties. Sintering process can take place in various mechanisms based on the driving energy and the material transport mechanism, as shown in Table 2.4 and in the form of phase diagram as shown in Figure 2.8. Solid state sintering and liquid phase sintering techniques are most commonly employed for ceramic materials.

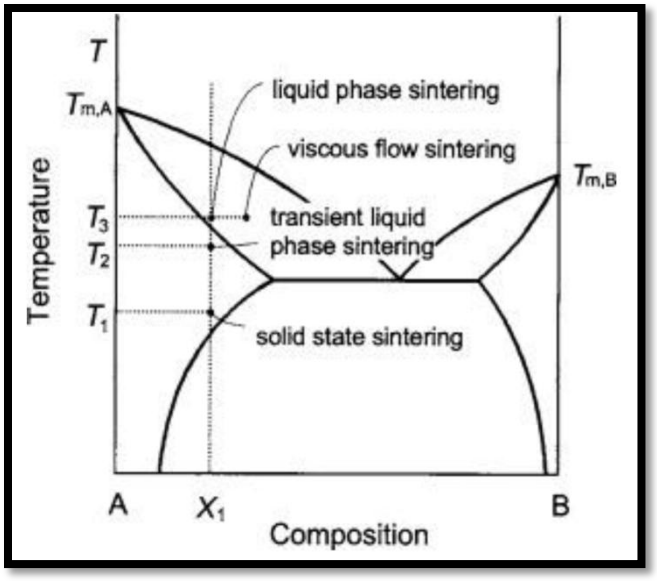

Figure 2.8: Various types of sintering techniques [62].

Solid state sintering: Surface free energy or chemical potential between the surfaces of the adjacent particles are the main driving forces for the solid state sintering process. The grain coarsening during the sintering process reduces the driving force for the densification and acting as an alternative route for densification. Carbon and boron are the most commonly used additives for sintering of SiC system [98–100].

Liquid phase sintering: This process involves sintering green compact under conditions where solid grains coexist along with liquid media. Usually this process is employed on hard materials where sintering is difficult e.g. Si_3N_4, SiC, WC etc [106-107]. The presence of viscous liquid provides the capillary force to pull the grains together, enhance the densification rate and accelerate grain growth. The identification of suitable liquid forming additives and its requirement based on the sintering material is the key point in obtaining the enhanced densification of the system [92]. Even though the liquid phase vigorously accelerates the sintering process and densifies the system, it remains a glassy intergranular phase, which in turn degrades the high temperature properties (creep and fatigue) of the component.

Table 2.4: Classification of sintering mechanisms [108].

S. No	Type of sintering	Material transport mechanism	Driving energy
1.	Vapour-phase	Evaporation-condensation	Differences in vapour pressure
2.	Solid-state	Diffusion	Differences in free energy or chemical potential
3.	Liquid-phase	Viscous flow, diffusion	Capillary pressure, surface tension
4.	Reactive liquid-phase	Viscous flow, solution precipitation	Capillary pressure, surface tension

The strong covalent bonding between silicon and carbon atoms of the SiC and the poor diffusivity of reactant species as well as the densification of SiC is a challenging task whether it is solid state or liquid phase. Sintering process often needs sintering additives with low melting temperatures to enhance densification. Carbon (C) and boron (B), either as elemental form or in the form of compounds, is mostly preferred as sintering aid for solid state densification process while aluminum or Yttrium and its compounds, mainly Al_2O_3/ Y_2O_3 are the liquid phase sintering additives [98, 103–106]. Alternately, recent studies have revealed sintering of SiC without sintering aids at high temperatures could be enhanced by using pressure assisted sintering processes such as hot isostatic press (HIP), hot press (HP), pulsed electric current pressure sintering (PECPS) and pressure assisted microwave sintering [107–109].

2.7 References:

[1] Przemyslaw Daniel Pastuszak and Aleksander Muc: *Key Eng. Mater.*, 2013, vol. 542, pp. 119–29.

[2] Azar Parvizi Majidi: *Compr. Compos. Mater.*, 2000, pp. 175–98.

[3] Jingbing Liu, Xiaoyue Ye, Hao Wang, Mankang Zhu, and Hui Yan: *Ceram. Int.*, 2003, vol. 29, pp. 629–33.

[4] Paul F. Becher: *Annu. Rev. Mater. Sci.*, 1990, vol. 20, pp. 179–96.

[5] Shigeaki Sugiyama, Daiki Kudo, and Hitoshi Taimatsu: *Mater. Trans.*, 2008, vol. 49, pp. 1644–49.

[6] Hison Xu, T A Martin, and Frederick Eichmiller: *J. Dent. Res.*, 1999, vol. 78, pp. 706–12.

[7] John J Brennan and Steven R Nutt: *J. Am. Ceram. Soc.*, 1992, vol. 75, pp. 1205–16.

[8] Hassan Mahfuz, Ashfaq Adnan, Vijaya K Rangari, Shaik Jeelani, and Bor Z Jang: 2004, vol. 35, pp. 519–27.

[9] J M Durand, M Vardavoulias, and M Jeandin: *Wear*, 1995, vol. 181–183, pp. 833–39.

[10] P J Withers: in *Ref. Modul. Mater. Sci. Mater. Eng.*, Elsevier, 2016.

[11] A. Riaz Ahamed, P. Asokan, and S. Aravindan: *Int. J. Adv. Manuf. Technol.*, 2009, vol. 44, pp. 520–28.

[12] M randall: *Particulate Composites: Fundamentals and Applications*, Springer, 2018.

[13] Bernd Clauß: in *Ceram. Matrix Compos. Fiber Reinf. Ceram. Their Appl.*, 2008, pp. 1–20.

[14] M Ozgur Seydibeyoglu, Amar K Mohanty, and Manjusri Misra: *Fiber Technology for Fiber-Reinforced Composites*, Woodhead Publishing, 2017.

[15] Soo-Jin Park and Min-Kang Seo: *Interface Science and Composites*, Academic Press, 2011.

[16] Krishan K Chawla: in *Compos. Mater. Sci. Eng.*, Springer International Publishing, Cham, 2019, pp. 251–96.

[17] S R Pemberton, E K Oberg, J Dean, Dimitris Tsarouchas, Athina Markaki, L Marston, and Bill

Clyne: *Compos. Sci. Technol.*, 2011, vol. 71, pp. 266–75.

[18] Kazuya Shimoda, Tatsuya Hinoki, and Akira Kohyama: *Compos. Sci. Technol.*, 2010, vol. 70, pp. 387–92.

[19] Johann Cho, Aldo R. Boccaccini, and Milo S.P. Shaffer: *J. Mater. Sci.*, 2009, vol. 44, pp. 1934–51.

[20] M. Belmonte, J. González-Julián, P. Miranzo, and M. I. Osendi: *J. Eur. Ceram. Soc.*, 2010, vol. 30, pp. 2937–46.

[21] P Xiao, J Chen, and X F Xu: *J Nanomater*, 2010, vol. 2010, p. 96389.

[22] Fengming Shi, Xiaowei Yin, Xiaomeng Fan, Laifei Cheng, and Litong Zhang: *J. Eur. Ceram. Soc.*, 2010, vol. 30, pp. 1955–62.

[23] D. Frazer, M. D. Abad, D. Krumwiede, C. A. Back, H. E. Khalifa, C. P. Deck, and P. Hosemann: *Compos. Part A Appl. Sci. Manuf.*, 2015, vol. 70, pp. 93–101.

[24] Eric Rohmer, Eric Martin, and Christophe Lorrette: *J. Nucl. Mater.*, 2014, vol. 453, pp. 16–21.

[25] Byeong Choon Goo: *Mater. Manuf. Process.*, 2016, vol. 31, pp. 979–88.

[26] Tiziano Minghetti, Christian Schelle, Thomas Graule, and Jakob Kuebler: 2011, vol. 37, pp. 3371–79.

[27] Pooja Bhatt and Alka Goe: *Mater. Sci. Res. India*, 2017, vol. 14, pp. 52–57.

[28] Tushar Kanti Das, Prosenjit Ghosh, and Narayan Ch. Das: *Adv. Compos. Hybrid Mater.*, 2019, vol. 2, pp. 214–33.

[29] Kamyar Shirvanimoghaddam, Salah U Hamim, Mohammad Karbalaei, Seyed Mousa, Hamid Khayyam, Amir Hossein, Ehsan Ghasali, Mahla Zabet, Khurram Shahzad, Shian Jia, J Paulo Davim, and Minoo Naebe: *Compos. Part A*, 2017, vol. 92, pp. 70–96.

[30] Subhranshu S Samal, Lanka Manoj: In *book on Encylopedia of Composites*, Wiley, 2012, pp. 1–9.

[31] Michio Inagaki: in *New Carbons - Control Struct. Funct.*, Elsevier Science, Oxford, 2000, pp. 82–123.

[32] James A Dicarlo and Hee-mann Yun: *Handbook of Ceramic Composites*, Springer, Boston, MA,

2005, pp. 33–52.

[33] Bhatt P, Goe A: *Mater. Sci. Res.India.*, 2017, vol. 14, pp. 52–57.

[34] Adrian B Mann, Mehdi Balooch, John H Kinney, and Timothy P Weihs: 1999, vol. 16, pp. 111–16.

[35] James A DiCarlo, Hee-Mann Yun: In *Handbook of Ceramic Composites*,Springer Link, 2005, ch. 2, pp. 1–20.

[36] Liang Guang Chen, Su Jien Lin, and Shou Yi Chang: *Metall. Mater. Trans. A*, Springer, 2005, vol. 36, pp. 1937–45.

[37] S. Tiwari and J. Bijwe: *Procedia Technol.*, 2014, vol. 14, pp. 505–12.

[38] I.C. Finegan, G.G.Tibbetts, D. G.Glasgow, J. M. Ting, M. L.Lake:*J. Mater. Sci.*, Sringer, 2003, vol. 38, pp. 3485–3490

[39] Haijiao Zhang, Huijiao Guo, Xiaoyong Deng, Ping Gu, Zhiwen Chen, and Zheng Jiao: 2010, vol. 21 (8), pp. 1–8.

[40] L Montoro, Carlos Luengo, Jose Rosolen, Enzo Cazzanelli, and Gino Mariotto: *Diam. Relat. Mater.*, 2003, vol. 12, pp. 846–50.

[41] T Savage, S Bhattacharya, B Sadanadan, J Gaillard, T M Tritt, Y P Sun, Y Wu, S Nayak, Roberto Car, and N Marzari: *J. Phys. Condens. Matter*, 2003, vol. 15, pp. 8969–9040.

[42] S C Tsang, P J F Harris, and M L H Green: *Nature*, 1993, vol. 362, pp. 520–22.

[43] Alexandre Felten, C Bittencourt, and Jean-Jacques Pireaux: *Nanotechnology*, 2006, vol. 17, p. 1954.

[44] Yu Li, Xiaobin Zhang, Junhang Luo, Wanzhen Huang, Jipeng Cheng, Zhiqiang Luo, Ting Li, Fu Liu, Guoliang Xu, and Xiaoxing Ke: *Nanotechnology*, 2004, vol. 15, p. 1645.

[45] Anil Suri and Karl S Coleman: *Carbon N. Y.*, 2011, vol. 49, pp. 3031–38.

[46] Fu-Hsiang Ko, Chung-Yang Lee, Chu-Jung Ko, and Tieh-Chi Chu: *Carbon N. Y.*, 2005, vol. 43, pp. 727–33.

[47] Kieran J MacKenzie, Oscar M Dunens, Monica J Hanus, and Andrew T Harris: *Carbon N. Y.*,

2011, vol. 49, pp. 4179–90.

[48] Jianggao Liu, Shubin Wang, Pengyang Li, Mengjie Feng, and Xinwang Yang: *Surf. Coatings Technol.*, 2016, vol. 286, pp. 57–63.

[49] Samuel J. Frueh, Timothy P. Coons, Justin W. Reutenauer, Rebecca Gottlieb, Michael A. Kmetz, and Steven L. Suib: *Ceram. Int.*, 2018, vol. 44, pp. 15310–16.

[50] Linlin Chen, Haihui Ye, and Yury Gogotsi: *J. Am. Ceram. Soc.*, 2004, vol. 87, pp. 147–51.

[51] Tao Li, Yu Duan, Kanghua Jin, Tao Suo, Xia Yu, and Yulong Li: *Int. J. Impact Eng.*, 2017, vol. 109, pp. 391–99.

[52] Chun Hway Hsueh: *Mater. Sci. Eng. A*, 1990, vol. 125, pp. 67–73.

[53] Gregory N. Morscher, Hee Mann Yun, James A. DiCarlo, and Linus Thomas-Ogbuji: *J. Am. Ceram. Soc.*, 2004, vol. 87, pp. 104–12.

[54] Wei Zhou, Peng Xiao, Yang Li, and Liang Zhou: *Ceram. Int.*, 2013, vol. 39, pp. 6569–76.

[55] Bei Yang, Xingui Zhou, and Yuxin Chai: *Ceram. Int.*, 2015, vol. 41, pp. 7185–90.

[56] R Naslain: *Compos. Interfaces*, 1993, vol. 1, pp. 253–86.

[57] R Naslain: *The Concept of Layered Interphases in SiC/SiC*, American Ceramic Society, Westerville, OH (United States), 1995.

[58] Suk-Joong L Kang: in *Sintering*, Suk-Joong L Kang, ed., Butterworth-Heinemann, Oxford, 2005, pp. 3–8.

[59] David W Richerson: *Modern Ceramic Engineering: Properties, Processing, and Use in Design*, CRC press, 2005.

[60] Tian-Quan Liu, Osamu Sakurai, Nobuyasu Mizutani, and Masanori Kato: *J. Mater. Sci.*, 1986, vol. 21, pp. 3698–3702.

[61] Suresh Kumar, K Chandra Shekar, B Jana, L M Manocha, and N Eswara Prasad: in *Aerosp. Mater. Mater. Technol.*, Springer, 2017, pp. 343–69.

[62] A. Ortona, T. Fend, H. W. Yu, K. Raju, P. Fitriani, and D. H. Yoon: *Sol. Energy Mater. Sol. Cells*, 2015, vol. 132, pp. 123–30.

[63] Wen Jin, Zhou Si, Yi Lu, Sun Bei-zhi, Wang Yi, Li Guang-de, Xing Zhong-fang, and Cao Jie: 2018, vol. 44, pp. 16583–88.

[64] Jing Wang, Xu Chen, Kang Guan, Laifei Cheng, Litong Zhang, and Yongsheng Liu: *Ceram. Int.*, 2018, vol. 44, pp. 16414–20.

[65] B Reznik, D Gerthsen, and K J Hüttinger: *Carbon N. Y.*, 2001, vol. 39, pp. 215–29.

[66] Lifeng Zhang, Chengzu Ren, Changling Zhou, Hongzhao Xu, and Xinmin Jin: *Appl. Surf. Sci.*, 2015, vol. 357, pp. 1427–33.

[67] Manish Patel, Kumar Saurabh, V V Bhanu Prasad, and J Subrahmanyam: *Bull. Mater. Sci.*, 2012, vol. 35, pp. 63–73.

[68] Hui Mei, Laifei Cheng, Litong Zhang, Xingang Luan, Peng Fang, and Jun Zhang: *J. Mater. Sci.*, 2005, vol. 40, pp. 4261–65.

[69] M Frieß, R Renz, W Krenkel, "Graded Ceramic Matrix Composites by LSI-Processing", in *Advanced Inorganic Structural Fiber Composites IV*, (ED.: P. Vincenzini, C. Badini), 2003, pp.141–148.

[70] Ilaria Corni, Mary P. Ryan, and Aldo R. Boccaccini: *J. Eur. Ceram. Soc.*, 2008, vol. 28, pp. 1353–67.

[71] Kun Yang, Hui Mei, Daoyang Han, and Laifei Cheng: *Ceram. Int.*, 2018, vol. 44, pp. 20187–91.

[72] Saša Novak, Katja König, Aljaž Ivekovič, and Aldo R. Boccaccini: *Key Eng. Mater.*, 2009, vol. 412, pp. 237–42.

[73] Joon-SooPark, Akira Kohyama,Tatsuya Hinoki, Kazuya Shimoda, Yi-Hyun Park: *J. Nucl. Mater.*, 2007, vol. 367-370, pp. 719–724.

[74] Dean-Mo Liu and Chen-Tsu Fu: *Ceram. Int.*, 1996, vol. 22, pp. 67–72.

[75] Bala Raghupathy and Jon Binner: *J. Nanoparticle Res.*, 2012, vol. 14.

[76] Michael Stuer, Zhe Zhao, and Paul Bowen: 2012, vol. 32, pp. 2899–2908.

[77] Prasenjit Barick, Dibyendu Chakravarty, Bhaskar Prasad Saha, Rahul Mitra, and Shrikant V. Joshi: *Ceram. Int.*, 2016, vol. 42, pp. 3836–48.

[78] Brita Nyberg, E Carlstrom, and Roger Carlsson: *Euro-Ceramics II.*, 1991, vol. 1, pp. 447–51.

[79] F Paul, J R Binder, H Gesswein, H-J Ritzhaupt-Kleissl, and J Hausselt: *Ceram. Int.*, 2009, vol. 35, pp. 479–86.

[80] Xing Zhong Guo and Hui Yang: *J. Zhejiang Univ. Sci.*, 2004, vol. 5, pp. 950–55.

[81] Martin Trunec and Karel Maca: in *Adv. Ceram. Dent.*, Elsevier, 2014, pp. 123–50.

[82] Isidoro Iván Cuesta, Emilio Martínez-Pañeda, Andrés Díaz, and Jesús Manuel Alegre: *Materials (Basel).*, 2019, vol. 12.

[83] P. Samal; J. Newkirk: *Book chapter on Milling of Brittle and Ductile Materials*, *Powder Metall.*, ASM International, 2015, vol. 7.

[84] Open university: *Science, Maths & Technology*, 2017, pp. 1–7.

[85] G. Ya Akimov, V. M. Timchenko, and É V. Chaika: *Refract. Ind. Ceram.*, 1997, vol. 38, pp. 310–14.

[86] Ramesh Singh, Christopher P., Tan Y., and Wd Teng: *Biomed. Eng. - Appl. Basis Commun.*, 2004, vol. 16, pp. 199–204.

[87] Ahmed Nassef, Waleed H. El-Garaihy, and Medhat El-Hadek: *Metals (Basel).*, 2017, vol. 7, pp. 1–12.

[88] J She, D Jiang, S Tan, and J Guo: *Mater. Lett. (General Ed.)*, 1992, vol. 14, pp. 240–44.

[89] Ranjit K Roy: *Handbook on Deign of Experimnts using the Taguch Approch*, Wiley, New York, 2001, pp. 1–560.

[90] S S Shinozaki, J Hangas, K R Carduner, M J Rokosz, K Suzuki, and N Shinohara: *J. Mater. Res.*, 1993, vol. 8, pp. 1635–43.

[91] Raghu N Kackar: *J. Qual. Technol.*, 1985, vol. 17, pp. 176–88.

[92] J. H. She and K. Ueno: *Mater. Res. Bull.*, 1999, vol. 34, pp. 1629–36.

[93] George Box: *Technometrics*, 1988, vol. 30, pp. 1–17.

[94] St, Lars, and Svante Wold: *Chemometrics and intelligent laboratory systems*, 1989, 259–272.

[95] Bala Murugan Gopalsamy, Biswanath Mondal, and Sukamal Ghosh: *J. Sci. Ind. Res. (India).*, 2009, vol. 68, pp. 686–95.

[96] Keselman HJ, Huberty CJ, Lix LM: *Review of Educational Research*, 1998, 350–386.

[97] S. El-Safty, N. Silikas, R. Akhtar, and D.C. Watts: *Dent. Mater.*, 2012, vol. 28, pp. 1171–82.

[98] Giuseppe Magnani, Giuliano Sico, Alida Brentari, and Paride Fabbri: *J. Eur. Ceram. Soc.*, 2014, vol. 34, pp. 4095–98.

[99] M. S. Datta, A. K. Bandyopadhyay, and B. Chaudhuri: *Bull. Mater. Sci.*, 2002, vol. 25, pp. 181–89.

[100] Julin Wan, Ren Guan Duan, and Amiya K. Mukherjee: *Scr. Mater.*, 2005, vol. 53, pp. 663–67.

[101] A. Can, M. Herrmann, D. S. McLachlan, I. Sigalas, and J. Adler: *J. Eur. Ceram. Soc.*, 2006, vol. 26, pp. 1707–13.

[102] F. K. Van Dijen and E. Mayer: *J. Eur. Ceram. Soc.*, 1996, vol. 16, pp. 413–20.

[103] Z H Huang, D C Jia, Y Zhou, and Y G Liu: *Ceram. Int.*, 2003, vol. 29, pp. 13–17.

[104] Joydeb Mukerji: *Def. Sci. J.*, 1993, vol. 43, p. 385.

[105] Oscar Borrero-López, Angel L Ortiz, Fernando Guiberteau, and Nitin P Padture: *J. Eur. Ceram. Soc.*, 2007, vol. 27, pp. 2521–27.

[106] Randall M German, *Æ* Pavan Suri, and *Æ* Seong Jin: 2009, pp. 1–39.

[107] Kurt A. Terrani, Caen Ang, Lance L. Snead, and Yutai Katoh: *J. Nucl. Mater.*, 2018, vol. 499, pp. 242–47.

[108] J E Garay: *J. Mater. Sci.*,2008, pp. 4050–4056.

[109] Joon Soo Park, Hiroshi Nishimura, Daisuke Hayasaka, Ju Hyeon Yu, Hirotatsu Kishimoto, and Akira Kohyama: *Fusion Eng. Des.*, 2016, vol. 109–111, pp. 1174–78.

CHAPTER 3

Experimental Methods

3.0 Introduction

In this chapter, an overview of various characterization techniques and design of experiments for the development of CNFs/ CNT dispersed SiC composites have been explained. Different processing techniques for the fabrication of composites are delineated. The optimization of processing parameters of SiC composites is carried out by using Taguchi's statistical design of experiments. The characterization techniques employed to investigate the properties of the samples are also discussed.

3.1 Characteristics of raw materials and methods

SiC powder (α-SiC (CUMI's M-15, M-25, India) of 0.6 μm and 0.4 μm size were used as matrix material. The β-SiC (particle size: 350 nm) (IAM, USA) with cubic structure and carbon nanofibers of length 35 μm, diameter 70 nm, (Grupo Antolin, Spain), and long carbon fiber bundles (C_f) (5-7K, IndiaMART, India) were used as secondary phase material. Boron (B) (from Sigma Aldrich, USA) and Carbon (C) in the form of sucrose (from SDFCL, India), were used as sintering additives. Sigma Aldrich, USA make Polyethylenimine (PEI-25000) was used as a dispersant of SiC in water media (freeze granulation process). Nitric acid (HNO_3) (Sigma-Aldrich, USA) and sulphuric acid (H_2SO_4) (Fisher Scientific, USA) were used to surface-treat the fibers while sodium dodecyl sulphate salt (SDS) (Fisher Scientific, USA) was used as a surfactant for well dispersion with the aqueous matrix. The long carbon fiber bundles (C_f) were coated with boron nitride (BN) by allowing polymeric precursors of boric acid (Fisher Scientific, USA) to react with urea (MERCK, USA). The overall work flow chart of the thesis experimental work is as given in Fig. 3.0.

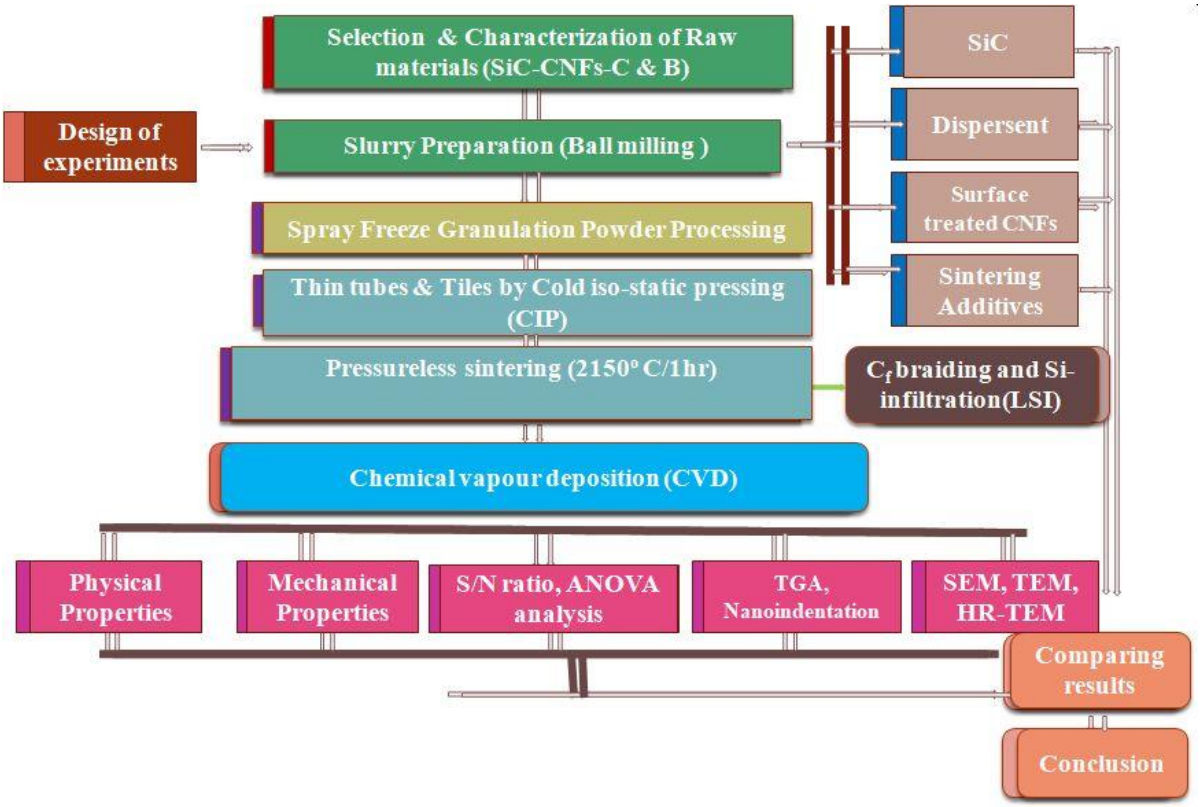

Figure 3.0: Overall workflow chart of the experimental work.Table 3.1: Information of the raw material for the fabrication of CVD SiC coated C_f/C-SiC hybrid composite tubes.

Raw material	Role	Specifications
SiC (CNFs) composite tube	Base matrix	In house fabricated dense and pressureless sintered SiC composite tube with 1 wt % CNFs reinforcement [1] Wall thickness: ~2 mm
High strength carbon fabric (HSC)	Reinforcement	TS 700S, TORAY, Japan Tensile strength 4900 MPa, Filament diameter: 7 µm Number of filaments per tow: 6K (K=1000), Density: 1.80 g/cc
Carbon non-crimped fabric (NCF)	Reinforcement	NCF W300C, SHIMTEQ, Japan Filament diameter: 6 µm, Number of filaments per tow: 7K Density: 1.80 g/cc
Spun yarn graphitized carbon	Reinforcement	Zoltek™ PX30, U.S, Filament diameter: 7 µm,

fabric (SYG)		Number of filaments per tow: 6K Density:1.75 g/cc
Coal-tar pitch	Binder as well as the precursor to the matrix	Carbon residue rate 46.3 %, IndiaMART, India
Silicon lumps	Infiltration material to form SiC matrix	Purity: 99 %, IndiaMART, India
Methyl-trichlorosilane (MTS)	Protective coating	Purity: 99 %, Sigma Aldrich, USA.

3.2 Taguchi designing of experiments

In this study, an attempt was made to process SiC – CNFs composite from establishing the influence of sintering parameters and secondary phase material (CNFs) on the properties of SiC composites. Experiments were designed by Taguchi statistical analysis. SiC-CNFs were prepared with varied CNFs composites at different sintering conditions and processed through solid state pressureless sintering technique. The physical and mechanical properties of the composites were then measured and analyzed statistically by Taguchi method.

3.2.1 Design of Experiment

The experiments were designed with Taguchi L_9 orthogonal array to minimise the number of experiments with the optimized combination of factors. The L_9 array contains 4 factors and 3 levels with a total degree of freedom (DF) of 8. Since the sintering parameters have a major impact on SiC-CNFs composite properties, the input sequence of the factors were given as sintering temperature (^oC), heating rate (^oC/min), holding time (hours) and CNFs composition (wt %), as listed in Table 3.2. Minitab 18 software version has been adopted for Taguchi analysis. The experimental results were studied with help of signal to noise (S/N) ratios, ANOVA, etc., as shown in flow chart given below (Figure 3.1). ANOVA helps in analyzing the influence of individual factors on total variance. The S/N ratio analysis will provide the most efficient set of operating conditions by the variation in the results. The signal-to-noise ratio measures how the response varies relative to the nominal or target value under different noise conditions. One can choose from different signal-to-noise ratios, depending on the goal of experiment. Out of three types of analysis based on characteristic S/N ratio viz. i.e, smaller is

better, normal is better and larger is better offered by Minitab, the last methodology i.e. larger is better was adopted and equation 3.1, shown below, was considered for analysis.

$$N = -10\text{Log}\left(\left(\frac{1}{n}\right)\sum\frac{1}{(y)^2}\right) \qquad \text{Equation (3.1)}$$

Where n is the number of experiments, y is observed data or results of the corresponding experiments carried out. The parameters consists the ANOVA tables such as DF, Adj SS, Adj MS, F and P values are default generated with the given inputs. P is probability that measures the significance of the term further. $P \leq 0.05$ is significance level. Each parameter value has its unique way of representing the influence of factors on the properties.

From the S/N ratio and ANOVA response tables, the major influencing factors of particular composite properties are studied.

Table 3.2: List of processing parameters and their respective levels for experimental design.

Processing parameters	Level 1	Level 2	Level 3
Sintering temperature (^{o}C) (A)	2125	2150	2175
Heating rate(^{o}C/min) (B)	6	8	10
Holding time (hours) (C)	1	2	3
CNFs composition (wt %) (D)	0	1	2

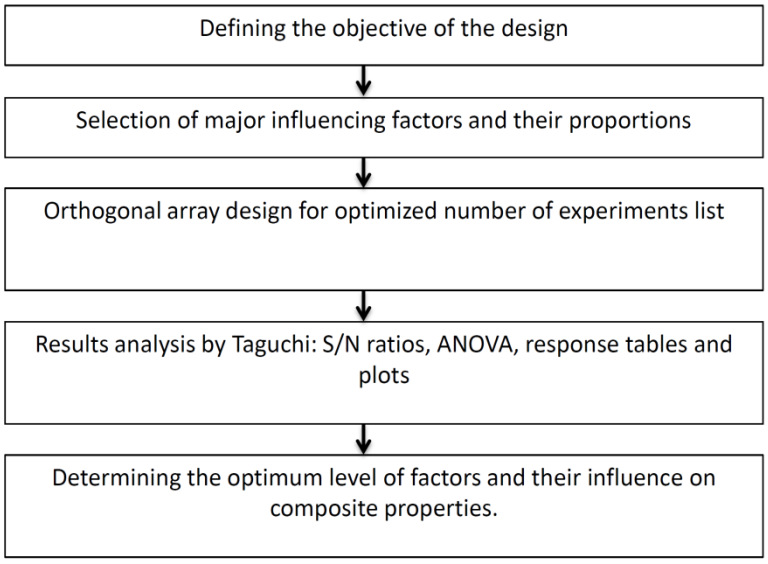

Figure 3.1: The sequential steps involved in the Taguchi analysis.

3.3 Surface treatment methodology of reinforcement materials

The CNFs offer superior support to SiC matrix with its unique combination of properties. However, avoiding micro segregation or bundling and uniform dispersion are challenges one faces while using carbon nanofibers as reinforcement. As explained in the previous chapter, extensive research work has been carried out to develop dispersion technologies of submicron to nanometer range reinforcement in various media. In the present study, chemical oxidation route was adopted for functionalization of carbon nanofibers and nano SiC powder particles. Long fiber filaments of carbon and SiC are coated hexagonal boron nitride (h-BN) an inter-phase material. The process details are as given below.

3.3.1 *Functionalization of CNFs using acid treatment*

In the present study, acid treatment of carbon nanofibers was carried out for improving their dispersibility in water. Nitric acid (HNO_3) and sulphuric acid (H_2SO_4) solution in the ratio of 3:1 at various concentrations were used to treat the fibers [2]. Zeta potential studies and FTIR Analysis were considered for fixing the acid concentration as 0.5 M so as to avoid the aggressive surface treatment of CNFs. The dispersion of fibers in the matrix was further enhanced by using suitable surfactant i.e sodium dodecyl sulfate salt (SDS) at optimized quantity and along with ultra-probe sonication. Ultra-probe sonication is a physical way of separating entanglement of carbon fibers using shear forces via sonication [3,4]. The literature studies, reveals that the SDS concentration used for CNFs or CNTs dispersion was minimum and the ratio of SDS to CNFs quantity is approximately 0.2:1 and further optimization of dispersion was carried out by zeta analyzer [5]. Vigorous mixing of composite slurry, before granulation, with an ultra-probe sonicator helped in removing air entrapment.

3.3.2 *Surface coating of long carbon fibers with BN using Sol-gel dip coating*

To improve the thermal stability and chemical inertness of long carbon fiber bundles (C_f) (IndiaMART, India), they were coated with boron nitride (BN) by allowing polymeric precursors of boric acid (Fisher Scientific, USA) to react with urea (MERCK, USA) [6]. The dip-coating technique in combination with sol-gel process was chosen to coat the fibers with BN. The carbon fiber filaments were separated from the bundle, cleaned and dried prior to coating and then subjected to dip-coating process at optimized experimental titration conditions, i.e. four cycles of

dip-coating. After the completion of each cycle, the dip-coated fibers were dried at 120 ^{o}C followed by curing at 800 ^{o}C for 2 hr at the rate of 5 ^{o}C/min under N_2 atm (Figure 3.2). BN coated C_f filaments thus synthesized were used as reinforcement for the fabrication of hybrid composite tubes.

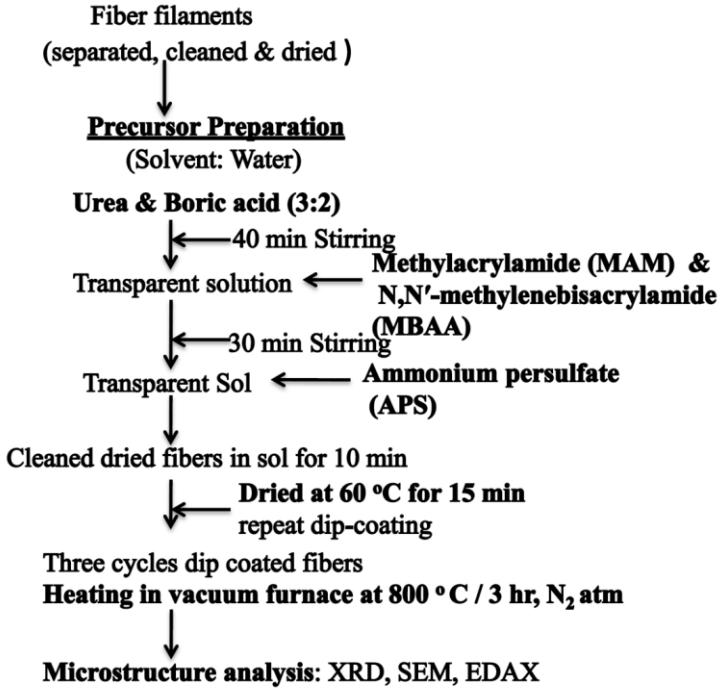

Figure 3.2: Process flow chart of interface coating of BN using sol-gel dip coating route [6,7].

3.4 Slurry preparation and powder processing of SiC based composites

The slurry preparation and powder processing are crucial steps in deciding the properties of the final product. In processing homogenous SiC based composite, lubricants, additives (sintering aids) and secondary phase material (carbon nanofibers) were mixed with the SiC matrix under wet conditions (aqueous solvent) using comminution methods. Some of the comminution techniques are crushing and grinding. In order to avoid the agglomerates or lump formation and to obtain the required particle size, milling was done. Ball milling is the most commonly employed comminution technique, where powders are ground or milled in a cylindrical container with the help of grinding media (suitable balls). The most commonly preferred grinding media is hard and inert material or similar type of material to avoid the contamination of media. In ball milling, slurry is homogeneously milled with applied mechanical forces. As the ball mill rotates, the slurry or ceramic powder lumps moves between the balls and the walls of the mill and hence

the agglomerates or lumps found reduces in size as represented in Figure 3.3. The rate of milling depends on the relative size and the density of the media.

In ball milling, the milling time, grinding media and applied mechanical force are the main parameters, which influence the properties of the powder largely. In the present study, powders were processed under optimized conditions of milling parameters such as the grinding media being twice the weight of the slurry or powders to be grounded, milling time of 20 min with a mechanical force rendered by 80 rpm.

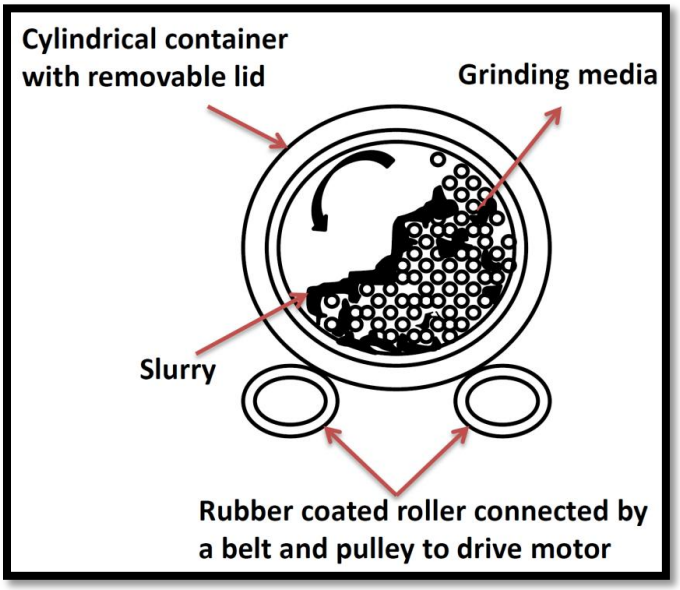

Figure 3.3: Schematic of ball milling process [8].

3.4.1 *Conventional and rotary evaporation powder processing methods*

The conventional powder process is a fast and economic processing technique. In this process the mixed or milled composite slurry is placed in a tray and dried in normal atmosphere or hot air oven. Hence the produced powder lumps are crushed and sieved.

Rotary evaporation is a controlled drying process to reduce the volume of solvent and commonly employed when compounds or additives in the slurry have lower boiling point than solvent. It is an effective technique to remove solvent from a compound of interest. In this process, slurry is placed inside a glass flask and mechanically rotated in hot water bath under controlled vacuum conditions; the set-up is shown in Figure 3.4. The flask rotation and the hot water bath helps in increasing the surface area of the compound thereby exposing the solvent for faster evaporation.

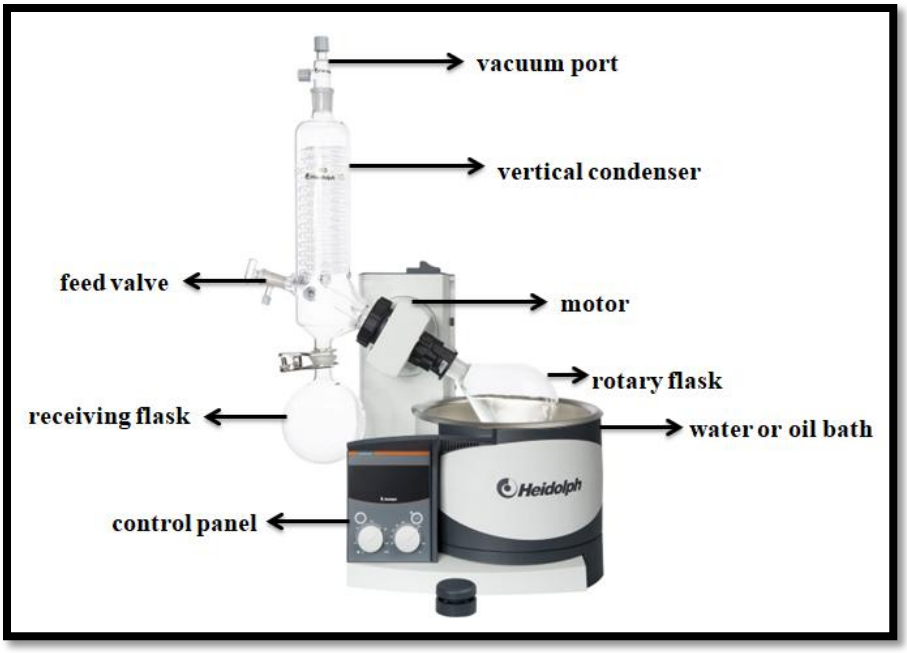

Figure 3.4: Schematic of rotary evaporator.

3.4.2 *Freeze granulation process*

SiC and its composite formulations were prepared with fixed carbon (2.4 wt %) in the form of sucrose, elemental boron (0.6 wt %) and varying CNFs content (1 to 3 wt %,). Sucrose was selected as carbon containing precursor for ease of subsequent aqueous processing of the slurries for freeze granulation. Prior to the addition of fibers in the matrix powder, acid treatment of the fibers were carried out for improving the dispersibility in water. The concentration of acids were optimised and fixed as 0.5M by mixing nitric acid and sulphuric acid in the ration 3:1.Surface modified fibers were dispersed in water with the help of sodium dodecyl sulfate salt (SDS) as a surfactant mixed using an ultra-probe sonicator. The dispersed CNFs solution was then added to SiC slurry to produce the composite powder of 30 vol % solid loading, which was then sprayed in the form of spherical granules into a chamber. The sprayed spherical granules were then frozen in liquid nitrogen gas using a freeze granulator (Powder Pro, Model: LS-2, Sweden) to make frozen granules, resembling spherical ice balls entrapping the well dispersed additives in the SiC matrix. Subsequently, drying of frozen granules through the sublimation of ice into vapour was carried out with the help of a freeze drier (SRK System Technik Gmbh, Model: LYO GT 2, Germany) at an initial temperature of less than -30 °C under constant vacuum level of 1.5 mbar. Thus, granules of CNFs containing SiC composite powders with fiber content varying from 1 to 3 wt % were prepared. The spherical shaped SiC/CNFs containing composite powder

with a bi-modal size distribution having a mean granule size of ~ 50 µm as shown in Figure 3.5 (c), was obtained which was used for further experiments.

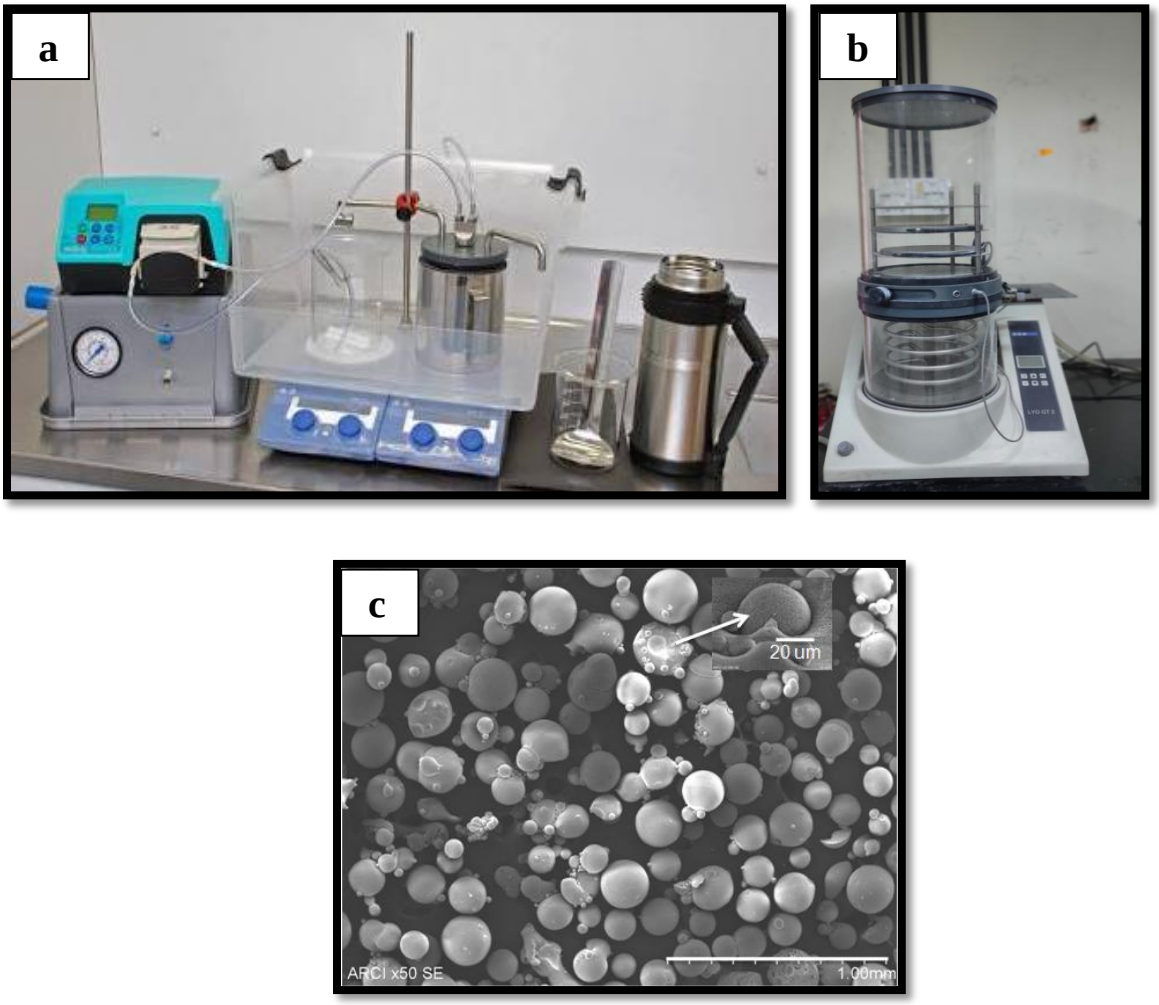

Figure 3.5: a) Spray freeze granulation set up b) freeze drying set up c) bi-model distribution of spray freeze granulated SiC composite powder.

3.5 Shaping, sintering and post sintering processes of the samples

Freeze granulated SiC-CNFs composite powder were used to produce highly dense green thin tubes of SiC based composites with dimensions 60-600 mm length, 1-10 mm wall thickness and 20-30 mm outer diameter in a cold isostatic press at 80 MPa pressure for 10 min using a specially designed neoprene mould as shown in the Figure 3.6. Green coupons of 32^{L} X 32^{W} X 4^{T} mm^3 size were also compacted at 491 MPa pressure using a uni-axial hydraulic press with an average density of 55-58 % to the theoretical value.

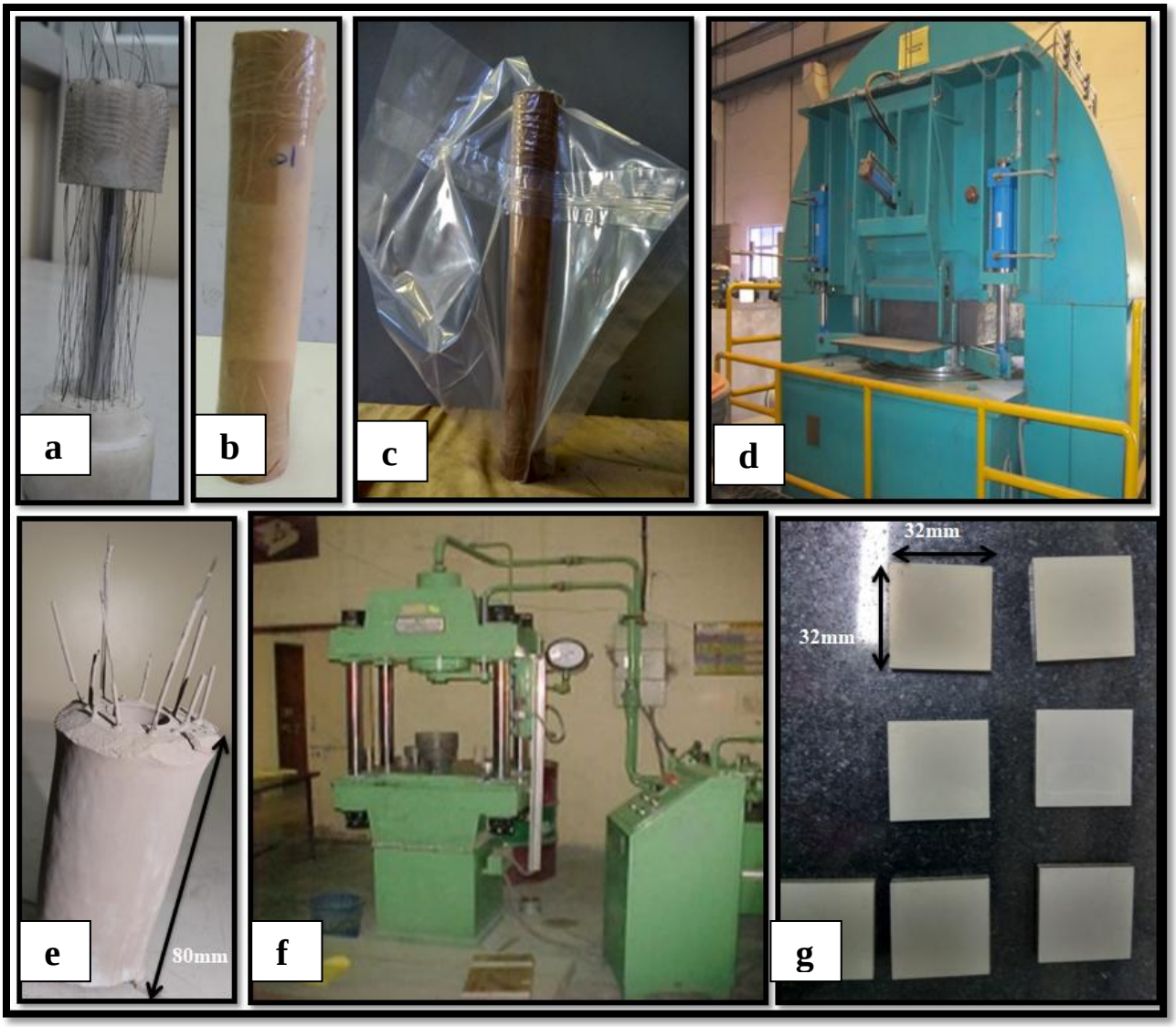

Figure 3.6: Processing steps involved in shaping a) fiber weaving around core rod b) substrate insertion inside the rubber bag c) vacuum tight sealing of bag d) cold isostatic press set up e) CIPed green SiC hybrid composite tubes with long fibers projections f) hydraulic uni-axial compaction press g) uniaxial pressed composite tiles.

The compacted green tubes along with the green coupons were then subjected to pressureless sintering at 2150 ^{o}C for a holding period of 1 hr in Argon atmosphere in a special holding arrangement to avoid warpage of the tube during sintering as shown in Figure 3.7. The time, temperature and heating rate variation of the sintering process are shown in Figure 3.8.

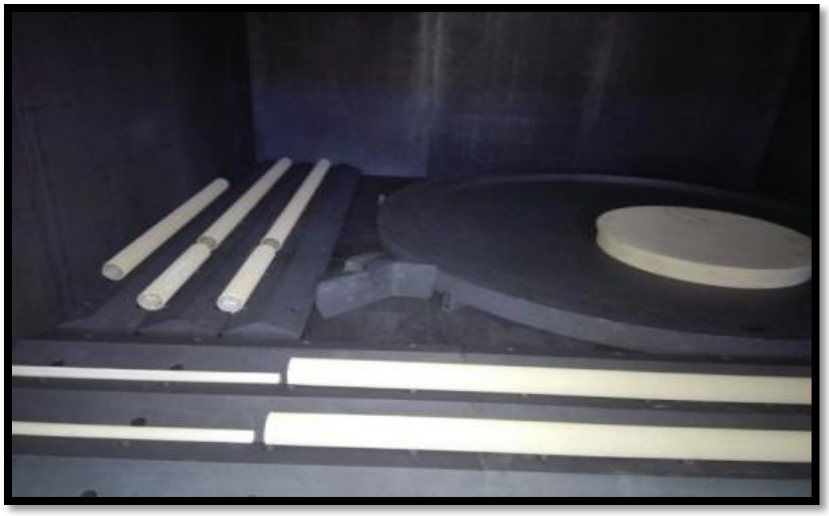

Figure 3.7: V-Channel arrangement for CIP tubes in the furnace.

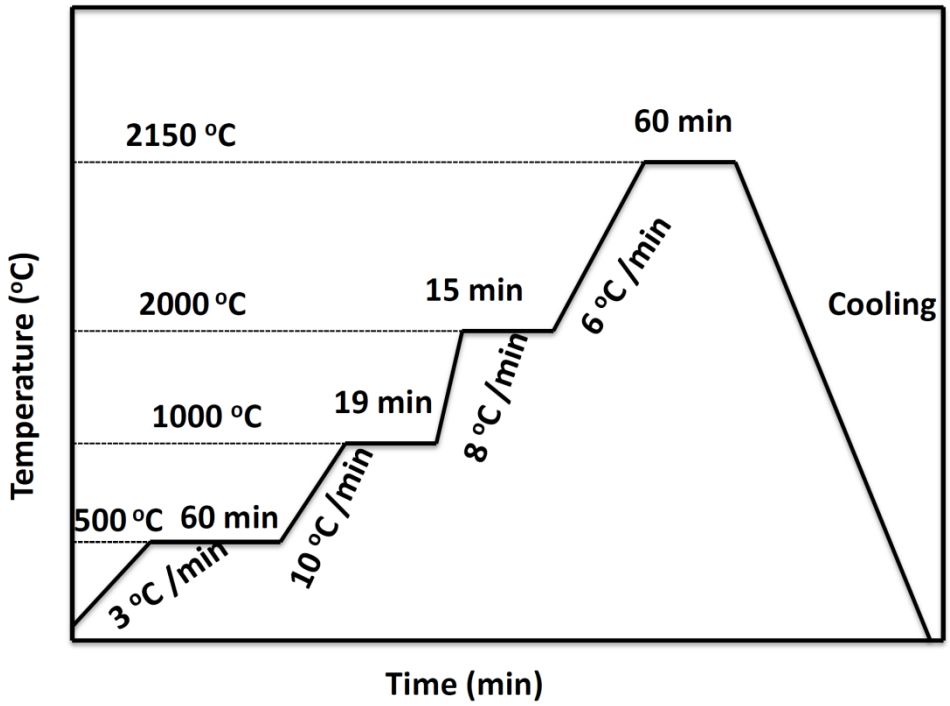

Figure 3.8: Pressureless sintering cycle.

3.5.1 *Fabrication of SiC hybrid composite tube through liquid silicon infiltration (LSI) and Chemical vapour deposition (CVD) techniques*

As a primary step of the process, a 2D conventional braiding of 8H satin of high strength carbon fibers (HSC), quadriaxial form of non-crimp carbon fabric NCF, and 8H satin form of spun yarn graphitized (SYG) fabric (using weaving machine) were produced on the in-house fabricated SiC (CNFs) composite tubes and the specifications of the fabric used are given in Table 3.1. The

process to produce the SiC (CNFs) composite tube is mentioned in previous section. The volume fraction of carbon fibers or fabric was maintained as 60 % [9]. The thickness of the fabric braiding was measured to be 8-9 cm with different types of braiding patterns as shown in Figure 3.9(a).

The schematic diagram of the fabrication process for CVD SiC-coated hybrid composite tubes is shown in Figure 3.10. The raw materials used for the processing of the composite tubes along with their specifications are shown in Table 3.1. As-received carbon fabric containing the active groups on the surface forms a strong bond with the polymer preform and avoids further interaction with liquid Si.

In the second step, processing and curing of porous preform on C_f braiding was carried out. The liquid Coal-tar pitch was used as carbon source and forms a layer during carbonization process, which produces porous C_f/C preform. Initially, the C_f braiding was impregnated with liquid coal-tar pitch at 280 ^oC for 2 hr and carbonized at 950 ^oC to form porous C_f/C composite. The porosity of the C_f/C composite was further increased by the graphitization process carried out at 2200 ^oC for 48 hrs. Graphitization facilitates interlocking of the elongated cracks in the porous C_f/C matrix, which interact with silicon and influence the infiltration process thereby enhancing SiC formation [10].

The third step, known as LSI process, consists of infiltration of the molten silicon into the cured porous C_f/C braided SiC (CNFs) composite tubes. The infiltration process is carried out with the help of capillary forces of liquid silicon under vacuum conditions to prevent oxidation and to obtain effective silicon infiltration. In the present study, LSI was carried out at 1700 ^oC for 1 hr by placing the tubes inside silicon lumps with an average size of 10 -20 mm in a graphite crucible in vacuum. During infiltration, silicon reacts with the carbon present in the preform and forms SiC matrix. The density of LSI C_f/C-SiC composites of differently braided carbon fabric was calculated.

Finally, the tubes were subjected to CVD coating. Prior to CVD coating, the Si infiltrated tubes were surface-smoothened by grinding operation for better adherence of coating. The ground hybrid composite tubes are shown in Figure 3.9(c).

The sintered SiC-CNFs composite tubes and liquid silicon infiltrated hybrid tubes were further densified by depositing a uniform 500-800 micron thick coating of SiC on the surface by CVD. The CVD was carried out at 1400 ^{o}C, maintaining 150-200 torricelli pressure with a deposition rate of 100 µm/hr using methyl-trichlorosilane (MTS) as a precursor in excess of hydrogen and argon as the carrier gas in a reactor as per the following reaction:

$$CH_3SiCl_3 \xrightarrow{H_2} SiC + 3\,HCl \qquad \text{where MTS: } H_2 \text{ is 1:1 mole ratio} \qquad \text{Equation (3.2)}$$

CVD-SiC coating was carried out at 1400 ^{o}C under 150 torr vacuum. A uniformly dense SiC coating with ~ 500-800 µm thick layer was formed on the composite and hybrid composite tubes. CVD SiC coated hybrid composite tubes and the coated layers are shown in Figure 3.9 (d) and (e) respectively.

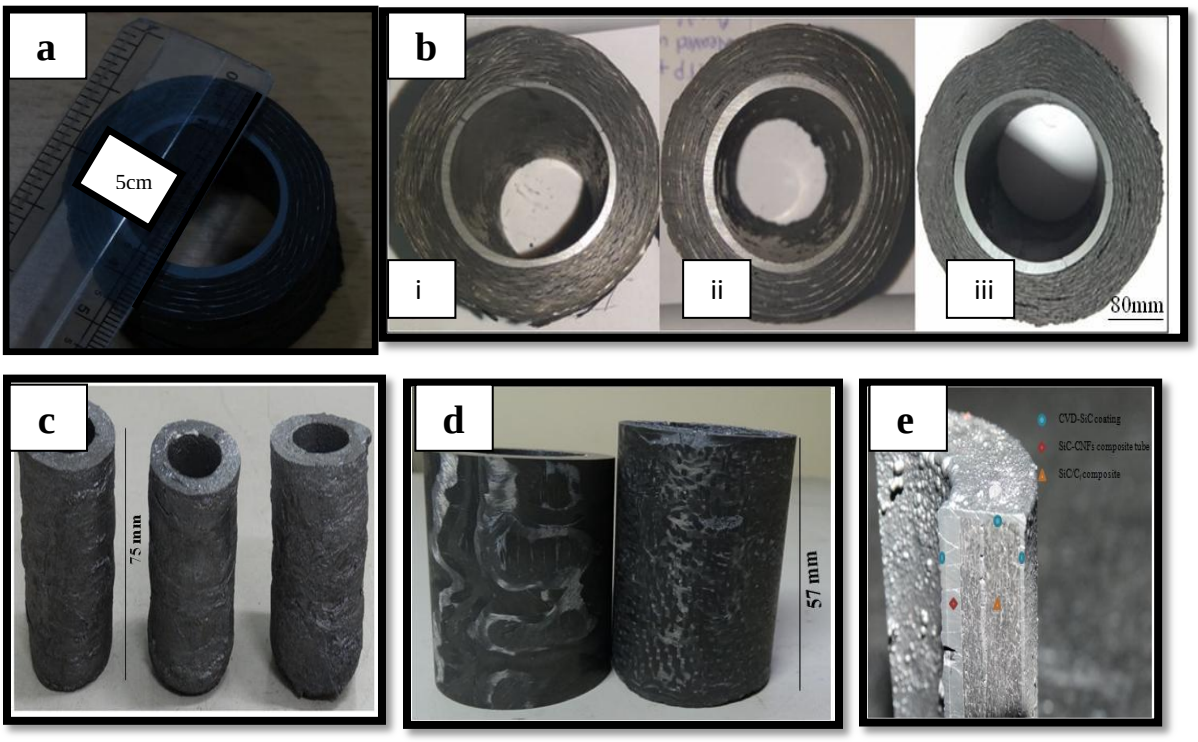

Figure 3.9: (a) C_f braided SiC/CNFs composite tubes before Si-infiltration (b) digital camera images of SiC (CNFs) tubes with different braided patterns i.e. i) HSC ii) SYG iii) NCF (c) C_f

braided SiC/CNFs composite tubes after Si-infiltration (d) grounded Samples for CVD SiC coating e) cross section of CVD SiC coated samples.

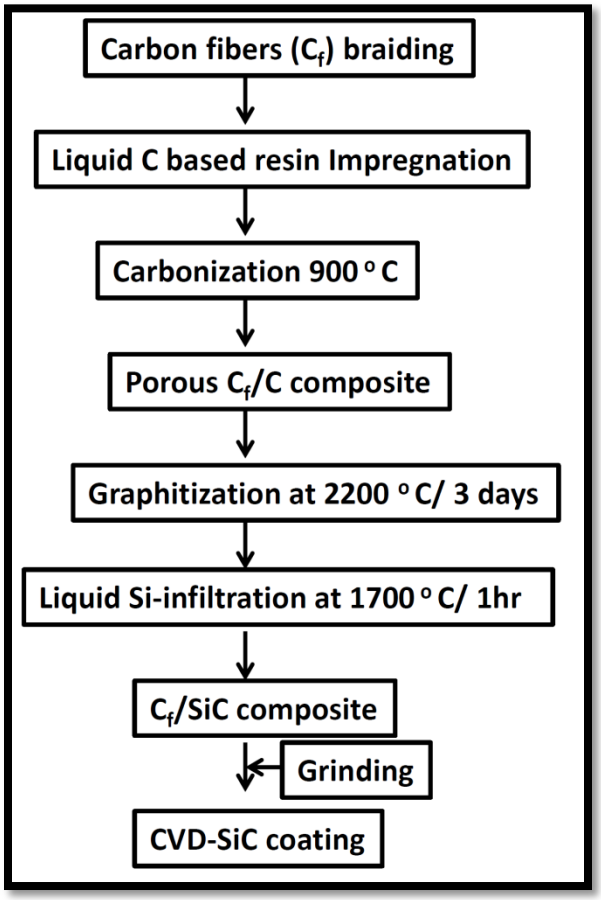

Figure 3.10: Flow chart of liquid silicon infiltration of hybrid composite tubes.

3.6 Materials characterization

3.6.1 *X-ray diffraction (XRD)*

The crystal structure analysis of raw SiC powders, secondary phase materials (raw and surface treated), sintered and post sintered samples were analyzed using high intensity multi-functional 2D X-ray diffraction system, shown in Figure 3.11. The RAPID-II-D/MAX (RIGAKU corp., Japan) was used to scan the samples under Cu-Kα radiation with the wavelength of 1.5406 Å and at an angle (2Θ) range from 20-90^{o}. The results obtained were analyzed and compared against the patterns found in international centre for diffraction date (ICDD) using crystal impact match software.

The structural and quantitative phase analysis of XRD data obtained from samples was carried out by Rietveld's refinement using MAUD software [11]. Rietveld's refinement is a software approach which is widely accepted to be an exceptionally valuable method for structural analysis of nearly all classes of crystalline materials. The various structural properties of the sample can be obtained including: accurate quantitative phase information, crystallite size, site occupancy factors etc. The refinement of structural information such as lattice parameters, atomic position, peak position, background parameters has been carried out while considering the standard reference crystal structure information (CIF). The symmetry and the space group considered for the refinement along with the refined structural parameters such as goodness of fit factor (χ^2) and R-factors: weighted residual error (R_{wp}), expected (R_{exp}), background (R_{wnb}) and Bragg (R_b). The values of χ^2 and R_{wp} acceptable for the effective refinement are very low ($\chi^2 < 2$, Rwp < 15). The refinement was carried out at a maximum number of cycles (21 cycles) until it matches with the standard reference peak positions.

Figure 3.11: X-ray diffractometer set-up.

3.6.2 *Zeta potential and UV-Vis spectroscopy analysis for dispersion stability of CNFs in the matrix*

In processing of nanomaterials reinforced composites, characterization of nanomaterials is a crucial step in studying the properties of the composite component. The nanomaterials (carbon nanotubes, carbon nanofibers, nanoparticles etc.,) have a tendency to form agglomerates in an aqueous media due to their inert surface properties, as discussed in section 3.4. In order to produce homogeneous dispersion of reinforcement in the matrix, it is important to study the dispersion stability of the same quantitatively. In the present study, to produce homogenous dispersion of CNFs in the SiC matrix, the standardization of surface treatment process by the titration of acid's ratio and surfactant quantity has been optimized with the help of i) UV-Vis spectroscopy (Model: Carry 5000, Varian Inc., US) in the wavelength range: 190-3300 /cm,

maximum , scan rate of 200 (UV-Vis) and 8000 (NIR) ii) Zeta potential analyzer (Model: Zeta-Meter Inc, Zeta-Meter 3.0+ Unit-ZM3-577, USA) at a potential range from -125 mV to + 125 mV, pH range: 2.5-11 and minimum of 20 ml sample volume.

Zeta potential analyzer was used to optimize acid concentration for CNFs surface treatment and concentration of surfactant (SDS) for homogenous dispersion in aqueous medium by analyzing the dispersion stability of CNFs. The dispersibility of fibers was measured by taking a dilute solution of 0.01 vol % in distilled water and the results obtained i.e zeta potential plots were compared.

The UV spectroscopy was employed to study the dispersion stability of CNFs in the wavelength range of 200-800 nm (Figure 3.12). The resulting spectrum was plotted with wavelength against the absorption. The absorption spectrums of the compounds were distinguished based on the specific wavelength of the dispersed CNFs in the solution by following Beer-Lambert law, as given in equation 3.3. In general, quality of dispersion was analyzed by the rate of absorption i.e more the absorbance, better the dispersion of CNTs or CNFs in aqueous media [12].

$$A = \log \frac{I_0}{I_t} \qquad \text{Equation (3.3)}$$

where A- absorbance, I_0- intensity of incident light, I_t- intensity of transmitted light.

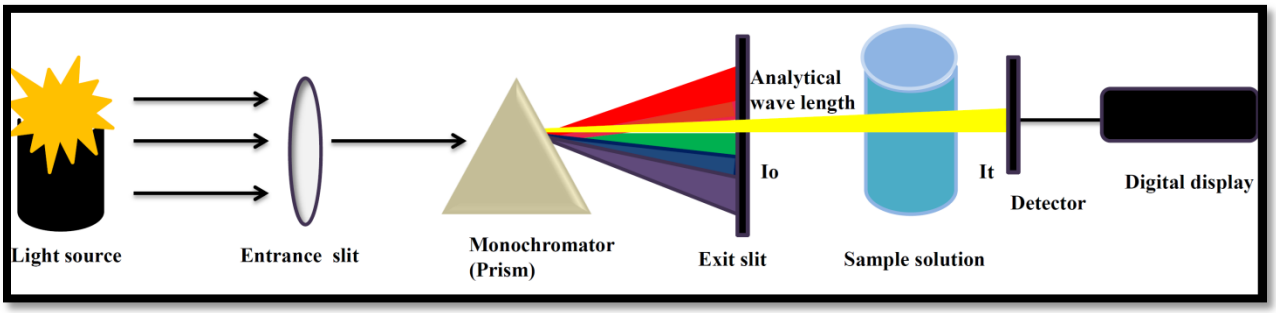

Figure 3.12: Schematic of UV-Vis spectroscopy mechanism.

3.6.3 *Laser diffraction analysis of the composite powders*

Particle size eanalysis is an important study in understanding the final property of a product and its appropriate application. The laser diffraction particle size analyzer provides the size measurement based on the variation in the intensity of light scattered or diffracted through a given angle from the particles to the incident laser beam. The as received SiC and spherical spray freeze granulated SiC-CNFs composite powder size analysis was carried out using laser diffraction technique (Model: MS3000, Malveren Instruments Ltd., UK) and the average size of granules was obtained from the plots i.e the plots of particle size against vol %.

3.6.4 *Fourier Transform Infrared Spectroscopy (FTIR)*

FTIR is a common laboratory spectroscopy instrument that deals with the infrared region of electromagnetic spectrum with the wave number ranging from 400-4000 cm^{-1}. The IR spectroscopy works based on the principle that the specific frequency of the IR radiation is absorbed by the molecules of the sample, which characterize the sample structure. FTIR is useful for several types of analysis, such as it can be employed to identify unknown materials, quality and consistency of samples, and provide quantitative results of components present in the mixture. In the current study, FTIR was employed (Model: Vertex 70; Bruker Optik GmbH, Germany) to analyze surface functionalities of as-received carbon fibers, acid treated CNFs and BN coated long carbon fibers at spectra resolution of 0.4 cm^{-1}. The picture of FTIR used for analysis if given in figure 3.13.

Figure 3.13: FT-IR instrument.

3.6.5 *Scanning Electron Microscope (SEM)*

SEM is one of the versatile instruments used to examine the surface, microstructure, composition and crystallographic analysis of samples (organic or inorganic) in nanometer to micrometer scale. It has been used in a wide range of medical fields and produces topographic image in the magnification range of 10x-10000x. The SEM produces images by scanning (raster scan pattern) the sample using a focused electron beam. When the electrons from the beam interact with the sample electrons produced various types of signals which contain the different types of information of the sample such as surface topography, composition and the crystallographic details. The types of signals produced by SEM are shown in Figure 3.14.

The microstructure, composition and phase analysis of secondary phase materials, sintered and post sintered samples were studied using field emission scanning electron microscope (FE-SEM) (Model: Gemini 5000). The elemental analysis and crystallographic studies were carried out with the help of the EDS and EBSD units attached with the FE-SEM equipment.

Prior to SEM analysis, the sample surface was polished to mirror finish. The sequence of the steps followed while sample preparation is as follows: The sintered and post sintered samples of

different dimensions were hot mounted for sample preparation. The flat-mounted samples were polished with fine-grit SiC paper (45-30 micron), followed by precise diamond cloth polishing (Buehler EcoMet® 4000, USA) (15 – 0.5 µm). Care was taken to avoid any deep scratches and damage of coating at each stage of polishing. As per the requirement of EBSD analysis, the samples were further polished using vibratory polishing (Buehler VibroMet® 2, USA) with colloidal silica (0.02 µm) for 5 hours.

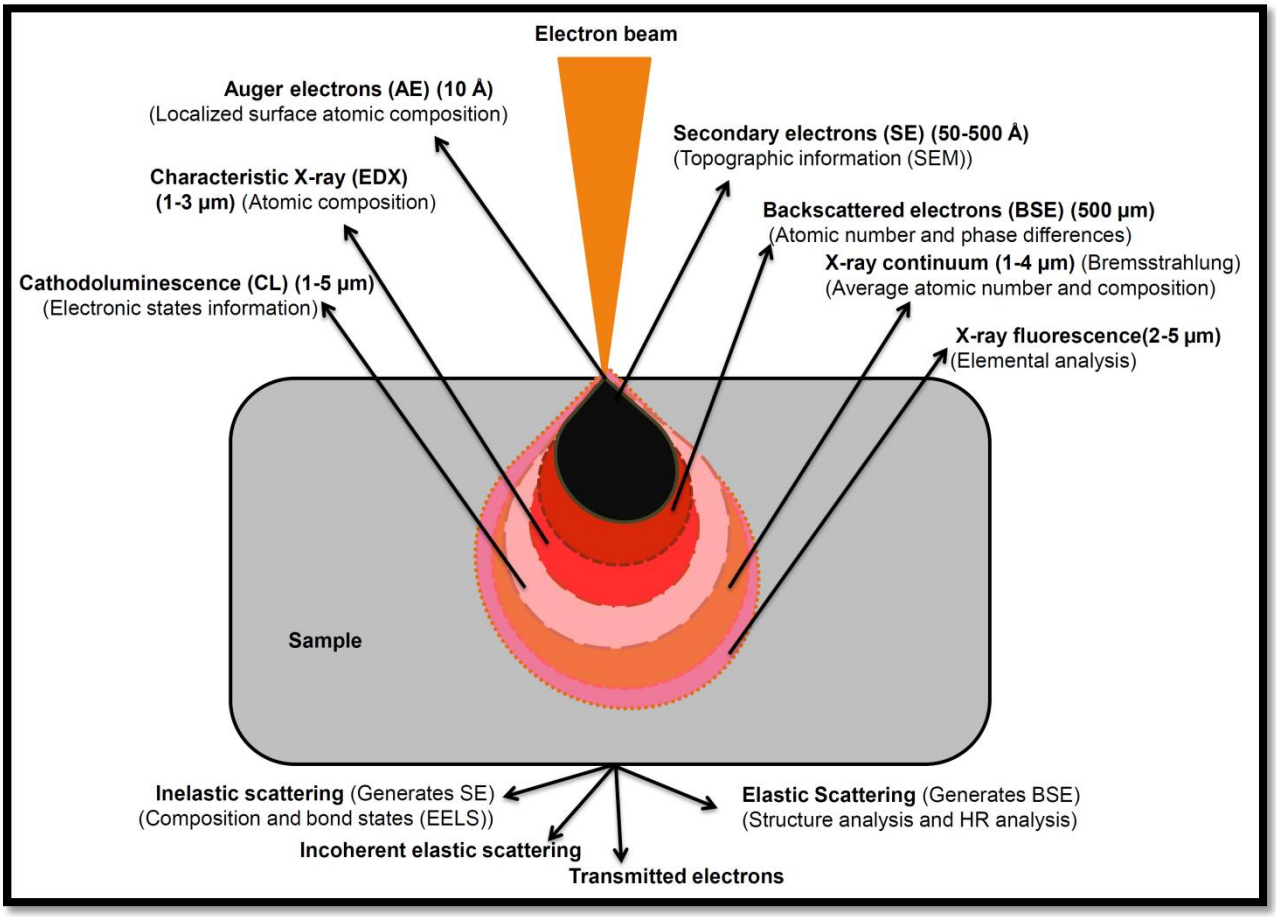

Figure 3.14: Illustration of SEM analysis and various types of signals emitted.

3.6.6 *Transmission electron microscope (TEM)*

The distribution of fibers and sintered SiC based composites samples was characterized by the transmission electron microscope (TEM) (Technai G^2, Netherland), operated at 200 kV (Figure 3.15). The EDS unit and electron energy loss spectroscopy setup were connected to TEM system. Hence, structural and chemical information of samples were obtained from TEM analysis at low and high resolutions (HR-TEM).

The sequential steps involved in TEM sample preparation were as follows:

i) As-sintered samples were cut into thin and disc shaped using ultrasonic disc cutter (Model: 601, Gatan Inc., USA) at slow speed.

ii) The discs were ground manually to nearly 150 µm.

iii) The surface of ground samples were dimpled by dimpler grinder (Model: 656, Gatan Inc., USA) to a thickness of about 30 µm.

iv) Samples were further polished with the precision ion polishing system (Model: PIPS, Gatan Inc., USA) at low kV for better electron transparency area.

Figure 3.15: TEM set-up.

3.7 Evaluation of properties

3.7.1 *Bulk density measurement*

The density of green compact, sintered and post sintered (CVD and LSI) samples was measured using Archimedes principle given in equation 3.4. The sintered and post sintered samples were cleaned with acetone before the measurement of mass. The dry mass measured samples were immersed in the deionized water and boiled for 2 hr from room temperature to 40 ^{o}C. The water was allowed to cool to room temperature and samples remained soaked in water (min. four hours) for better results. The samples were taken out, dabbed with cotton cloth to remove excess water and immediately the soaked mass was measured and the samples were suspended in water to measure the suspended weight.

$$\text{Bulk density} = \frac{\text{Dry mass (D) X Density of water}}{\text{Soaked mass(W)} - \text{Suspended mass(S)}} \times 100 \qquad \text{Equation (3.4)}$$

Principle: weight loss of the sample in water is equal to the weight of the equivalent volume of the water displaced by the sample.

3.7.2 *Mechanical properties*

3.7.2.1 *Vickers micro-indentation*

Average hardness and indentation fracture toughness values of the sample were evaluated using a Vickers micro-hardness tester (Wateruhl technische Mikroscopie GmbH & Co. KG, Model: UHL VMHT, Germany) under a load of 4.9 and 9.8 N (1 kgf). Indentation fracture toughness of the samples was calculated with an average of ten indents using Anstis' empirical equations 3.5 [13]. The indented surface of the sintered samples were polished to mirror finish without any surface scratches and cleaned ultrasonically before the testing.

$$K_{IC} = 0.016 * \left(\frac{E}{H}\right)^{\frac{1}{2}} * \left(\frac{F}{c^{\frac{3}{2}}}\right) \qquad \text{Equation (3.5)}$$

where

K_{IC} = fracture toughness (MPa $m^{1/2}$),

E = young's modulus (GPa),

H = Vickers hardness (GPa),

F = indentation load (N),

c = half crack length (m).

3.7.2.2 *Three-point bend test*

Strength was measured through 3-point bend test as per ASTM standards C1161-13 and samples with dimension $25^{L}x4^{W}x2^{T}$ mm^3 were made using the universal testing machine (UTM, INSTRON-4483, UK) under the 0.5 mm/min of cross head speed and a span length of 20 mm.

3.7.2.3 *Nano-indentation*

In this study, an iNano® nanoindenter (Nanomechanics, INC., Oak Ridge, USA) equipped with a pyramidal Berkovich (three-faced) diamond tip indenter was used for the analysis, as shown in Figure 3.16. The geometrical inconsistency of the diamond indenter tip was calibrated with fused silica before the measurement. Continuous stiffness measurement (CSM) test was carried out as a function of indentation depth (maximum 200 nm) up to a maximum load 50 mN for mechanical properties measurement (15 x 15 indents with 10 μm apart). The average hardness and the elastic modulus of the samples were measured continuously throughout the indentation. The large indentation load and indent spacing of conventional nano indentation or CSM make it difficult to measure the properties of individual phases present in the matrix such as secondary phase, agglomerates or pores, etc. On the other hand, high-speed nano indentation mapping was conducted at a maximum load of 20 mN in 150 x150 μm^2 area with 10000 indents (100 x 100), with a spacing of 1.5 μm apart from one another. Hence, hardness and the elastic modulus values of individual phases from the maps can be measured and correlated with the microstructure. All the averaged test results of the samples were measured and compared with one another [14–16]. The sample preparation for high-speed nano-indentation mapping is very critical as the nano range tip is used for indentation. The samples were flat mounted as per the nano-indenter system's stage requirement and evenly polished without any deep scratches. The procedure followed was similar to EBSD sample preparation.

.

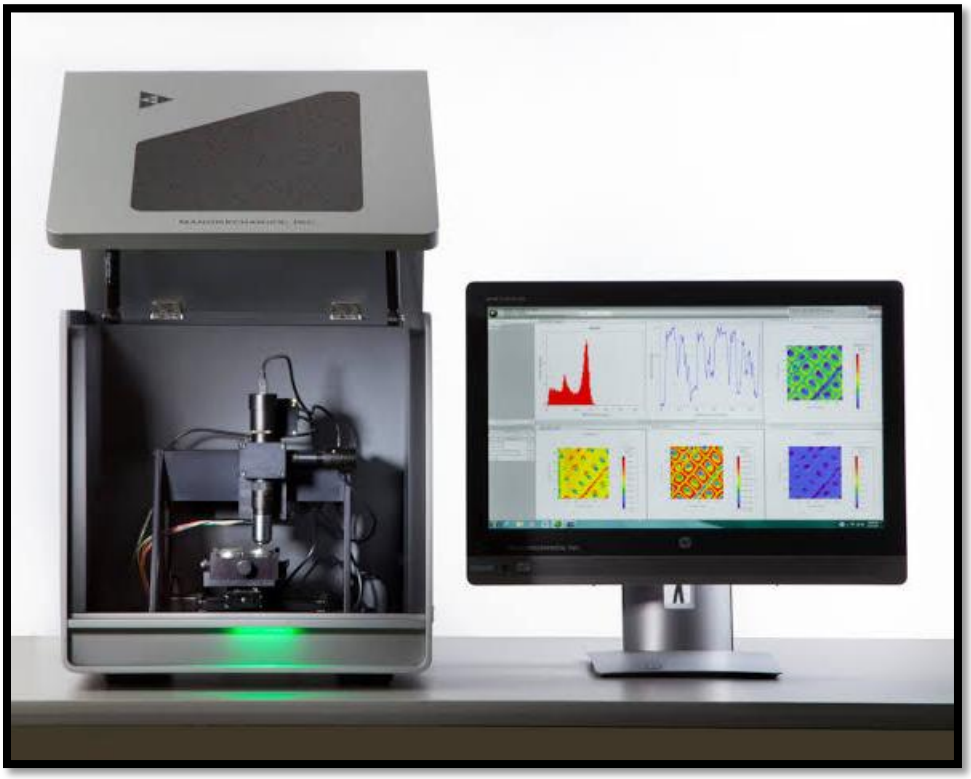

Figure 3.16: Advanced high-speed nanoindentation set-up.

3.7.3 Thermal Properties

3.7.3.1 ***Thermal conductivity*** Thermal conductivities (K) of the composites were calculated with DSC (STA 449 Jupiter- Netzsch GmbH, Germany) by Laser flash technique up to 1000 ^{o}C. The conductivity was calculated using equation (3.6), given below:

$K = \alpha \rho C_v$ where Equation (3.6)

α - thermal diffusivity, ρ- density and C_v - specific heat.

3.7.3.2 ***Thermo gravimetric analysis*** The oxidation study of the composites samples was carried out by thermogravimetric analysis (TGA) (STA 449 F3; NETZSCH, Germany) in the ambient air. A constant heating rate of 10 ^{o}C/min and 80 ml/min oxygen gas flow rate were maintained from the beginning (room temperature) till the experiment was completed at 1450 ^{o}C in oxygen or air (~ atmospheric pressure). The sample of dimensions 4 X 4 X 3 mm^3 was prepared using slow speed iso-Met cutting machine (isoMet^{TM} Low Speed Saw, Buehler, USA).

The weight (< 200 mg) and dimensions (< 6 X 6 X 6 mm^3) of the samples was maintained according to the sample holder (pure alumina crucible) design in TGA setup. The samples were cleaned in an ultrasonic bath and dried at 100 ^oC before testing. Weight changes in the samples with respect to the temperatures were recorded by an automated weighing balance connected with the crucible. Considering the statistical significance of the analysis, the average of a total of five samples were taken for the oxidation analysis as well as for other property measurements.

The residual mass or weight change (Δm) of the samples after the TG test was calculated from the following equation 3.7:

$$\Delta m = \frac{m_o - m}{m_o} X\ 100\%$$

Equation (3.7)

Where m_o: initial mass, m: mass after the test [17].

3.8 References:

[1] Mubina Shaik, Asit Kumar Khanra, and Bhaskar Prasad Saha: *Mater. Chem. Phys.*, 2018, vol. 220, pp. 225–32.

[2] Yang Kun, Y I Zili, Jing Qingfeng, Y U E Renliang, Jiang Wei, and L I N Daohui: 2013, vol. 58, pp. 2082–90.

[3] Jing Zhang and Lian Gao: 2007, vol. 61, pp. 3571–74.

[4] Yunhua Shi, Lingling Ren, Dianqing Li, Huifang Gao, and Bing Yang: 2013, vol. 2013, pp. 6–12.

[5] M. F. Islam, E. Rojas, D. M. Bergey, A. T. Johnson, and A. G. Yodh: *Nano Lett.*, 2003, vol. 3, pp. 269–73.

[6] Jianggao Liu, Shubin Wang, Pengyang Li, Mengjie Feng, and Xinwang Yang: *Surf. Coatings Technol.*, 2016, vol. 286, pp. 57–63.

[7] Wei Zhou, Peng Xiao, Yang Li, and Liang Zhou: *Ceram. Int.*, 2013, vol. 39, pp. 6569–76.

[8] P R Soni: *Handbook on Mechanical Alloying: Fundamentals and Applications*, Cambridge Int Science Publishing, 2000, pp. 1–200.

[9] Chunhong Ma, Lingjun Guo, Hejun Li, Wenlong Tan, Tao Duan, Ningkun Liu, and Maoyan Zhang: *Mater. Des.*, 2016, vol. 90, pp. 373–78.

[10] Guangpeng Jiang, Jianfeng Yang, Yongdong Xu, Jiqiang Gao, Junzhan Zhang, Litong Zhang, Laifei Cheng, and Jianjun Lou: *Compos. Sci. Technol.*, 2008, vol. 68, pp. 2468–73.

[11] L Lutterotti, S Matthies, and H R Wenk: *IUCr Newsl. CPD*, 1999, vol. 21, pp. 14–15.

[12] Jidraph Njuguna, O Arda Vanli, and Richard Liang: *Hindawi Publishing Corporation*, 2015, pp. 1–12.

[13] Anstis GR, Chantikul P, Lawn BR, Marshall DB: *J. Ameri. Ceram. Soc.*, 1981, vol. 64, pp. 533–538.

[14] Tobias Beirau, Warren C. Oliver, Claudia E. Reissner, William D. Nix, Herbert Pöllmann, and Rodney C. Ewing: *Appl. Phys. Lett.*, 2019, vol. 115, pp. 1–6.

[15] A. Bolshakov and G. M. Pharr: *J. Mater. Res.*, 1998, vol. 13, pp. 1049–58.

[16] G. M. Pharr: *Mater. Sci. Eng. A*, 1998, vol. 253, pp. 151–59.

[17] T. C. Vaimakis, *Thermogravimetry (TG) or thermogravimetric analysis (TGA)*, Chemistry department, Univeristy of Ioannina, Greece, 2013.

CHAPTER 4

Optimization of processing parameters and fabrication of CVD coated SiC-CNFs thin composite tubes using Taguchi statistical analysis

4.0 Introduction

This chapter deals with the optimization of material properties of CNFs composite tubes through Taguchi experimental design method to optimize processing parameters such as sintering temperature, heating rate and holding time for different CNFs compositions. Further, experiments were designed at the optimized processing conditions to evaluate the effect of particle size of SiC and CNFs loading on the properties of CNFs composites by choosing an L_9 (3^3) orthogonal array of design. The experimental results i.e. performance parameters were analyzed by Taguchi optimization method and microstructure analysis. The effect of variables on the properties of the composites were studied from the signal to noise ratio (S/N), analysis of variance (ANOVA), and interaction plots. At optimized conditions of processing parameters reported by Taguchi analysis, the fabrication and characterization of CVD coated CNFs thin composite tubes were also discussed. The impact of surface treatment of CNFs and CVD SiC coating on the properties of SiC composite tubes were also analyzed.

4.1 Results and Discussion

4.1.1 Taguchi analysis of the CNFs composite properties for anticipation of the optimal experimental condition by

4.1.1.1 *S/N ratio analysis of CNFs composites properties- density, hardness and fracture toughness*

The S/N ratio of CNFs composites properties i.e, average values of density, hardness and fracture toughness were calculated using larger is better criterion though Equation 4.1 as given in experimental section. Based on the S/N ratio difference obtained from Table 4.1, the rank of the variables (A, B, C, D) was calculated and given in the S/N ratio response (Tables 4.2 and 4.3) of its properties. From the S/N ratio value and ranks from the properties response Tables 4.1 and 4.2, it was observed that factor A has major influence on optimizing density and hardness. The main effect plots of density and hardness of CNFs composites reveals that factors A and C were exercising a combined influence on optimizing the density, whereas factors A and B were primarily influencing the hardness, as depicted in Figure 4.1(a & b) respectively. The SEM images of sintered SiC composites at 0-1 wt % CNFs variation in Figure 4.1(c & d) respectively, show packed grain structures, which provide supporting evidence for optimum density of

particular processing conditions of variables as mentioned above. The microstructure has few closed pores with CNFs dispersion (marked with arrows).

The S/N ratio and response Tables 4.1 and 4.3 shows that factor D has greater impact on fracture toughness of CNFs composite than other factors , which was also apparent based on the main effect plot given in Figure 4.2(a). It was observed that as CNFs wt % increases from 0-3 wt %, the increase in non-homogeneous dispersion of CNFs leads to the formation of CNFs bundling or agglomerates, as evident from Figure 4.1(c & d) and Figure 4.2(b).

Table 4.1: Experimental layout along with and the S/N ratio CNFs composites average ρ (g/cc), Hv (GPa) and F.T (MPa $m^{1/2}$).

Sintering temperature (^oC) (A)	**Heating rate (^oC/min) (B)**	**Holding time (hour) (C)**	**CNFs Composition (wt %) (D)**	**Avg. ρ g/cc**	**S/N ratio (Density)**	**Avg. H_v (GPa)**	**S/N ratio (Hardness)**	**Avg. F.T (MPam $^{1/2}$)**	**S/N ratio (Fracture toughness)**
2125	6	1	0	2.91	9.6289	22.8	26.6891	3.33	12.4856
2125	8	2	1	3.03	9.7992	21.6	27.2722	4.21	11.4806
2125	10	3	2	3.09	9.9662	23.1	28.3660	3.75	13.6067
2150	6	2	2	3.15	10.1301	26.2	27.7833	4.79	11.5268
2150	8	3	0	3.21	9.9109	24.5	28.4649	3.77	13.7684
2150	10	1	1	3.13	10.0212	26.5	27.8187	4.88	14.1854
2175	6	3	1	3.17	9.8831	24.6	27.0437	5.12	11.9539
2175	8	1	2	3.12	9.9662	22.5	28.3991	3.96	11.4574
2175	10	2	0	3.15	9.6289	26.3	26.6891	3.74	12.4856

Table 4.2: Response table of S/N ratio (Larger is better) for a) density b) hardness.

a Level	Density				b Hardness			
	Sintering temp (^{o}C) (A)	Heating rate (^{o}C/min) (B)	Holding time (hour) (C)	CNFs Composition (wt %) (D)	Sintering temp (^{o}C) (A)	Heating rate (^{o}C/min) (B)	Holding time (hr) (C)	CNFs Composition (wt %) (D)
1	9.569	9.755	9.691	9.791	27.04	27.78	27.56	27.78
2	10.002	9.881	9.854	9.854	28.20	27.17	27.82	27.66
3	9.957	9.892	9.983	9.883	27.75	28.05	27.62	27.56
Delta	0.434	0.137	0.293	0.091	1.16	0.87	0.26	0.22
Rank	1	3	2	4	1	2	3	4

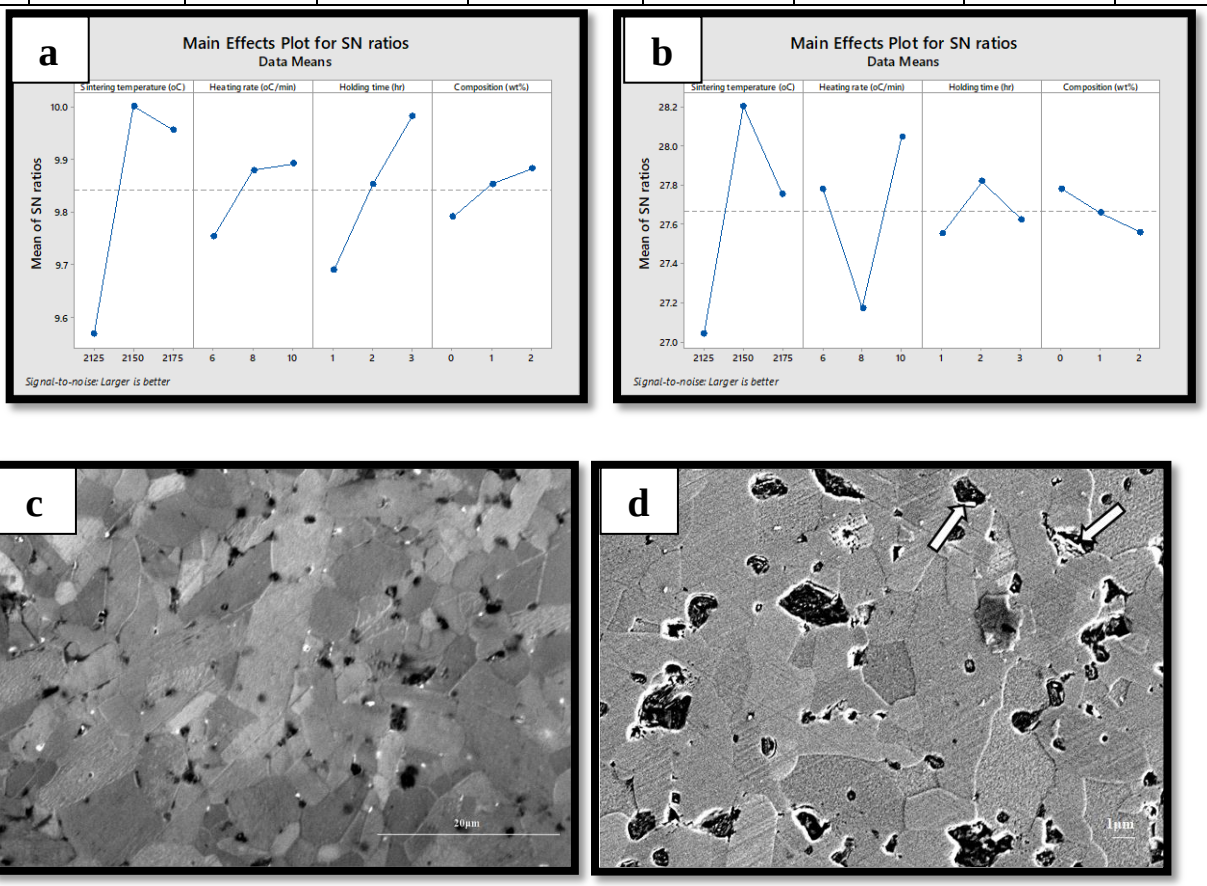

Figure 4.1: a) Main effect plot for S/N ratio in density b) Main effect plot for S/N ratio in hardness; Scanning electron microscope (SEM) image of c) monolithic SiC d) 1 wt % CNFs composites.

Table 4.3: Response table of S/N ratio (Larger is better) for fracture toughness of CNFs composites.

Level	Sintering temperature (^{o}C) (A)	Heating rate (^{o}C/min) (B)	Holding time (hour) (C)	CNFs Composition (wt %) (D)
1	11.47	12.75	12.06	11.14
2	12.97	11.99	12.52	13.48
3	12.53	12.24	12.40	12.35
Delta	1.50	0.76	0.46	2.34
Rank	2	3	4	1

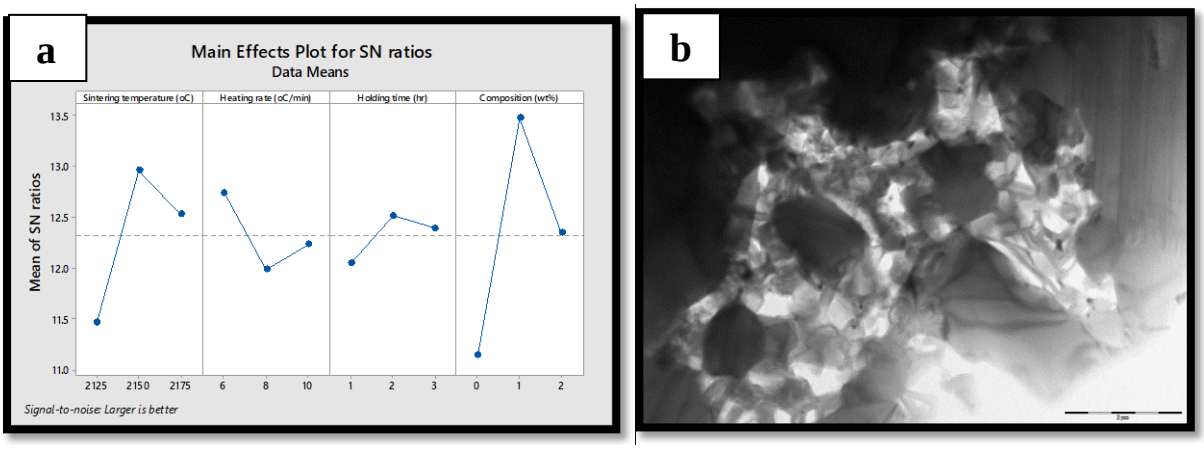

Figure 4.2: a) Main effect plot for S/N ratio in fracture toughness b) TEM image of CNFs distribution in 2 wt % CNFs composite.

4.1.1.2 *Analysis of variance of density, hardness and fracture toughness*

ANOVA helps to study the contribution of each factor for attaining the optimum process outcome. ANOVA helps in analyzing the influence of individual factors on total variance. In ANOVA table, DF is defined as degree of freedom which provides detailed information of the factors used in analysis. Total DF was determined based on the total number of experimental observations. Adj SS quantifies the amount of variation in the response data explained by each term in the model. Adj MS measures the amount of variation of a factor, regardless of order in which they are entered. Large F-value was used to determine the statistical significance of the term or factor

and its association with the response. P is probability that measures the significance of the term further. $P \leq 0.05$ is significance level.

The ANOVA response tables of density, hardness and fracture toughness report that the first two large Adj MS value and lowest P-values (< 0.05) were observed to increase in case of A & C, A & B, D & A respectively shown in tables (4.4, 4.5 and 4.6).

Table 4.4: ANOVA analysis table for density.

Factors	**DF**	**Adj SS**	**Adj MS**	**F-Value**	**P-Value**
Sintering temperature (^{o}C) (A)	2	0.042467	0.021233	30.33	0.032
Heating rate (^{o}C/min) (B)	2	0.004067	0.002033	2.90	0.256
Holding time (hour) (C)	2	0.016067	0.008033	11.48	0.080
Error	2	0.001400	0.000700		
Total	8	0.064000			

Table 4.5: ANOVA table for hardness.

Factors	**DF**	**Adj SS**	**Adj MS**	**F-Value**	**P-Value**
Sintering temperature (^{o}C) (A)	2	15.9267	7.9633	29.49	0.033
Heating rate (^{o}C/min) (B)	2	9.2867	4.6433	17.20	0.055
Holding time (hour) (C)	2	1.0067	0.5033	1.86	0.349
Error	2	0.5400	0.2700		
Total	8	26.7600			

Table 4.6: ANOVA analysis table for fracture toughness.

Factors	DF	Adj SS	Adj MS	F-Value	P-Value
Sintering temperature (^{o}C) (A)	2	0.81642	0.40821	13.22	0.070
Heating rate (^{o}C/min) (B)	2	0.29242	0.14621	4.74	0.174
CNFs Composition (wt %) (D)	2	1.89296	0.94648	30.65	0.032
Error	2	0.06176	0.03088		
Total	8	3.06356			

4.1.1.3 *Anticipation of the optimal experimental condition of processing parameters w.r.t the properties by interaction plot*

Interaction plot helps in analyzing the effect of interaction between the two variables on the properties of CNFs composites, while the other two factors are fixed to the optimized level. The interaction between sintering temperature and heating rate has shown an increase in mean value of density till a certain heating rate, after which it goes down, as depicted in Figure 4.3(a).

The S/N ratio response tables and ANOVA response tables would aid us in understanding the individual and combined effects of factors that impact certain properties of CNFs composites. Interaction plots exhibited that density (ρ) continuously increased with A and C values from low to high, hardness (H_v) and fracture toughness (F.T) improved during the interaction of A and B, D and A respectively, up to maximum experimental temperature.

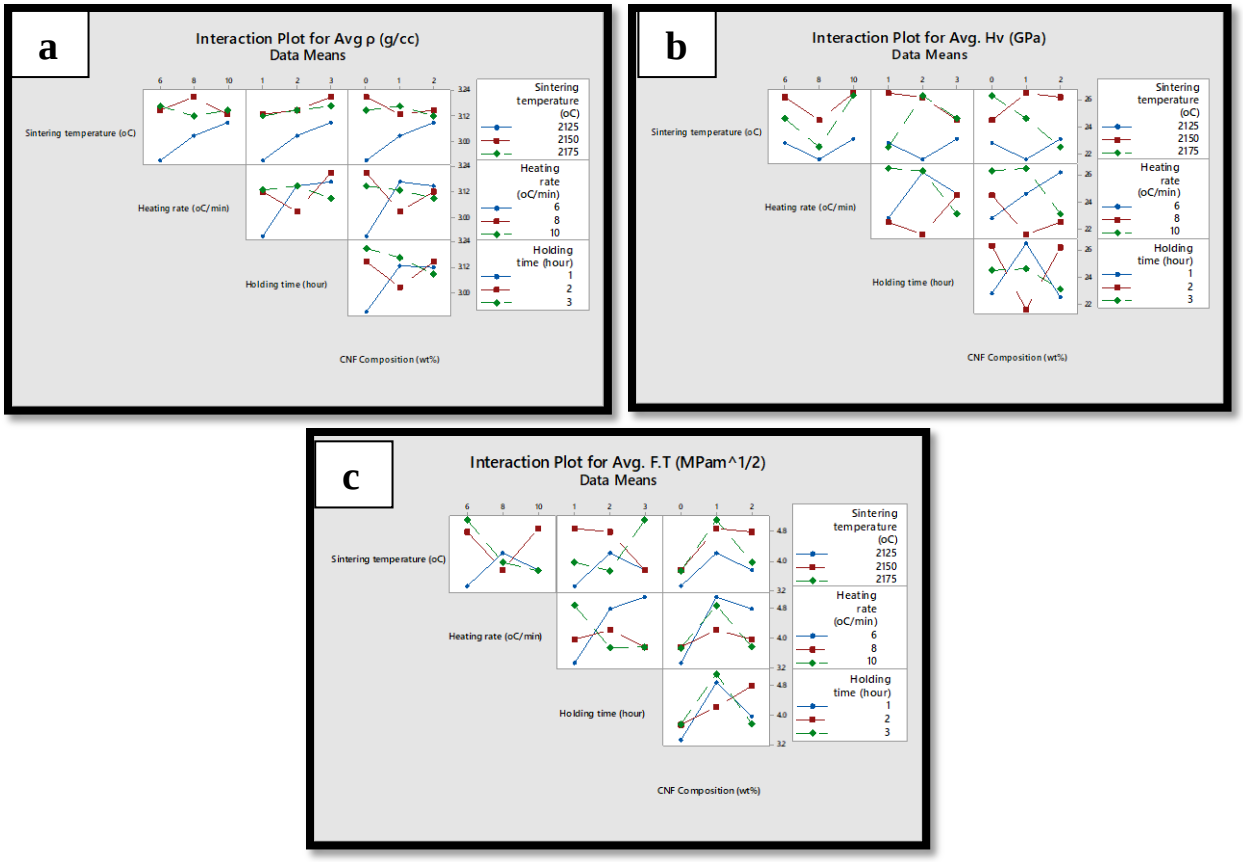

Figure 4.3: Interaction plot of a) density b) hardness c) fracture toughness with the parameters.

4.1.1.4 *Confirmation test*

To validate the experimental results and to evaluate the analysis, confirmation tests were conducted. At optimized condition of the previous analysis, experiments were designed and evaluated by choosing SiC powders of three different particle size and CNFs wt % as influencing factors using L_9 (3^2) array (experimental layout as given in section 3.2). The results are given in the Tables 7, 8, 9, which show that the results were comparable with previous analysis and that the particle size was the major determining parameter, which was directly proportional to properties of the composite.

Table 4.7: Confirmation test results.

Particle size	CNFs composition (wt %)	Relative Density (%)	Hardness (GPa)	Fracture toughness (MPa $m^{1/2}$)	S/N ratio
M-15 (0.6µm)	1	98.4	26.30	4.92	18.4507
M-15	2	97.5	23.53	4.17	17.0319
M-15	3	96.2	22.07	3.99	16.6438
M-25 (0.4 µm)	1	97.5	25.01	4.12	16.9453
M-25	2	96.6	23.24	3.89	16.4434
M-25	3	95.3	21.03	3.64	15.8589
Beta SiC (0.350 µm)	1	90.2	25.54	3.76	16.1745
Beta SiC (0.350 µm)	2	87.5	24.03	3.42	15.3581
Beta SiC (0.350 µm)	3	83.1	21.98	3.59	15.7509

Table 4.8: Response table of S/N ratio (Larger is better).

Level	Particle size	CNFs composition
1	17.38	17.19
2	16.42	16.28
3	15.76	16.08
Delta	1.61	1.11
Rank	1	2

Table 4.9: Analysis of Variance.

Source	DF	Adj SS	Adj MS	F-Value	P-Value
Particle size	5	1.50392	0.30078	14.58	0.026
Error	3	0.06190	0.02063		
Total	8	1.56582			

4.1.2 Processing and properties analysis of sintered and CVD coated CNFs thin composite tubes

The dense CVD SiC coated CNFs thin composite tubes were fabricated at optimized processing condition as obtained through Taguchi statistical analysis. In addition, to avoid entanglement or bundling during the dispersion, the CNFs were surface modified or acid treated at optimized titrations.

4.1.2.1 ***Dispersibility and stabilization of CNFs in the suspension for uniform distribution in the composite matrix***

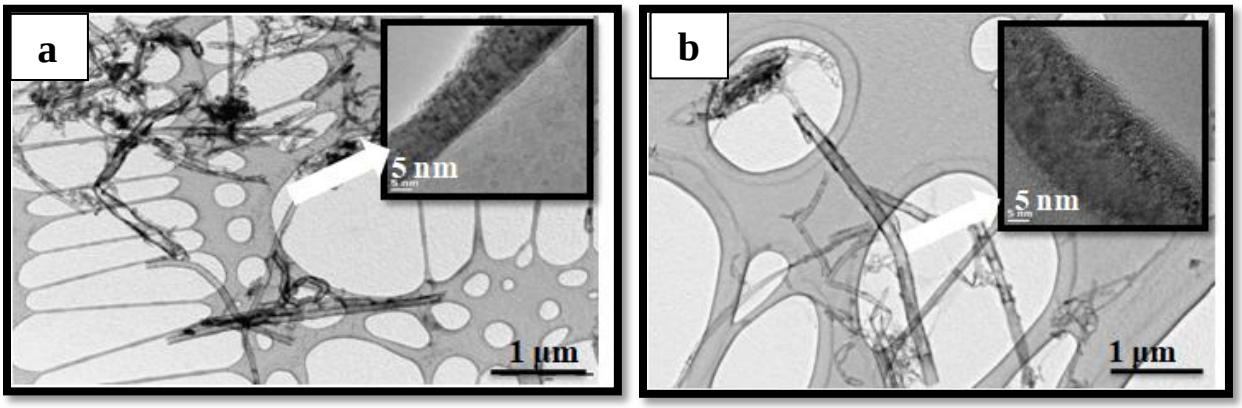

Figure 4.4: TEM images of a) bare b) acid treated CNFs.

Acid treatment, also known as chemical treatment, was carried to reduce hydrophobicity, inertness and impurity of as received CNFs or CNTs [1]. Further, the concentrated acids form oxygen-containing functional groups on the surface of the CNFs which help to reduce entanglements and improve dispersion of CNFs in the matrix. The TEM image of as received CNFs shows (Figure 4.4(a)) that the fibres were mostly bundled which got separated after acid treatment as shown in Figure 4.4(b). The acid treatment was conducted at elevated temperature involving only surface bonding with oxygen functional groups without changing any internal structure of CNFs. Hence, the crystallinity of CNFs remained intact even after acid treatment which was evident from XRD peak positions (Figure 4.5) and high resolution image as shown in Figure 4.4 (a & b). The XRD peaks corresponding to 26^{o}, 43^{o}, 45^{o} reflected from (002), (100), and (101) planes respectively, were identified as diffraction peak of graphite. The FTIR analysis of as received and surface treated CNFs is as shown in Figure 4.5 (b). Carbon materials usually show very weak IR response. In the FT-IR spectrum of the acid-treated CNFs the peaks which

are identified at 1515, 1682 and 3738 cm^{-1} corresponds to O-H stretching, and 2331, 3081 cm^{-1} corresponds to C-H stretching. As received CNFs have shown FTIR peaks at 1047, 1543 cm^{-1} which correspond to C-O and C-H stretching respectively.

The effect of acid treatment and surfactant on the dispersion of CNFs in aqueous media was analyzed at different titration conditions using Zeta Potential Analyzer. Average zeta potential of bare CNFs was 19.6 mV and surface modified CNFs treated with acids of 0.3 M & 0.5 M concentration was reported to be 35.1 mV & 55.4 mV respectively. Good dispersibility as indicated by high zeta potential value of acid treated CNFs in the matrix is shown in Figure 4.6.

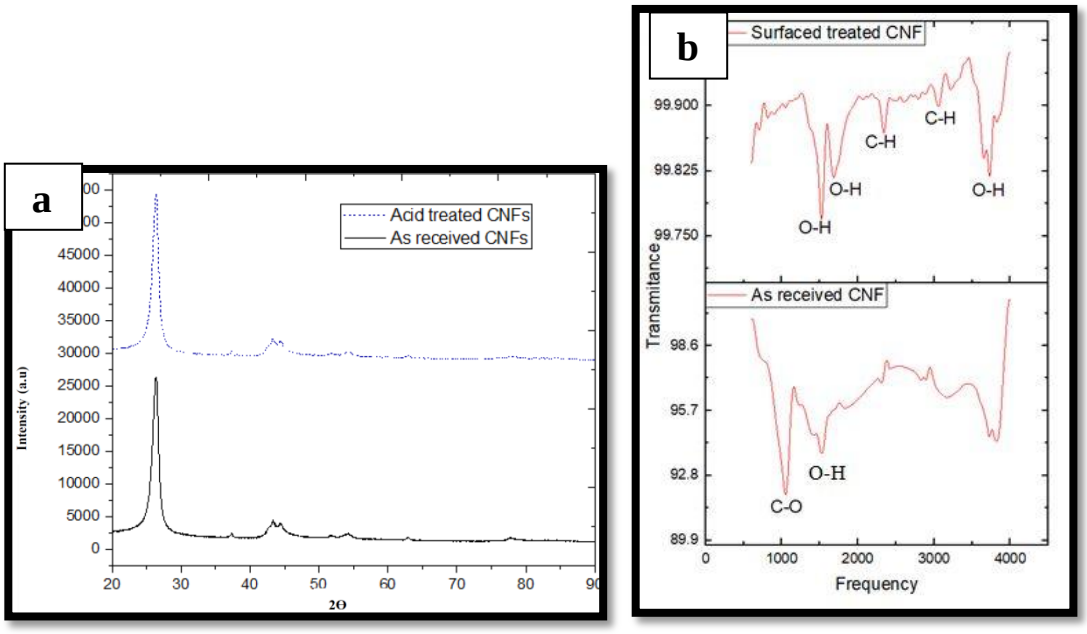

Figure 4.5: a) X-ray diffraction patterns and b) FTIR analysis of CNFs before and after treatment.

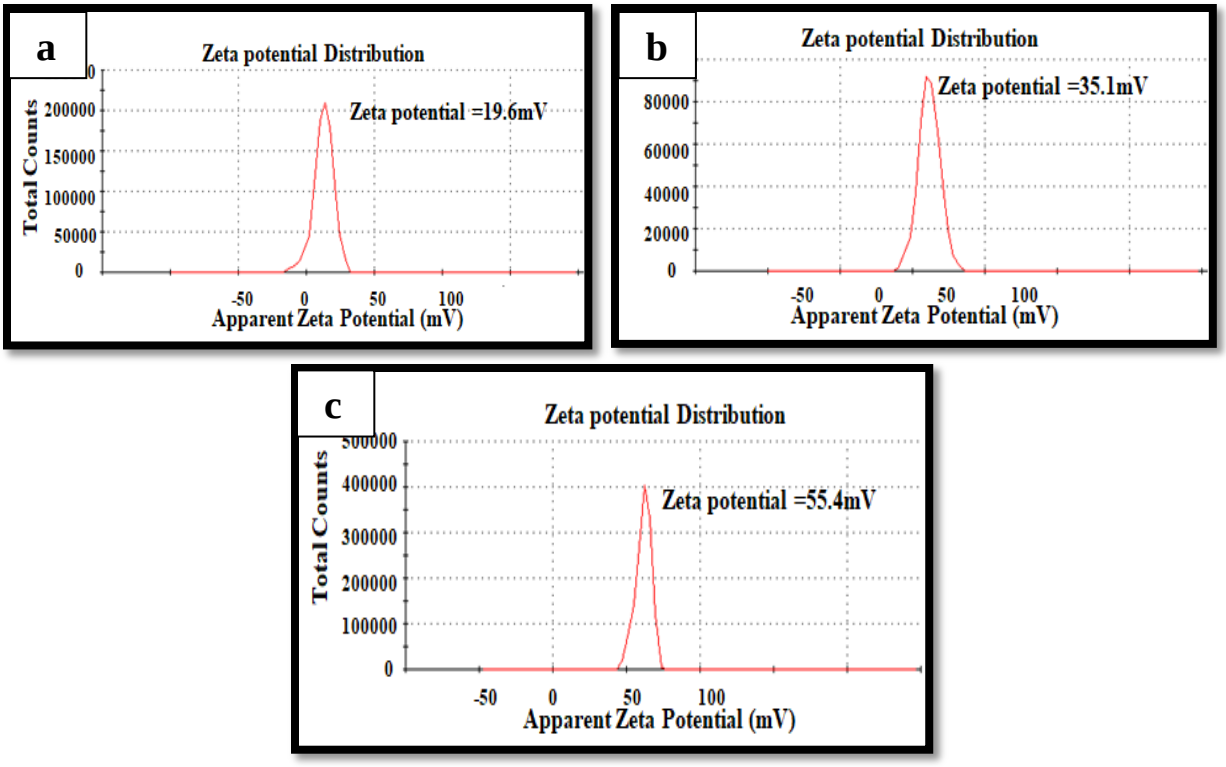

Figure 4.6: Apparent zeta potential of a) bare CNFs b) & c) acid treated CNFs at 0.3M and 0.5M respectively.

4.1.2.2 *Microstructure analysis of SiC and its composite samples*

Scanning electron microscopy images of polished SiC and its CNFs containing composites were shown in Figure 4.7 (a-d). The microstructures of both bare and fiber containing composites comprised equiaxed, elongated and platy grains. A few carbon-rich, non-stoichiometric SiC phase originating from sucrose was also observed in the matrix. The SEM image molothic SiC, in Figure 4.7 (a), shows a mixture of two morphologies i.e., elongated and equiaxed grain structures. In case of 1 wt % CNFs composite, more equiaxed grains were observed as shown in Figure 4.7(b), indicating that the grain growth was inhibited by fibers due to entrapment in the junctions of SiC grain boundaries (Figure 4.7(e)). SiC composites with more than 1 wt % CNFs content showed agglomerated regions. A representative microstructure of composites containing more than 1 wt % CNFs shows the presence of agglomerated regions which were marked with an arrow in Figure 4.7(c). Investigation of the fracture surface reveals the presence of toughening mechanisms like fiber pull-out and fiber bridging from the SiC-CNFs composite fracture surface, as may be seen from Figure 4.7(d), indicated by a circle and this was correlated to the improved

mechanical properties of the composite. TEM images of SiC-CNFs composite as depicted in Figure 4.7(e) show densely packed grain with CNFs entrapment (marked with arrow) at triple point junction of the grains.

EBSD studies on SiC-1 wt % CNFs composite also confirms the presence of equiaxed grains as shown in image quality map Figure 4.8(a). In EBSD grain boundary maps and table as shown in Figure 4.8(b), the grain boundaries were differentiated with colour coding with respect to the angles, where red coloured boundaries represent the sub-grain boundaries (1^o - 5^o), green denoting the small angle grain boundaries (5^o - 15^o) and blue is for high angle boundaries (15^o - 180^o). As SiC-1 wt % CNFs composite contain predominantly high angle grain boundaries with regular grain orientation, it is expected that the presence of dislocations or lattice defects are fewer , with minimal residual stress in SiC crystals [2].

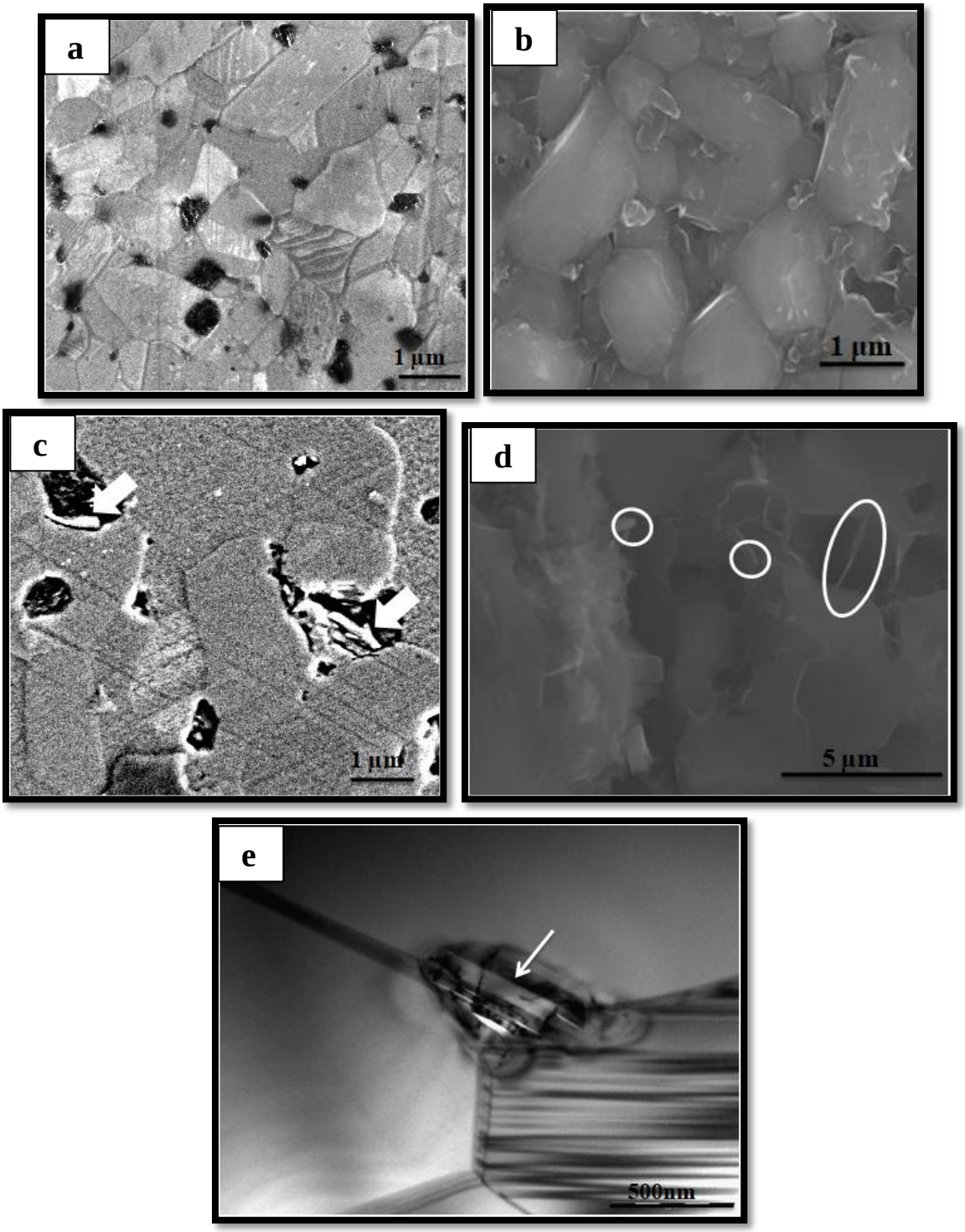

Figure 4.7: Field emission scanning electron micrographs (FE-SEM) of a) SiC bare b) SiC-1 wt % CNFs c) SiC-2 wt % CNFs d) fracture surface of SiC-CNFs composite e) TEM image of CNFs entrapment.

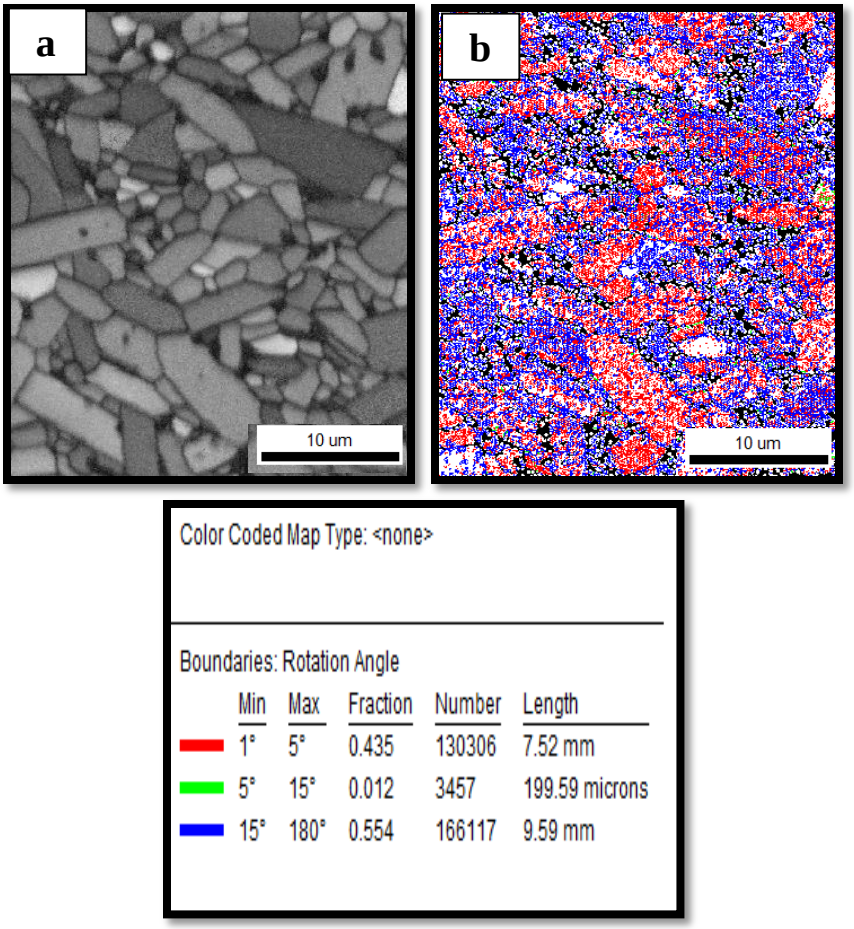

Figure 4.8: Electron backscatter diffraction (EBSD) of SiC-1 wt % CNFs a) image quality map b) grain boundary map with the boundaries table.

4.1.2.3 *Characterization & Micro-structural analysis of CVD-SiC coated tube*

In case of sintered SiC substrate, the XRD patterns correspond to the diffraction planes of intense peaks (102), (103), (104), (110), (202) with the diffraction angles 36.4^{o}, 38.2^{o}, 42.7^{o}, 60.1^{o} and 73.3^{o} respectively, indicating the presence of α-SiC with hexagonal crystal structure in Figure 4.9(a). The XRD pattern of CVD coated layer is also shown in Figure 4.9(b), indicating diffraction angles at 35.6^{o}, 41.3^{o}, 60.1^{o}, 72.1^{o} and 75.5^{o} respectively, corresponding to the diffraction planes of β-SiC such as (111), (200), (220), (311) and (222). The angle at nearly 29.4 ^{o} and ~ 33.7^{o} corresponds to graphitic carbon and 6H-SiC, respectively. Normally, CVD coated SiC deposits grow preferentially either in (111) or (220) plane, depending on the processing parameters [3]. In the present work, the deposits are preferentially oriented along (111) plane as shown in Figure 4.9(b). Considerable growth was also observed in (222) and (311) planes.

However, with varying processing parameters such as deposition temperature and H_2 / MTS ratio, the growth of deposits can preferentially be oriented in different planes.

From the SEM - EDS area mapping it is assumed that the stoichiometric SiC compositions at different regions of CVD coating confirming uniform coating which formed on the tube surface, as evident from Figure 4.9 (c, d) and Table in 4.9(d).

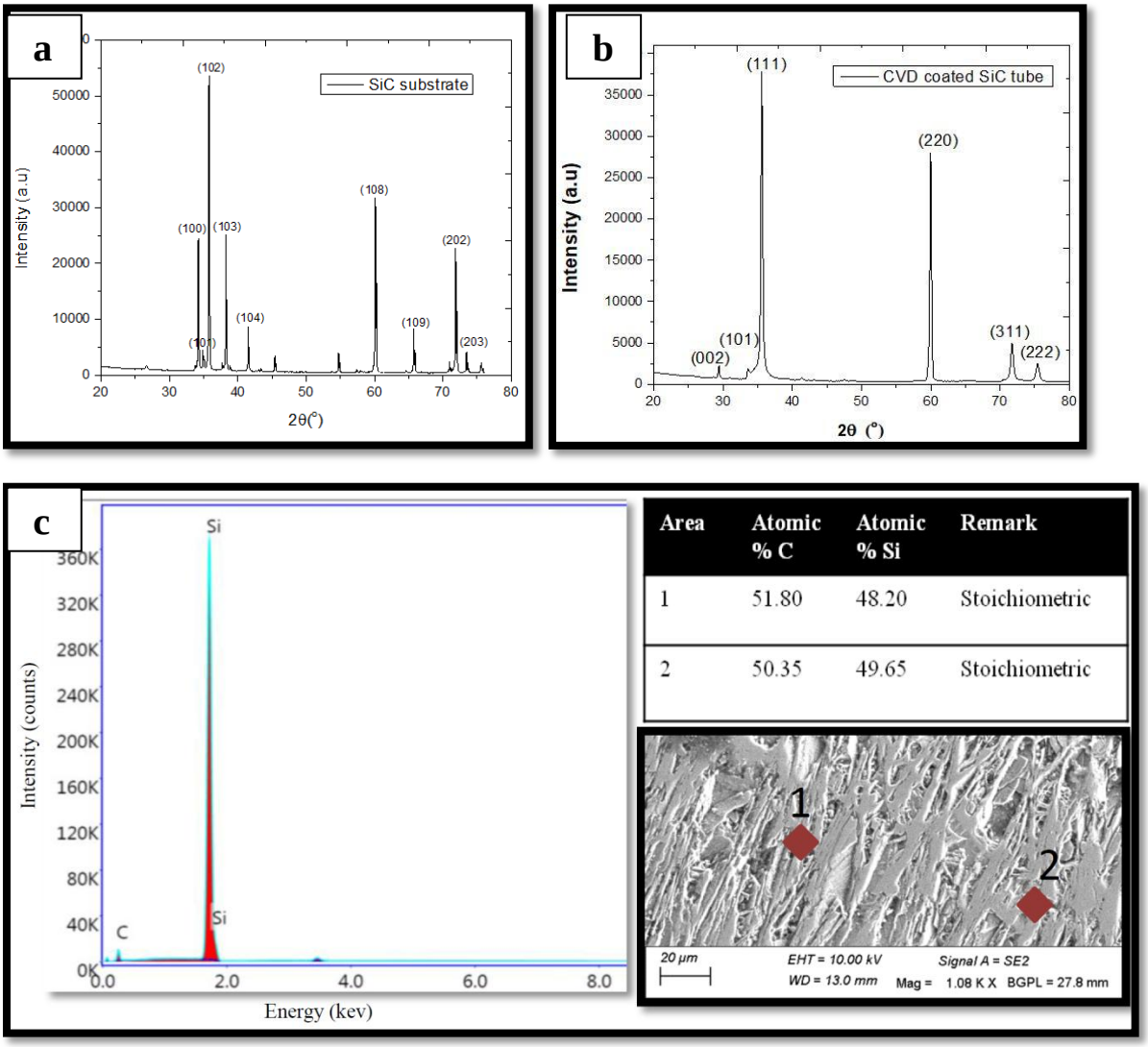

Figure 4.9: X-ray diffraction patterns of a) substrate before the CVD coating b) CVD coated SiC tube c) Energy dispersive spectroscopy (EDS) d) area mapping and stoichiometric atomic ratios of Si & C of selected regions.

4.1.2.4 *Physical and mechanical properties of sintered and CVD coated SiC and its composite tubes*

The physical and mechanical properties of sintered SiC and its composite tubes are listed in Table 4.10 and depicted as a Figure 4.10. As compared with Taguchi analysis results, it is evident that the superior properties of the composites were achieved through proper surface treatment and dispersion of CNFs in SiC matrix employing advanced freeze-dried powder processing technique. In this study, the surface modified 1 wt % CNFs containing composite achieved the highest density, which is 98.5 % of its theoretical value. Consequently, the hardness, strength and fracture toughness values were measured (average of ten samples) and found to be superior, corresponding to an average value of 25.62 GPa, 464.79 MPa and 5.14 $MPam^{1/2}$ respectively, compared with bare SiC. However, the density of the composites decreases with increase in CNFs content which can be attributed to the agglomeration of carbon fibres in the matrix. It is worth mentioning that the properties of surface modified 1 wt % CNFs containing composite processed through pressureless sintering technique is superior to the properties reported in the literature for the same composite, processed through advanced processing techniques such as Pulsed electric current-pressure technique, Hot-pressing which are highly cost-intensive processes [4, 5].

Table 4.11 shows the density and hardness values of CVD SiC coating which comprises β – phase corresponding to cubic structure deposited on monolithic SiC substrate having α – phase corresponding to the hexagonal structure. The density of CVD coating applied on monolithic SiC tube was noted to be 3.20 g/cm^3 i.e. more than 99 % of its theoretical value. Hardness and indentation fracture toughness values were measured as 28.97 GPa and 3.87 $MPam^{1/2}$ respectively.

Table 4.10: Relative densities of monolithic SiC and SiC-CNFs composites.

Composition	0 wt % CNFs	1 wt % CNFs	2 wt % CNFs	3 wt % CNFs
Relative density (%)	99	98.5	97.5	96.3

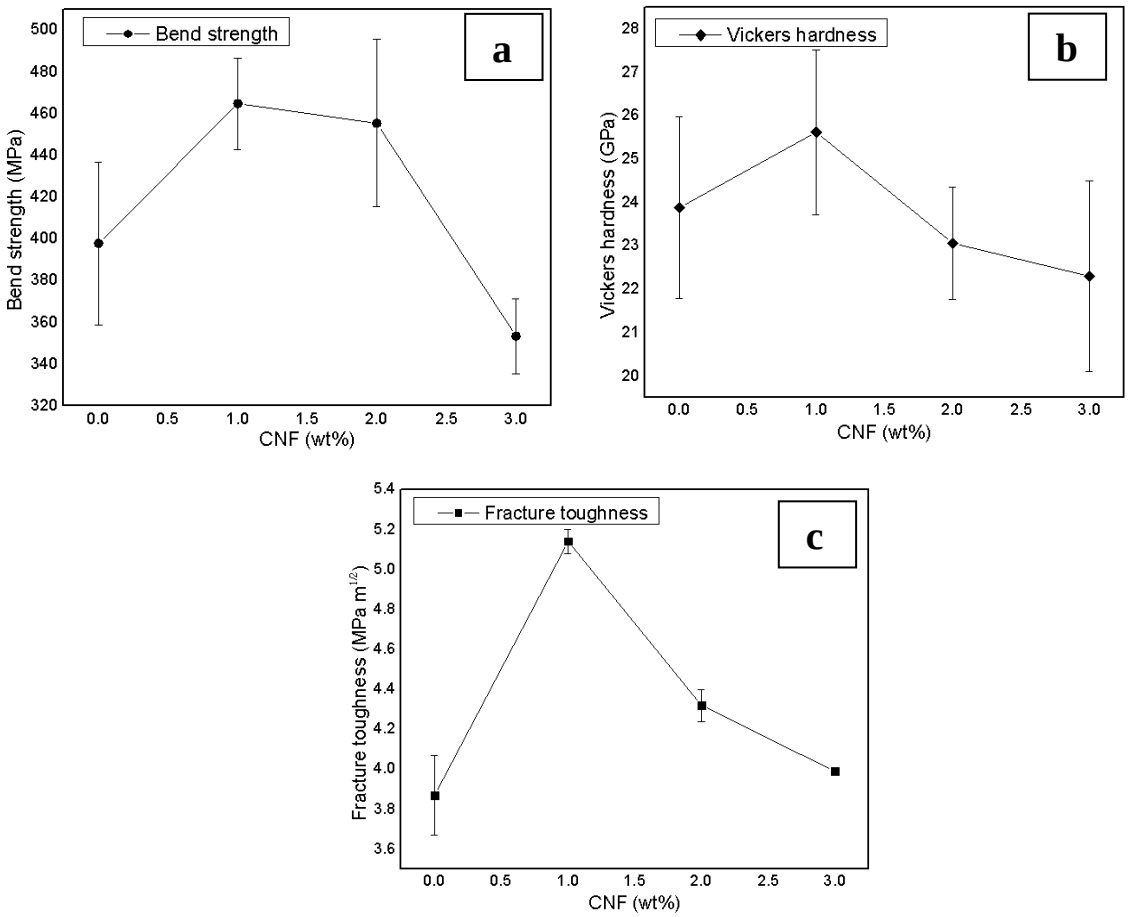

Figure 4.10: Mechanical properties of SiC-CNFs composites with respect to the CNFs content a) wt % CNFs vs bend strength b) wt % CNFs vs hardness c) wt % CNFs vs fracture toughness.

Table 4.11: Properties comparison of sintered SiC tubes (SSiC) and CVD coated SSiC tubes.

Properties	**SSiC**	**CVD SiC**
Coating thickness (μm)	---	500-600
Density (g/cm^3)	3.17	3.20
Vickers Hardness (GPa at 1kg load)	27.12	28.97
Phase	α (Hexagonal)	β (cubic)
Indentation fracture toughness ($MPam^{1/2}$)	4.02	3.87

4.1.2.5 *Thermal properties of SiC and its Composites*

The thermal conductivity value of CNFs containing SiC composites along with monolithic SiC processed out of spray freeze-dried powders was determined with respect to temperature by laser flash method and compared with values in the literature [6]. The overall thermal conductivities of in-house processed monolithic SiC and SiC-1 wt % CNFs composite are shown in Figure 11(a). Porosity or defects, grain boundaries orientations and impurities at the grain boundaries are known to be the main parameters in materials which determine and control thermal conductivity. High-resolution TEM image (HR-TEM) as shown in Figure 4.11(b) depicts good bonding between the SiC matrix and highly conductive CNFs, leading to more than two-fold increment in thermal conductivity value for SiC-CNFs composite even at the high temperature compared to monolithic SiC i.e. thermal conductivities of monolithic at 100 ^{o}C was 149 W/mK ; for the composite it was 158 W/mK and at high temperature i.e at 1000 ^{o}C, the monolithic SiC was having 30 W/mK, while that for the composite**,** it was reported as 74 W/mK. The superior thermal conductivity value for 1wt % CNFs containing SiC composites compared to that reported in the literature may be attributed to better green and sintered properties of the composite.

The use of advanced spray freeze granulation technique helped in obtaining strong bonding between the matrix and the fiber in the sintered tubes. The detailed analysis of SiC-1 wt % CNFs composites was carried out using TEM, EBSD and HR-TEM images, as illustrated by Figures 4.7, 4.8 and 4.9. The high thermal conductivity value of SiC-1 wt % CNFs composite can be attributed to the fine and uniform dispersion of secondary fiber phases, minimization of porosity due to improved density as revealed by TEM. Further, the HR-TEM shows good bonding between CNFs and the SiC matrix causing the thermal conductivity of the composite to increase. Finally, the EBSD mapping shows regular grain orientation with high angle clean grain boundaries confirming vastly improved thermal conductivity.

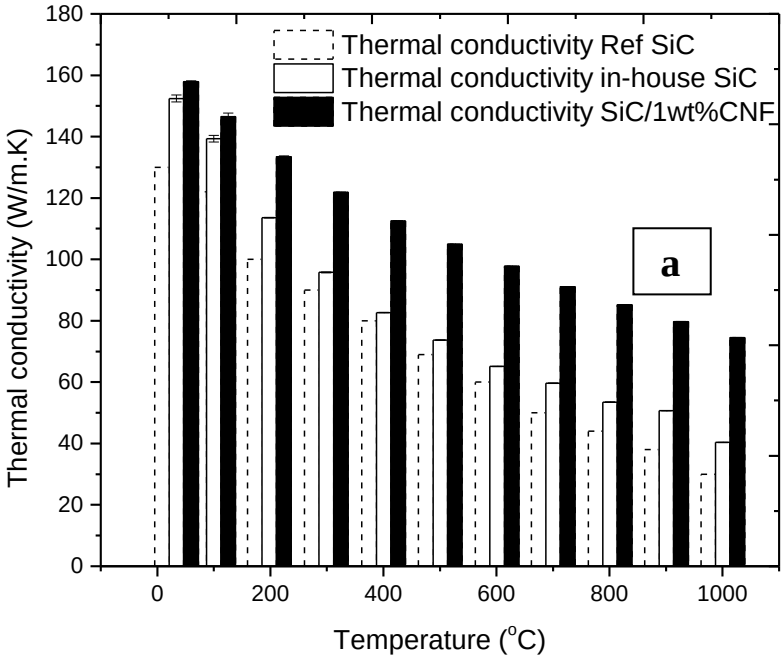

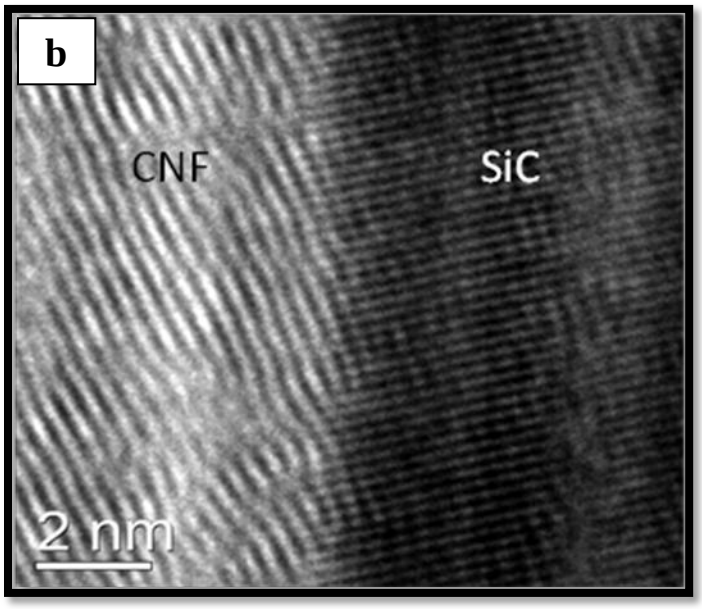

Figure 4.11: a) Thermal conductivity variation of monolithic SiC & SiC-1 wt % CNFs composite with respect to temperature b) HR-TEM image of SiC & CNFs interface.

4.2 Conclusions

1. The following conclusions are drawn from the S/N ratio and ANOVA analysis of Taguchi design of experiments,
   i. The best combination of optimized sintering parameters was obtained when composites were sintered at 2150 ^{o}C with heating rate of 8 ^{o}C/min for 1 hr holding time.
   ii. Sintering temperature and CNFs wt % were identified to be major factors impacting directly the physical and mechanical properties, in particular, one of the most important parameters i.e., fracture toughness of CNFs composite tubes. As the CNFs quantity increased, the decrease in the fracture toughness of the composite was observed due to the agglomeration or bundling of CNFs. The superior fracture toughness obtained in this study was 5.12 MPam$^{1/2}$ with 1 wt % CNFs dispersion in SiC matrix.
2. The best combination of properties i.e. density (ρ): 3.21 g/cc (at 0 wt % CNFs), hardness (H_v): 26.5 GPa (1 wt %), and fracture toughness (F.T): 5.12 MPam$^{1/2}$ (at 0 wt % CNFs) of CNFs composites was obtained through adopting Taguchi statistical analysis with an L_9 (3^4) orthogonal array.
3. Tests were conducted at optimized set of conditions to establish the effect of SiC powder particle size and CNFs loading, which confirms the physical and mechanical properties of the composites determined from results of previous analysis.
4. Fine particle powders with large surface area have a high tendency to form agglomerate. Confirmation test with CNFs composite of M-15 grade having relatively larger particle size than other grade powders**,** reveals superior properties of the particles processed though the present experiments.
5. The thin and dense CVD SiC coated CNFs composite tubes were fabricated at optimized processing condition obtained through Taguchi statistical analysis. In addition, to avoid the entanglement or bundling during dispersion, the CNFs were surface modified or acid treated at optimized titrations.
6. Spray freeze granulation process was used to produce well-dispersed spherical SiC composite powder at variation of CNFs from 0–3 wt %.
7. Cold isostatic pressing was employed to shape thin and dense green SiC tubes and it's composite.

8. Sinterability of the composites was enhanced due to the use of spray freeze granulated composite powder. Hence, produced superior physical and mechanical properties of SiC-CNFs composites.
9. Highly dense green tubes produced out of surface modified 1 wt % CNFs composite spherical granules could achieve 98.5 % theoretical density and exhibited 25.62 GPa, 464.79 MPa and 5.14 MPa $m^{1/2}$ hardness, strength and fracture toughness values respectively which are the highest amongst all other composites.
10. The thermal conductivity value of 1wt % CNFs containing composite was measured from room temperature to 1000 ^{o}C and found to be more than a monolithic SiC sample, which can be attributed to the strong bond between high thermal conductive CNFs with SiC matrix and high angle grain boundaries with less phonon scattering, made evident from the HR-TEM & EBSD analysis.
11. Highly dense CVD coating was employed on SiC tubes to form uniformly distributed stoichiometric coating with improved physical & mechanical properties, which was revealed by SEM & EDAX analysis.

4.2 References:

[1] Fatin MF, Ruslinda AR, Norhafizah S, Farehanim MA: *IEEE Conference on Biomedical Engineering and Sciences (IECBES)*, Kuala Lumpur, 2014, pp. 686–689.

[2] Li Y, Yin J, Wu H: *J. Euro. Ceram. Soc.*, 2014, vol. 34, pp. 2591–2595.

[3] Seo YH, Nahm KS, Suh EK, Lee HJ: *Korean J Chem Eng*, 1996, vol 13, pp. 522–529.

[4] Jing X, Yang X, Shi D, Niu H: *Ceram. Int.*, 2017, vol. 43, pp. 6721–6729.

[5] Shimoda K, Hinoki T, Kohyama A: *Compo. Sci. Technol.*, 2010,vol. 70, pp. 387–392.

[6] Blumm Johannes JO, Opfermann J: *High. Temp. Pressure.*, 2003,vol. 35, pp. 513–520.

CHAPTER 5

Fabrication of BN coated long carbon and carbon nanofibers reinforced SiC based hybrid tubes through CIP and pressureless sintering

5.0 Introduction

In this chapter, fabrication of boron nitride coated continuous carbon fiber (BN-C_f) reinforced SiC based hybrid composite tubes (BN-C_f/SiC-CNFs) and its characterization have been discussed. The hybrid composite tubes were fabricated by systematically laying long carbon fiber in spray granulated premixed CNFs dispersed SiC composite powder. High-density hybrid composite tubes were processed by cold isostatic pressing (CIP) of the aforementioned powder in a specially designed mould followed by pressureless sintering. The microstructure and phase analysis of the raw materials, BN coated $C_{f,}$ and sintered hybrid composite samples etc., were characterized using SEM, FTIR, XRD and TEM. The fractographic analysis of the fracture surface of the hybrid composite tubes was also carried out to understand the influence of long fibers on the improvement of fracture toughness of nanofibers containing a hybrid composite matrix.

5.1 Results and Discussion

5.1.1 *Phase and chemical composition analysis*

The XRD pattern of as received and BN coated carbon fibers and the hybrid composite tube is shown in Figure 5.1. A broad diffraction peak is seen from Figure 5.1(a) at 25^o, corresponding to (002) plane, which is identified to be the common peak for both carbon fibers and BN coating with hexagonal crystal structure. The diffracted peaks from the surface of BN coated carbon fibers were observed at 2Ɵ value 25.80^o, 43.54^o, 53.43^o corresponding to (002), (100), and (004) diffraction planes respectively, representing hexagonal h-BN phase. An intense peak was observed at 28.15^o corresponding to (310) plane, revealing the presence of B_2O_3 phase, which can be expected due to the processing method adopted for BN coating (will be discussed in the upcoming sections).

The XRD pattern of the hybrid composite is identified in three different phases, as shown in Figure 5.1(b). The corresponding 2Ɵ value and diffraction planes of the phases represent hexagonal crystal structured SiC, BN. The XRD peak at 37.32^o with (021) as the reflection plane identified to be boron carbide (B_4C) with rhombohedral crystal structure [ICDD file no: 00-006-0555] [1]. The formation of B_4C phase may be attributed to the reaction between the free carbon

and excess boron oxide (B_2O_3) deposited on the surface of BN coated C fiber taking place at high temperature [2].

FTIR spectrum of as-received and BN coated carbon fibers are shown in Figure 5.1(c). From FTIR spectroscopy principle, it is known that the absorbed light energy of the material can be converted into rotational and vibrational energy to make the absorption peaks visible. The FTIR spectra of as-received carbon fiber have shown the bands at 1525 cm^{-1}, 1732 cm^{-1}, 2349 cm^{-1}, 2914 cm^{-1}, and 3712 cm^{-1}, which correspond to the bonding of C-N, C=O, C-H, O-H, N-H, respectively. In the case of BN-C_f, the bands observed at 738 cm^{-1} and 1401 cm^{-1} are attributed to B-N-B in-plane bending, B-N stretching vibration, respectively [3,4].

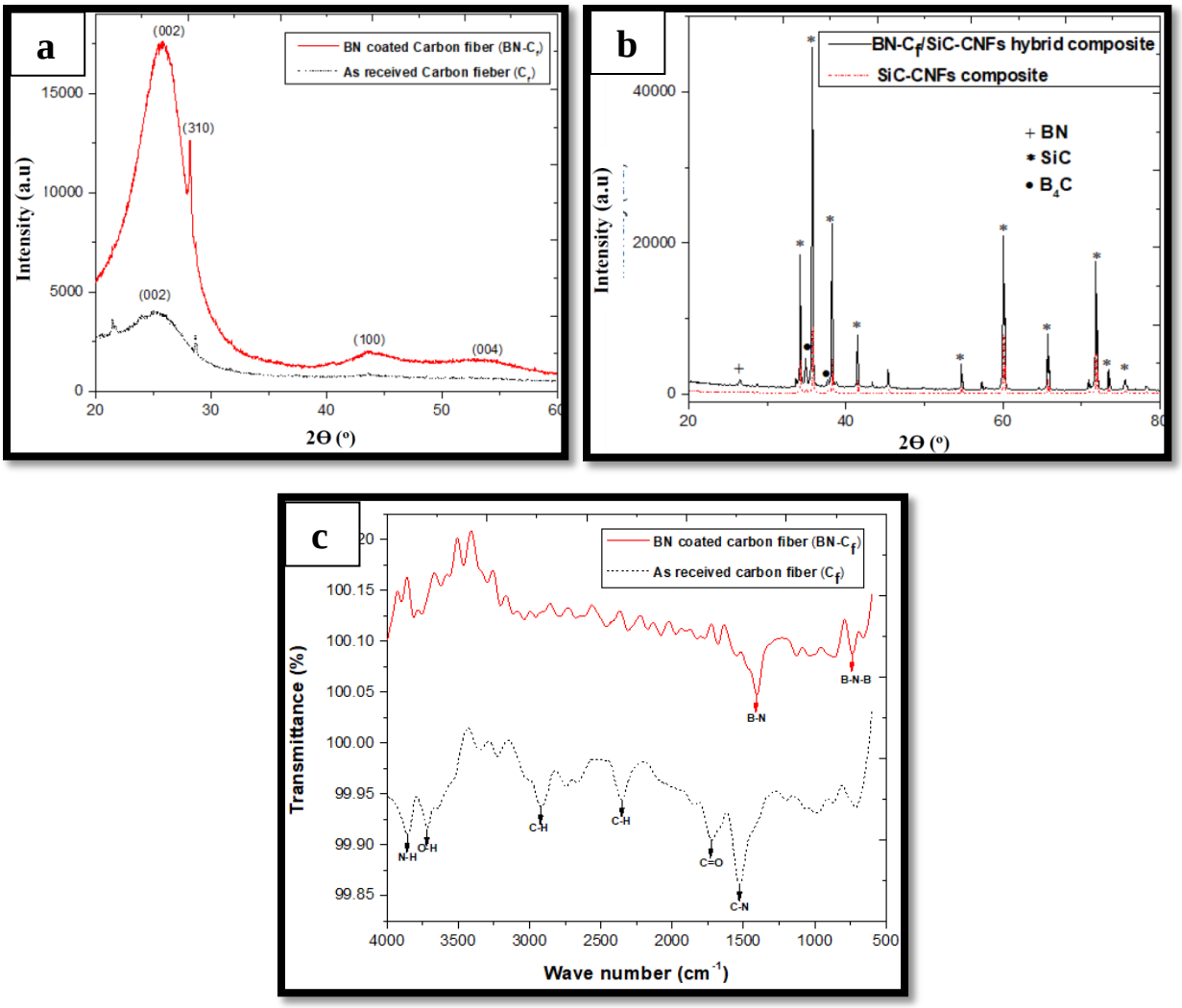

Figure 5.1: XRD pattern of a) as received and BN coated carbon fibers b) BN-C_f /SiC-CNFs hybrid composite; FTIR spectra of c) as received and BN coated carbon fibers.

5.1.2 *Rietveld refinement analysis*

The structural and quantitative phase analysis of XRD data obtained from composite samples (i.e., SiC-CNFs composite sample and SiC-based hybrid composite sample) was carried out by Rietveld's refinement using MAUD software [24–26]. Refining structural information such as lattice parameters, atomic position, peak position, background parameters were carried out while considering the standard reference crystal structure information from crystallographic information file (CIF). The symmetry and the space group considered for the refinement along with the refined structural parameters, such as goodness of fit factor (χ^2) and R-factors: weighted residual error (R_{wp}), expected (R_{exp}), background (R_{wnb}) and Bragg (R_b) are given in Table 5.1. The values of χ^2 and R_{wp} acceptable for the effective refinement were very low ($\chi^2 < 2$, Rwp < 15) [26]. The refinement was carried out at a maximum number of cycles (21 cycles) until it matched the standard reference peak positions. Figure 5.3 shows that the calculated (black line) and observed (red lines) data have completely coincided with each other and the multi-phase peaks matched well with the respective standard reference files. The observed and standard lattice parameters (a, b, and c) were found to be nearly equal (Table 5.1). The refinement output values such as χ^2 (1.710 and 1.125), R_w (13.7222 and 9.014) indicate good refinement. Rietveld refinements of the composites also identified the presence of multi-phase in the samples which was also confirmed by XRD phase analysis. The SiC-CNFs composite sample is identified with two phases, whereas hybrid composites comprises of three phases. The phases were measured quantitatively considering the influence of all sharp or intense and small broad peaks. The phase analysis reveals that the amount of SiC and B_4C present in SiC-CNFs composite is 84.981 % and 15.018 % respectively whereas SiC hybrid composite contains 79.942 % SiC and 18.897 % B_4C and 1.160 % BN respectively.

The B_4C phase was found to be slightly more in the case of hybrid composite than SiC-CNFs composite sample. The formation of B_4C in SiC-CNFs composite may be attributed to the reaction between the free carbon and boron**,** which were added to the matrix as sintering additives. On the other hand, in case of SiC hybrid composites, the source of B_4C was expected due to the reaction between the free carbon, boron and excess boron oxide (B_2O_3).

Table 5.1: Rietveld refined structural parameters and quantitative phase contents of the samples.

Sample	Phase	Space groups	Lattice parameters (Å)		Crystallite size (nm)	Phase present (wt %)	Sig / GOF	R_w	R_{wnb}	R_b	R_{exp}
			a=b	c							
SiC-CNFs composite	SiC	$P6_3mc$ [186]	3.084	15.136	54.1832	84.981±0.00	1.710	13.722	14.603	9.590	8.024
	B_4C	$R\bar{3}m$ [166]	5.618	12.119		15.018±3.014					
SiC-based hybrid composite	SiC	P63mc [186]	3.081	15.117	54.1832	79.942±0.00	1.125	9.014	9.650	8.085	8.012
	B_4C	$R\bar{3}m$ [166]	6.129	10.708		18.897±1.088					
	BN	$P6_3/mmc$ [194]	2.013	6.730		1.160±0.116					

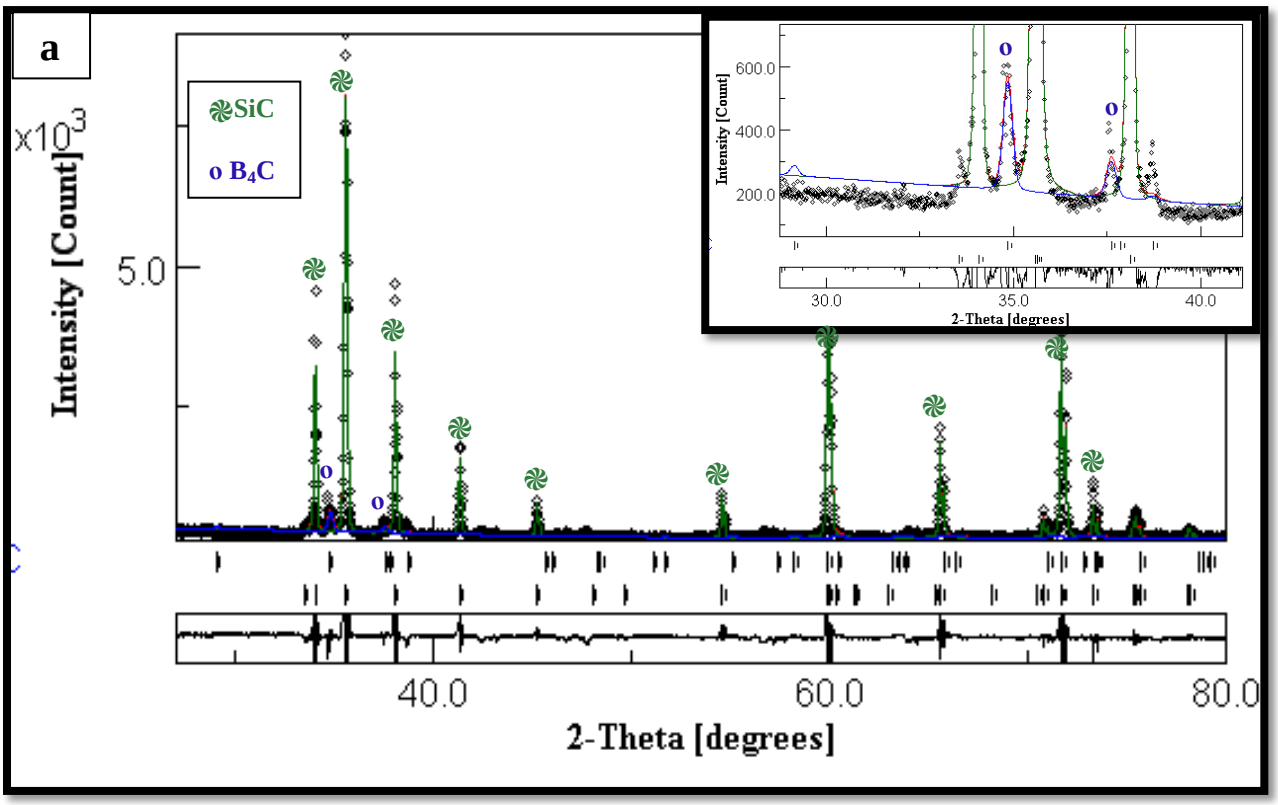

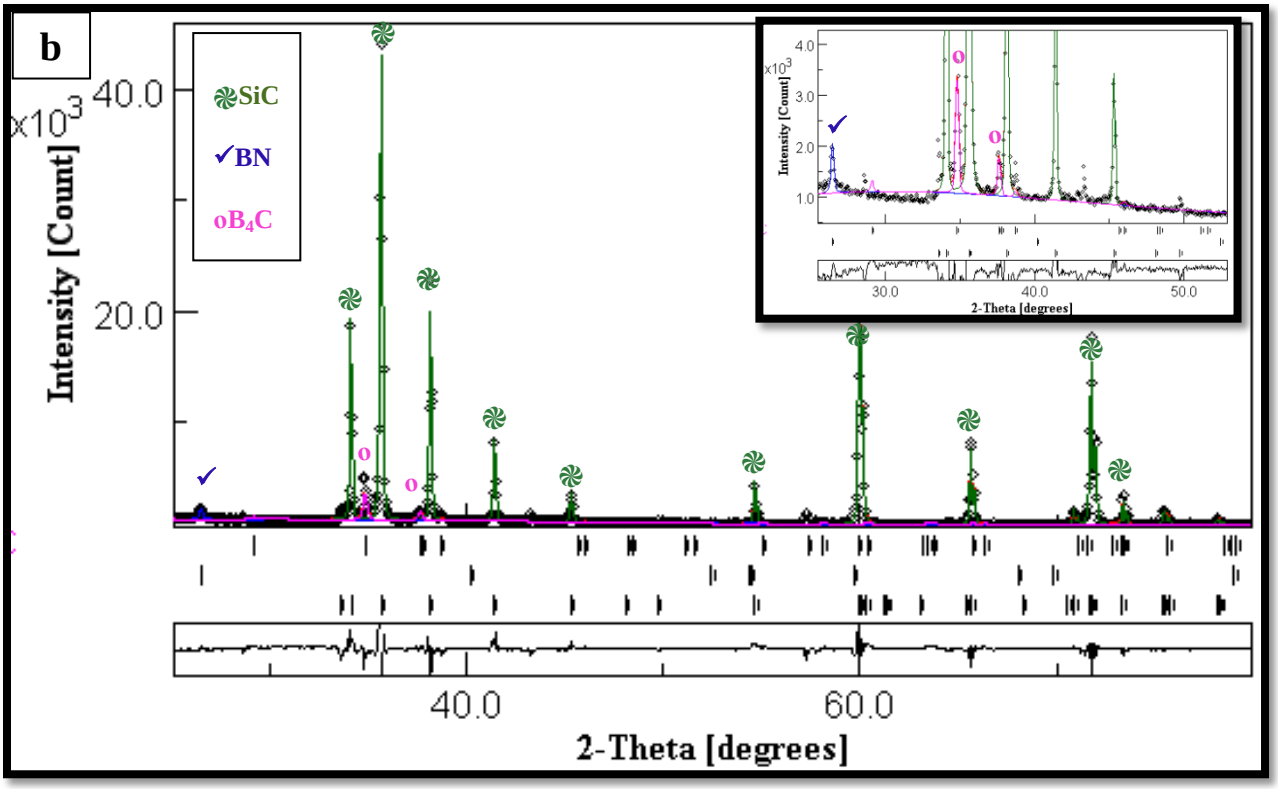

Figure 5.2: Rietveld refinements of XRD patterns of a) SiC-CNFs composites b) BN-C_f /SiC-CNFs hybrid composites.

5.1.3 *Formation mechanism of BN coating on C fibers*

The dip-coating technique in combination with sol-gel process was chosen to coat the long carbon fibers with BN, adopting the process mentioned in the previous section. The difference in the surface morphology of the fibers before and after the coating process was evident from SEM images as shown in Figure 5.3 (a) and (b). The dip-coating and curing process forms a rugged surfaced thin film with adherence of different sized clusters on the evenly surfaced carbon fibers, as shown in Figure 5.3(b).

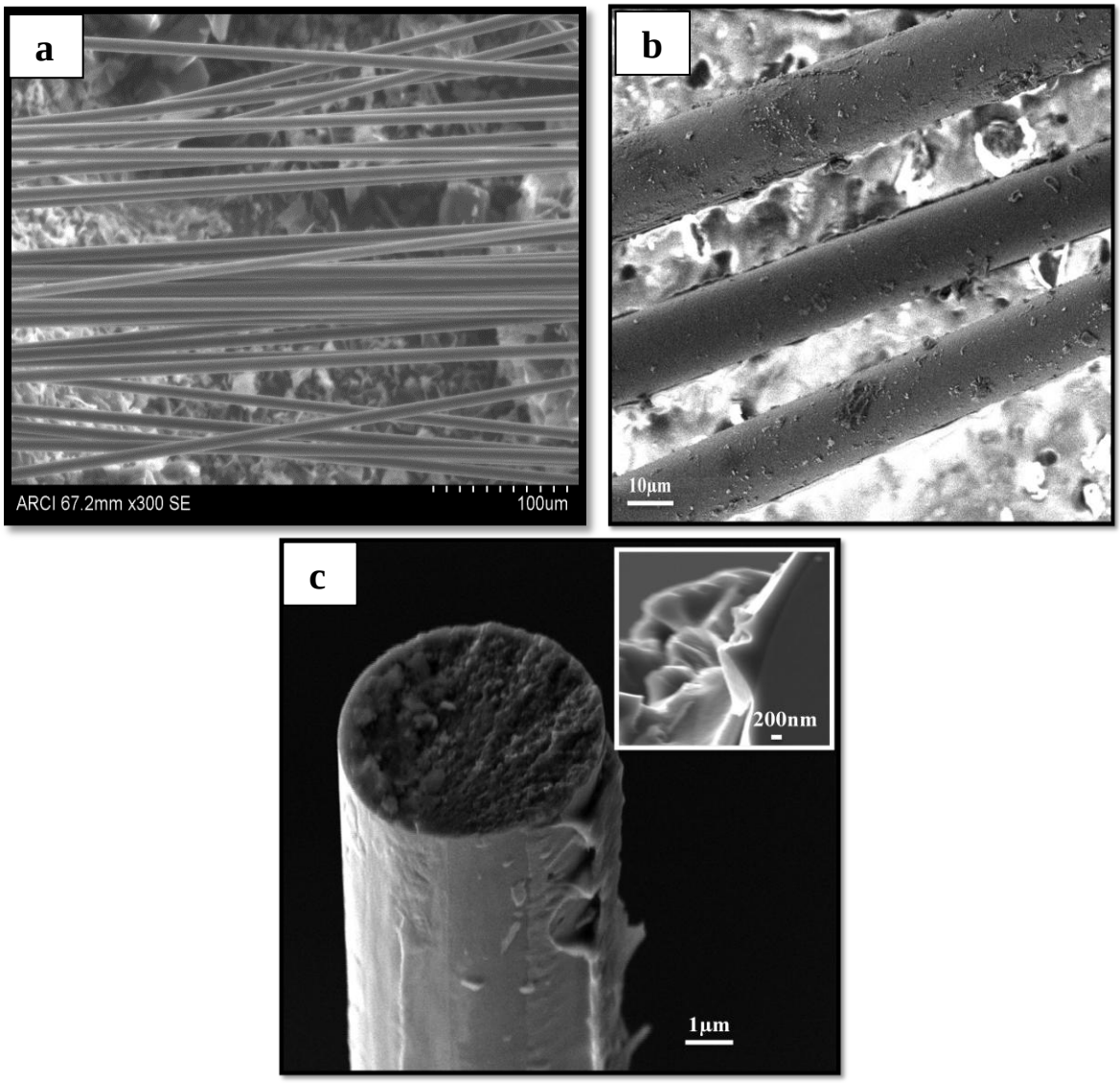

Figure 5.3: SEM image of a) as-received b) BN-coated c) cross-sectional view of carbon fibers.

The possible chemical reactions and the mechanism involved in the synthesis of BN protective coating on carbon fibers using urea and boric acid have been reported to follow the equations given below [7]. The initial reaction of BN coating starts with dehydration of boric acid at elevated temperatures**,** which results in the formation of boric oxide (B_2O_3) (Eq 5.1).

$$2H_3BO_3 \rightarrow B_2O_3 + 3\ H_2O \qquad \text{Equation (5.1)}$$

Boric acid (H_3BO_3) reacts with urea ($CO\ (NH_2)_2$) at temperature ranges of 250-300 ^oC and forms ammonium polyborate ($(NH_4)_2B_4O_7$). In aqueous media, urea thermally decomposes into

ammonia and carbon dioxide. At further high temperatures, ammonium polyborate reacts with ammonia (NH_3) and forms ~ 300 nm thin layer of h-BN on the fibers, as evident from Figure 5.3(c) (Eq 5.2-5.4) [8].

$4H_3BO_3 + CO(NH_2)_2 \rightarrow (NH_4)_2B_4O_7 + CO_2 + 4H_2O$ at 250-300 ^oC Equation (5.2)

$CO(NH_2)_2 + H_2O \rightarrow 2NH_3 + CO_2$ Equation (5.3)

$½ (NH_4)_2B_4O_7 + NH_3 \rightarrow 2h\text{-}BN + 7/2H_2O$ at 750-800 ^oC Equation (5.4)

The reaction between boric oxide and ammonia at high temperatures also results in the formation of BN layer on the fiber surface (Equation 5.5) [7].

$B_2O_3 + 2NH_3 \rightarrow 2BN + 3H_2O$ Equation (5.5)

The BN layer thus produced helps in protecting the carbon fiber from high-temperature oxidizing atmosphere.

At temperatures above 1350 ^oC, the un-reacted excess boron oxide clusters adhering to the long carbon fiber surface react with the free carbon added as sintering additive to SiC hybrid composite matrix to form boron carbide as per the following reaction (Equation 5.6):

$2B_2O_3 + 7C \rightarrow 6CO + B_4C$ Equation (5.6)

The B_4C phase was also identified from XRD analysis (Figure 5.1(b)) [9,10].

5.1.4 Microstructure and properties correlation

A detailed microstructural analysis highlighting the interfacial bonding of different phases present in the matrix and its correlation with the properties of the hybrid composites was carried out by means of SEM imaging, SEM-EDS mapping, TEM, HR-TEM, and EELS analysis.

The high thermo-mechanical properties of BN coating protect the long carbon fibers from higher temperature oxidation to retain the properties of hybrid composite tubes [11]. Superior thermal

conductivity of many structural ceramic composites at high temperatures is also attributed to stable crystalline C_f reinforcement and CNFs dispersion in the matrix [12]. The fracture surface of fiber-matrix bonding is shown in Figure 5.4 (a) & (b). The weak BN interface provides toughness for the composite by de-bonding and sliding between fiber and coating, which shield the matrix from cracking at higher loads [13]. The fiber pull-out from the matrix was observed from Figure 5.4(a), indicating improved fracture toughness of the composite, which is also evident from the values given in Table 5.2. The distribution of BN on the surface of continuously coated carbon fibers that protruded from the fracture surface of the hybrid composite tube was evident from EDS X-ray mapping and line scan analysis, as shown in Figure 5.5(a, b) which is further confirmed by FTIR analysis (Figure 5.1(c)).

The interfaces between BN coating, long carbon fibers, and SiC matrix are shown in Figure 5.6(a) at high magnification using TEM. The dispersion of CNFs in the SiC matrix was evident from Figure 5.6(b). High-resolution TEM image acquired from Figure 5.6(a) shows the interface between the BN coating and the SiC grain, with a lattice spacing of 0.33 nm, 0.27 nm respectively, as shown in Figure 5.6(c). The uniform distribution of CNFs and crystalline BN-C_f makes a major contribution in leading to superior properties of the hybrid composite tube.

SEM observations and the properties measured to justify the influence of BN coating on the stability of C_f. The influence of other parameters like improved green density of green tubes formed by cold isostatic pressing and optimized sintering parameters helped in achieving superior properties of hybrid composite tubes. The properties of the hybrid composites such as relative density hardness and fracture toughness obtained through the novel process were measured to be 96.4 %, 22.68 GPa, 5.26 $MPam^{1/2}$ respectively (Table 5.2). The results were observed to be comparable with the base matrix (SiC-CNFs composite) properties with slight variation (less). This variation, mainly the density of hybrid tubes was expected due to the loose bonding between the BN-coated continuous carbon fibers with the matrix. However, a small improvement in fracture toughness of the matrix was observed with the reinforcement of the continuous carbon fiber, in the case hybrid composite as shown in Table 5.2.

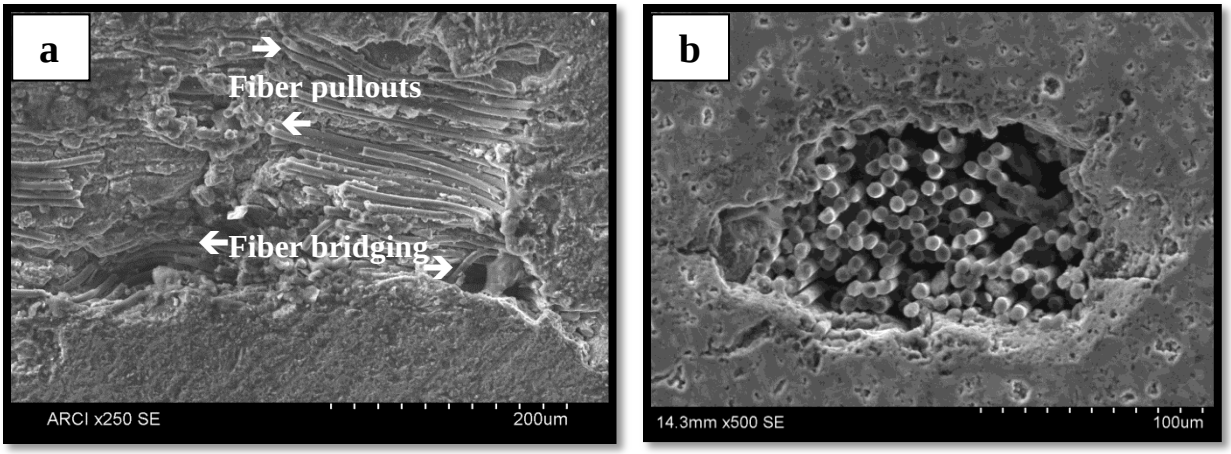

Figure 5.4: SEM image of the fracture of the hybrid composite tube a) surface view b) cross-sectional view.

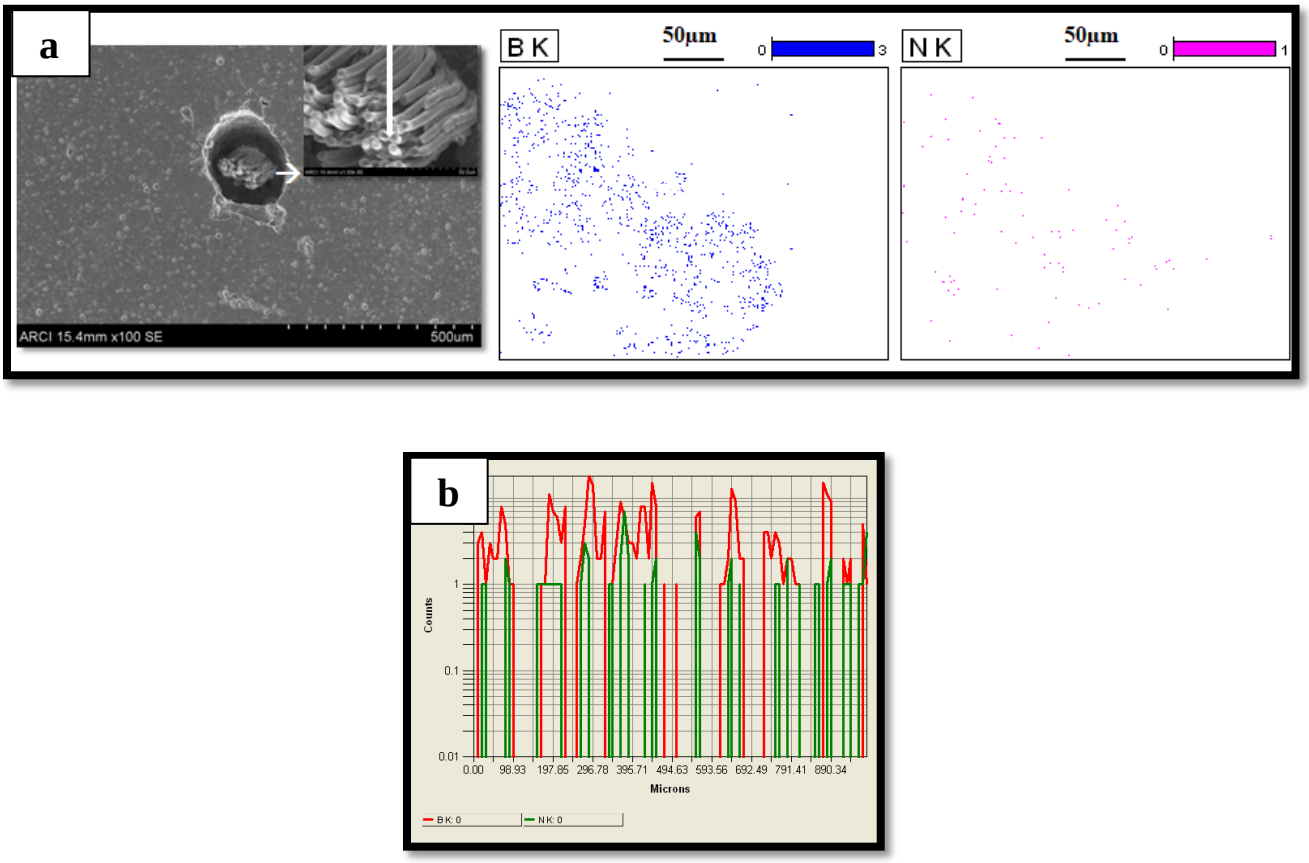

Figure 5.5: SEM-EDS mapping of BN coated C_f in the hybrid composite matrix a) X-ray mapping b) line scanning.

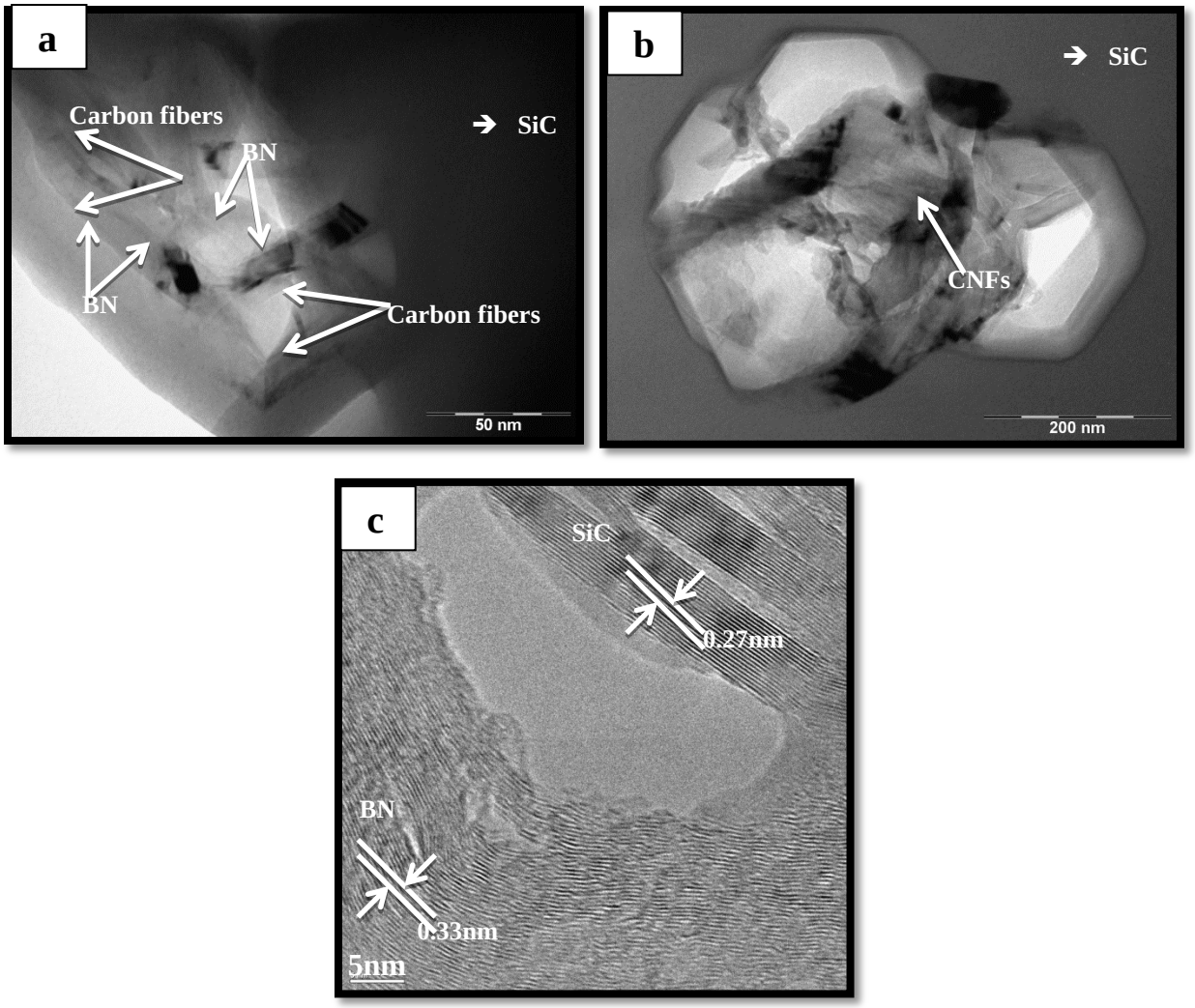

Figure 5.6: TEM characterization of a) magnified interface image of SiC grain and BN coated long carbon fibers b) CNFs dispersion in the SiC matrix c) HR-TEM interface image of BN coating and SiC grain.

Table 5.2: Physical and mechanical properties of the pressureless sintered hybrid composite tube.

Sample	**Relative density (%)**	**Vickers hardness (GPa)**	**Indentation fracture toughness (MPa $m^{1/2}$)**
BN-C_f/SiC-CNFs hybrid composite tube	96.4	22.68 ± 2.17	5.26 ± 0.74

Figure 5.7 (a), TEM image of hybrid composite shows the presence of the boron carbide (B_4C) phase (size 60-90 nm) within the matrix at the triple point junction of SiC grains [14]. The EEL study also confirms the new phase as boron carbide by identifying B and C elements in the area analysed, as shown in Figure 5.7(b). The grain refinement assisted by B_4C phase with strong interface bonding between SiC matrix interns resulted in excellent physical and mechanical properties of the hybrid composite, as mentioned earlier. A high-resolution TEM image of Figure 5.7(a) shows strong crystalline interface bonding between B_4C phase and SiC phase with a lattice spacing of 0.36 nm as shown in Figure 5.7(c).

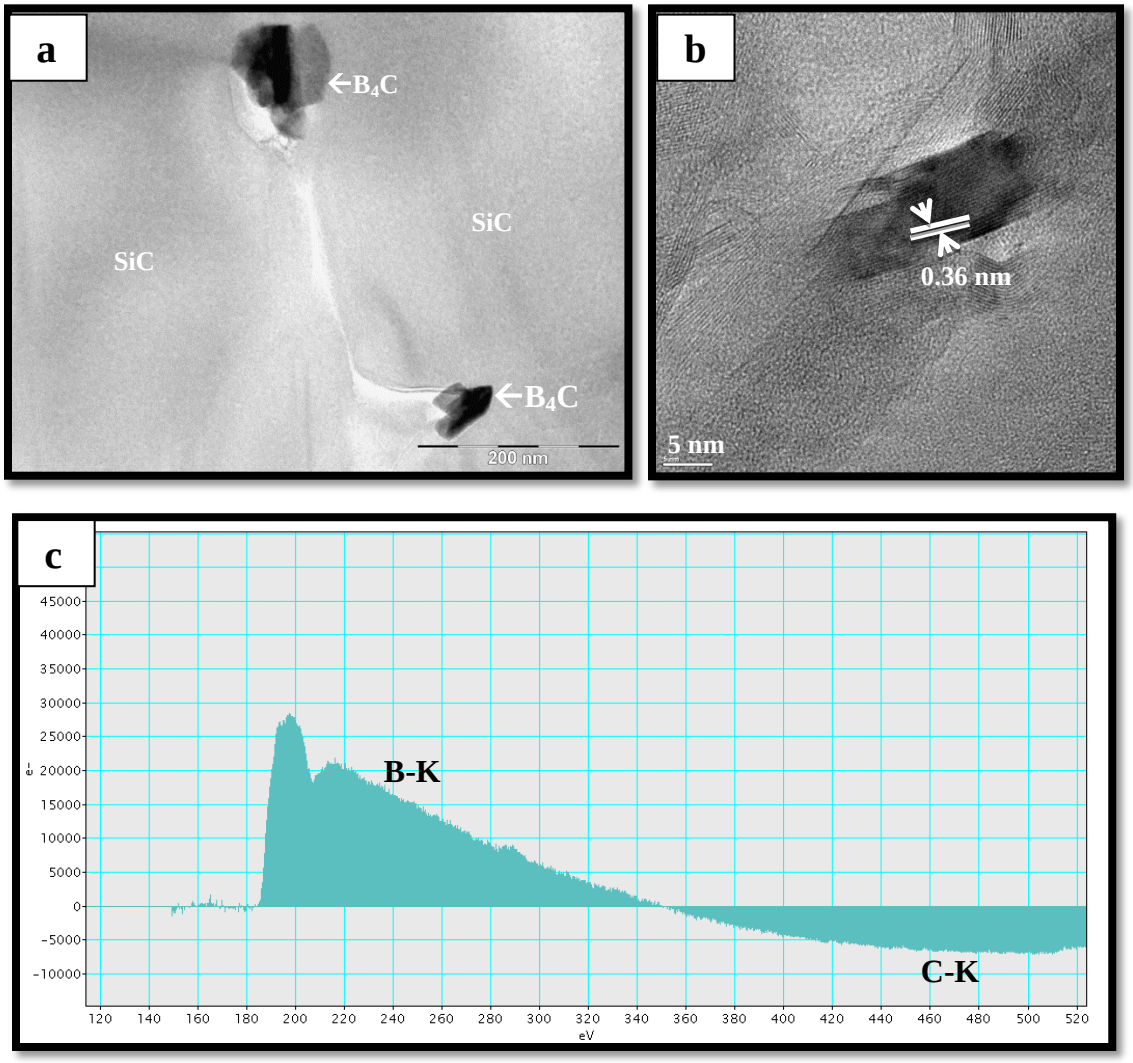

Figure 5.7: TEM image of hybrid composite a) B_4C phase at the junction of SiC grains b) EELS spectra of B_4C phase c) HR-TEM image of B_4C phase.

5.2 Conclusions

A novel approach was adopted for the fabrication of dense BN coated continuous carbon fiber reinforced SiC-CNFs hybrid composite tubes to exploit the dual benefit of nanocarbon fiber dispersion with long carbon fibers in the matrix. Highly dense composite tubes of SiC-CNFs host matrix with systematically laid BN coated long C_f was produced by cold isostatic pressing followed by pressureless sintering.

The highly dense hybrid composite tubes (relative density-96.4 %) showed superior mechanical properties in terms of hardness and fracture toughness of 22.68 GPa, 5.26 $MPam^{1/2}$ respectively. The XRD phase analysis and FTIR studies on BN coating and its interface bonding showed that the stability of BN coating even after high temperature sintering (2150 ^{o}C), which had a great impact on C_f stability. The improved fracture toughness and other mechanical properties of the composite tube reveal combined contribution of fibers in the matrix, such as uniform distribution of CNFs in the matrix and long carbon fiber pullouts from the matrix.

The systematic phase and microstructural analysis have shown that highly stable and weak interface BN bonding with long C_f, helped in fiber pullouts as revealed in the fractographic study. TEM analysis and EELs studies reveal the presence of B_4C phase within the matrix and its grain refinement action, which in turn contributed to the enhancement of density as well as mechanical properties of the composite.

5.3 References:

[1] R M Mohanty, K Balasubramanian, and S K Seshadri: in *Adv. Ceram.*, Costas Sikalidis, ed., IntechOpen, London, 2011.

[2] Masaki Kakiage, Naoki Tahara, Satomi Yanagidani, Ikuo Yanase, and Hidehiko Kobayashi: *J. Ceram. Soc. Japan*, 2011, vol. 119, pp. 422–25.

[3] Jianbin Song, Quanping Yuan, Xueshen Liu, Dong Wang, Feng Fu, and Wenbin Yang: *BioResources*, 2015, vol. 10, pp. 5820–29.

[4] Wei Zhou, Peng Xiao, Yang Li, and Liang Zhou: *Ceram. Int.*, 2013, vol. 39, pp. 6569–76.

[5] N Sehab, A Amara, and Y Mebdoua: *Mater. Manuf. Process.*, 2017, vol. 32, pp. 1260–64.

[6] Victor Ioan Stanciu, Véronique Vitry, and Fabienne Delaunois: *Mater. Manuf. Process.*, 2020, pp. 1–6.

[7] Linlin Chen, Haihui Ye, and Yury Gogotsi: *J. Am. Ceram. Soc.*, 2004, vol. 87, pp. 147–51.

[8] Suna Balci, Naime Sezgi, and Esin Eren: *Ind. Eng. Chem. Res.*, 2012, vol. 51, pp. 11091–11096.

[9] Dina H.A. Besisa, Mahmoud A.A. Hagras, Emad M.M. Ewais, Yasser M.Z. Ahmed, Zaki I. Zaki, and Adel Ahmed: *J. Ceram. Process. Res.*, 2016, vol. 17, pp. 1219–25.

[10] J A Bigdeloo and A M Hadian: *Int. J. Recent Trends Eng.*, 2009, vol. 1, pp. 44–49.

[11] Rodolfo F.K. Gunnewiek, Pollyane M. Souto, and Ruth H.G.A. Kiminami: *J. Nanomater.*, 2017, pp. 1–9.

[12] Junfeng Liang, Mrinal Saha, and M Altan: *Procedia Eng.*, 2013, vol. 56, pp. 814–20.

[13] Gregory N. Morscher, Hee Mann Yun, James A. DiCarlo, and Linus Thomas-Ogbuji: *J. Am. Ceram. Soc.*, 2004, vol. 87, pp. 104–12.

[14] G. I. Kalandadze, S. O. Shalamberidze, and A. B. Peikrishvili: *J. Solid State Chem.*, 2000, vol. 154, pp. 194–198.

CHAPTER 6

Enhancement of oxidation resistance of CVD SiC coated C_f/SiC-SiC(CNFs) hybrid composites processed through Si-infiltration

6.0 Introduction

Three different types of C_f/SiC-SiC(CNFs) hybrid composite tubes were fabricated by LSI process. The surface of the preprocessed dense CNFs containing silicon carbide composite tubes (SiC(CNFs)) wrapped with carbon fiber (C_f) of different braiding patterns was used as base matrix material for LSI. The steps involved in LSI process are as follows: precursor impregnation (liquid coal-tar pitch) of the brandings, carbonization to form C/C_f porous structure, graphitization, pyrolysis and liquid Si-infiltration. Further, a dense and uniform cubic β-SiC coating was applied on the surface of the above-mentioned hybrid composite tubes using chemical vapor deposition process to improve its oxidation resistance property. The oxidation behavior of bare C_f, C_f/SiC composite and CVD-SiC coated C_f/SiC composite was examined separately using TGA at a temperature between room temperature to 1350 ^oC. The influence of individual phases on the oxidation resistance of the hybrid tube was studied thoroughly using XRD, SEM-EDS analysis and its results are discussed in detail.

6.1 Results and Discussion

6.1.1 *Microstructure and phase analysis*

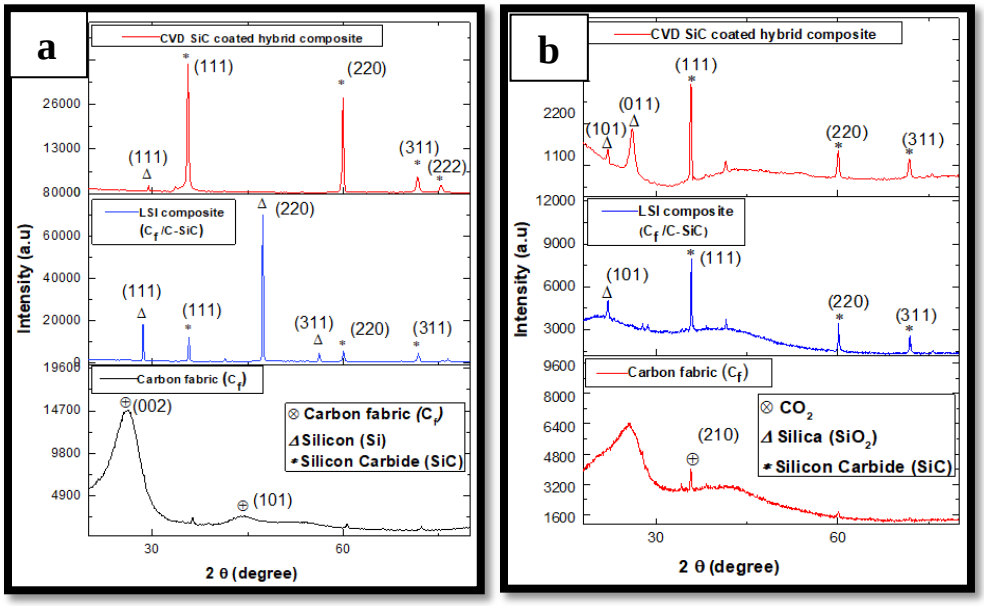

Figure 6.1: XRD phase analysis of carbon fabric (C_f), LSI composite (C_f/C-SiC), and SiC coated C_f/C-SiC hybrid composite a) before and b) after TGA.

Phase analysis of as-received carbon fabric (C_f), C_f/C-SiC composites, and SiC coated C_f/C-SiC hybrid composite cross-sectional samples before and after TG analysis was carried out using XRD and the evolution of phases are shown in Figure 6.1(a) and (b) respectively.

The phase analysis of as-received C_f reveals peaks at 26.12^o, 44.25^o reflecting from (002), (101) planes respectively before TG analysis (Figure 6.1(a)), confirming crystallinity with a regular hexagonal arrangement of C atoms [ICDD no: 04-015-2407]. The high-intensity peaks at 28.51^o (111), 44.94^o (220), 56.19 ^{o} (311) were seen (Figure 6.1(a)) in the case of LSI composite (C_f/C-SiC) indicating the presence of free Si [ICDD no: 01-071-3770]. The peaks at 35.78^o (111), 60.08^o (220), 71.83^o (311) (Figure 6.1(a)) confirm the formation of textured β-SiC (cubic) phase [ICDD no: 00-001-1119]. The presence of free Si and β-SiC was also observed in the XRD pattern of SiC coated hybrid composite cross-sectional area as well as LSI composite sample.

The XRD pattern of C_f samples after TG test, shown peak at 35.69^o (210), which corresponds to the presence of CO_2 and represents the formation of amorphous structure [ICDD no: 04-007-0541]. The peaks at 21.96^o (101) and 26.04^o (011) corresponds to presence of quartz [ICDD no: 04-008-8228] and cristobalite [ICDD no: 04-006-2056] structures as shown in Figure 6.1(b). The peaks at 35.78^o (111), 60.08^o (220), 71.83^o (311) (Figure 6.1(b)) confirm the stability of the textured β-SiC (cubic) phase of LSI composite sample and SiC coated hybrid composite sample. It was observed that the XRD pattern of TG tested SiC coated hybrid composite sample has showed less amorphous nature than LSI composite sample and also retained all the major intense peaks of cubic SiC along with few low-intensity peaks of SiO_2.

SEM analysis also reveals the presence of three different phases in LSI composite. This can be identified by color contrast i.e, bright-greyscale, dull greyscale, and black scale regions corresponding to Si, SiC and C_f respectively and the same is shown clearly in Figure 6.2(a). Densely packed columnar grains of SiC coating were noticed in Fig. 6.2(b) [1,2].

The distribution of elements present in the composites was studied by the EDS elemental mapping and line scanning as shown in Figure 6.3. This shows that the variation of Si and C was more prominent (Figure 6.3(a)) in the case of LSI composite. Whereas, in the case of the SiC

coating and SiC(CNFs) composite surface regions, Si and C variations were almost stoichiometric as evident from elemental analysis, line scan graph and also from the table, given in Figure 6.3(b). TG analysis shows that SiC coated hybrid composite samples formed an oxide layer of Si on the surface, which was confirmed by SEM-EDS as well as XRD analysis, as shown in Figure 6.1(b). After the TG test, the distribution of elemental oxygen was observed to be more on the surface of C_f/C-SiC composite compared to SiC coating and bare SiC(CNFs) region, as shown in Figure 6.3(c).

The microstructural change and elemental analysis of the LSI composites before and after the TG test is shown in Figure 6.4(a) and (b) respectively. It was observed that due to high-temperature oxidation, LSI composite formed an oxide layer on the surface and the presence of oxygen was also detected by the SEM-EDS study, as shown in Figure 6.4(b).

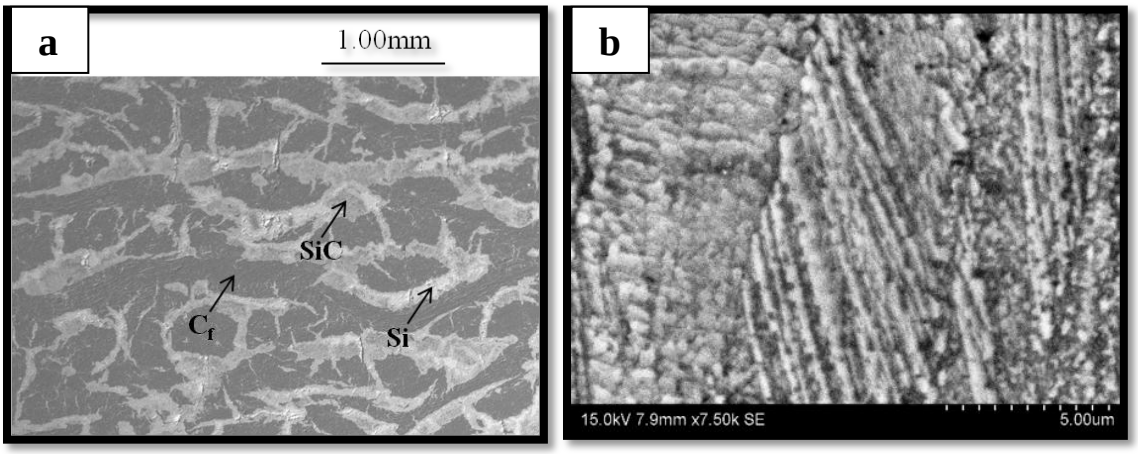

Figure 6.2: SEM image of a) cross-section of LSI composite (C_f/C-SiC) b) SiC-CVD coating.

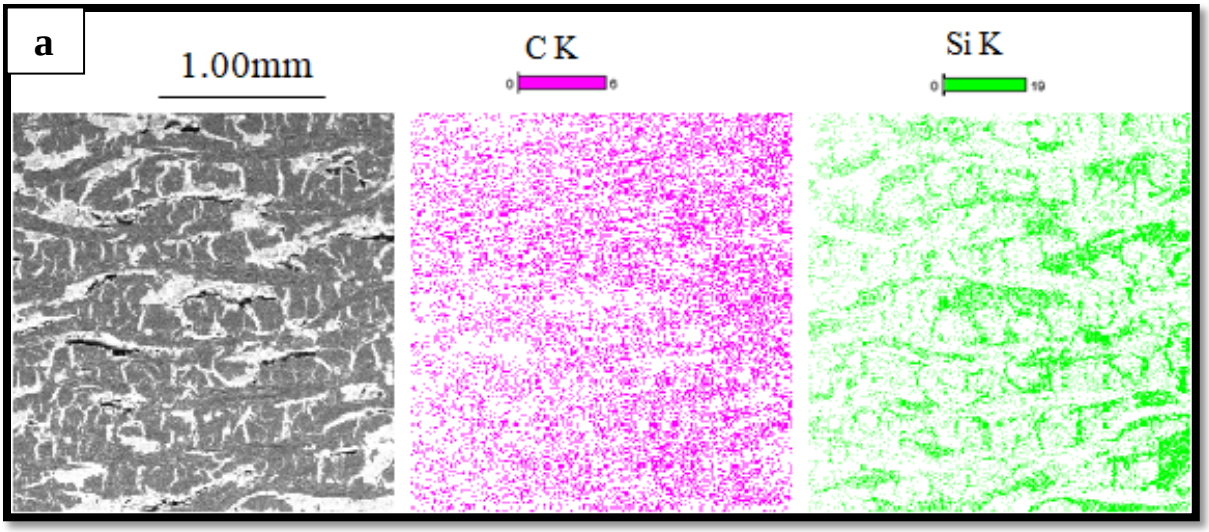

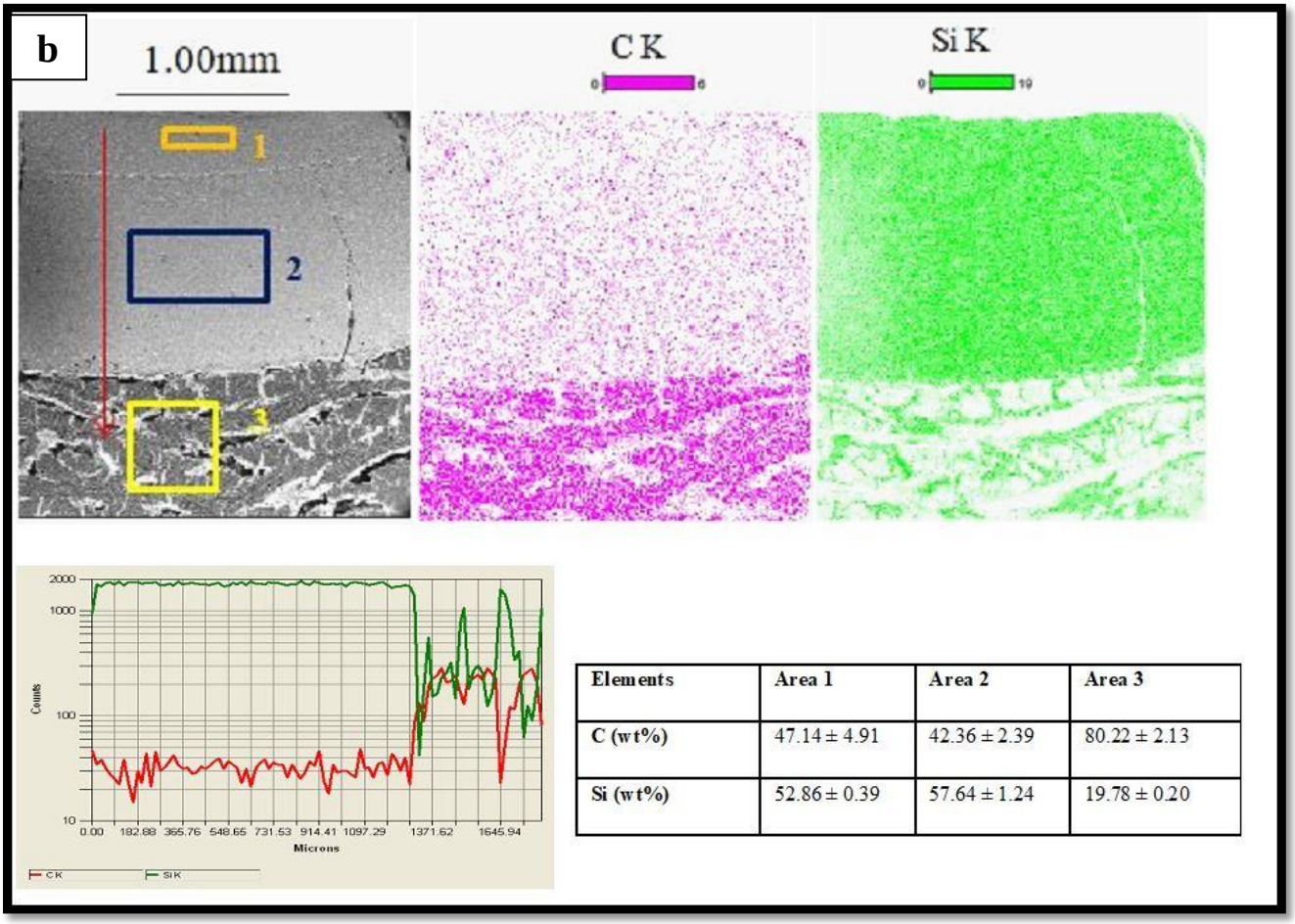

Elements	Area 1	Area 2	Area 3
C (wt%)	47.14 ± 4.91	42.36 ± 2.39	80.22 ± 2.13
Si (wt%)	52.86 ± 0.39	57.64 ± 1.24	19.78 ± 0.20

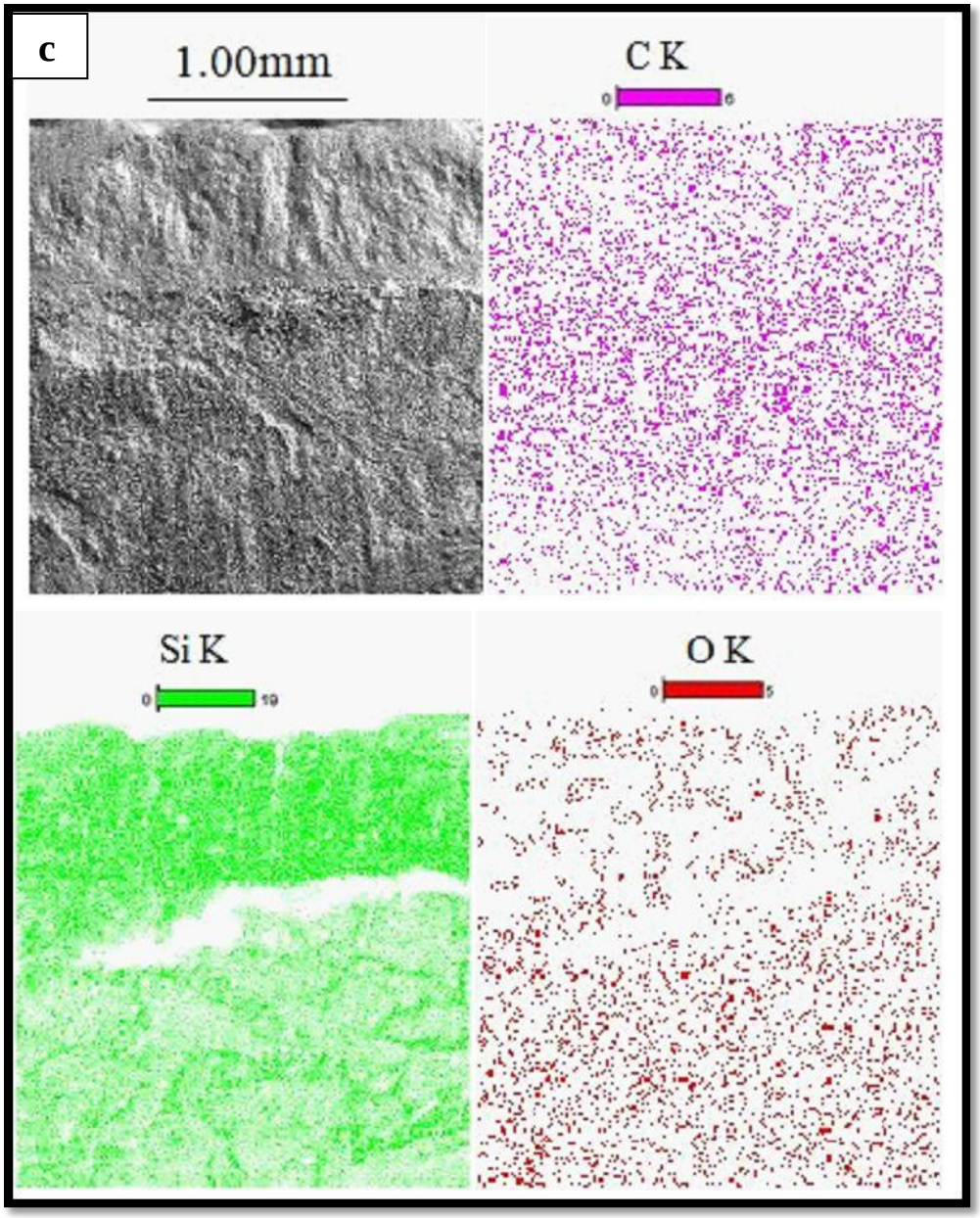

Figure 6.3: SEM, EDS (X-ray mapping, line scanning) analysis of a) C_f/C-SiC matrix b) and c) cross-section image of CVD SiC coated hybrid composite sample before and after TGA test respectively.

6.1.2 *Physical and mechanical properties analysis of hybrid composite tubes*

The density of LSI C_f/C-SiC composites of differently braided carbon fabric was measured using Archimedes principle, and the results were as listed Table 6.1. From the results, a slight variation in the density of the infiltrated tubes with respect to the type of braiding pattern was observed

and expected due to the braiding process of the fabric. Finally, the tubes were provided with CVD coating. Prior to CVD coating, the Si infiltrated tubes were surface smoothened through grinding for better adherence of coating. The density of the applied CVD-SiC coating was measured to be 3.20 g/cc, which is nearly equal to the theoretical value, as shown in Table 6.2. The mechanical properties of the coating were evaluated as per ASTM standard, which is discussed in subsequent sections.

Table 6.1: Densities of the LSI composites (C_f/C-SiC).

Samples	**SiC (CNFs) tubes**	**8H satin HSC**	**Quadriaxial NCF**	**8H satin SYG**
Avg. Density (g/cc)	3.13 ± 0.01	2.08± 0.03	2.11± 0.02	2.35± 0.02

Table 6.2: Physical and mechanical properties of CVD SiC coating.

Samples	**Avg. Density (g/cc)**	**Avg. Hardness (GPa)**	**Avg. Fracture toughness ($MPam^{1/2}$)**
CVD SiC coating	3.20± 0.01	28.76± 0.23	3.94± 0.11

6.1.3 *Thermogravimetric analysis (TGA)*

To investigate the influence of CVD-SiC coating on the oxidation resistance of C_f/C-SiC composites, TGA was conducted in the air (ambient), from room temperature (RT) to 1450°C. Oxidation process was at work as shown by weight change of the compositions which is captured in TG analysis. A slight increase in the weight of the samples was seen in the early stage of oxidation (25-100 °C), which could be attributed to the buoyancy effect of TGA equipment [3,4]. The onset of the oxidation process of as received C_f was observed to be around 300 °C and the whole oxidation process was completed at 500 °C, shown in Figure 6.1(a). In the case of LSI composite, the reaction between the oxygen and the exposed C_f/C preform resulted in rapid weight loss due to the evolution of carbon oxides at a temperature beyond 650 °C till

1350 ^{o}C. This process was very rapid and substantial weight change was observed as a result of the release of gaseous by-products formed through reactions (6.1) and (6.4) [5].

$C(s) + O_2(g) \rightarrow CO_2(g)$ Equation (6.1)

$C(s) + \frac{1}{2} O_2(g) \rightarrow CO(g)$ Equation (6.2)

$CO(g) + \frac{1}{2} O_2(g) \rightarrow CO_2(g)$ Equation (6.3)

$2C(s) + O_2(g) \rightarrow 2CO(g)$ Equation (6.4)

The oxidation of SiC at high temperature may be either passive or active based on the factors mentioned earlier. Active oxidation is prevalent at low oxygen pressure (< 1 bar), where the reaction between SiC and oxygen leads to the formation of a gaseous form of SiO as per equation (6.5). With active oxidation, rapid change in the weight leading to a catastrophic decrease in the strength of the composite can be observed [6].

$SiC(s) + O_2(g) \rightarrow SiO(g) + CO(g)$ Equation (6.5)

The passive oxidation is preceded by oxygen pressure close to one bar (high oxygen pressure) and forms a solid SiO_2 layer based on the following equations (6.6), (6.7) and (6.8).

$SiC(s) + 2O_2(g) \rightarrow SiO_2(s) + CO_2(g)$ Equation (6.6)

$2SiC(s) + 3O_2(g) \rightarrow 2SiO_2(s) + 2CO(g)$ Equation (6.7)

$Si(s) + O_2(g) \rightarrow SiO_2(s)$ Equation (6.8)

The passive oxide layer makes SiC stronger by blunting the strength limiting surface flaws [7]. Deposition of the oxide layer (SiO_2) on the surface of SiC coating leads to a net increase in the mass of the sample. In the present study, the test conditions were suitable for the formation of a passive oxide layer on the surface of SiC coated hybrid composite samples. LSI composite has shown weight gain beyond the temperature range of 200-1350 $^{\circ}$C due to simultaneous oxidation of free Si and SiC. Hence, the overall residual mass of LSI composite during the test from RT to 1450 $^{\circ}$C was observed to 24 %, as shown in Figure 6.5(a).

The CVD SiC coating forms a smooth and dense SiO_2 oxide layer than the SiC processed through other routes [8]. Hence, unlike LSI composite, the diffusion and further reaction with the oxygen was restricted in CVD SiC coated composites. Therefore, no significant weight change was observed even at high temperatures. On the other hand, in the case of LSI composite, after gaining weight in the initial oxidation process, continuous weight loss was observed at later stages at a temperature beyond 650 ^{o}C as shown in Figure 6.5(a). In the present study, the weight gain in the SiC coating was marginal which can be attributed to the formation of a few nanometer thin SiO_2 layers. The literature has also revealed that pure SiC processed through CVD allows the formation of a very thin (~100-300 nm) layer of SiO_2 scale on the surface [9]. Also, in our present study, the CVD coating with enough thickness (500-800 µm) was able to prevent further penetration of oxygen through the thin SiO_2 layer. Hence, no further oxidation or weight change was observed and a more linear TGA graph can be seen in Figure 6.5(a). SiC coated hybrid sample has retained its crystal structure and shown the formation of SiO_2 with low-intensity XRD peaks. However, XRD analysis of TG tested LSI composite samples show an amorphous structure. The TG tested CVD SiC coated C_f/C-SiC hybrid composite samples showed overall residual mass of 0.7 %, which shows the excellent oxidation resistance of hybrid composite tubes when provided with dense and uniform SiC coating.

Literature survey also reveals that high-temperature oxidation kinetics of SiC follows parabolic law of oxidation, which can be expressed as

$$X^2 = K_p t \qquad \text{Equation (6.9)}$$

Where X is scale (SiO_2) thickness, t- time, K is parabolic rate constant.

Therefore, the rate of oxidation is inversely proportional to the oxide layer thickness.

The residual mass and oxidation time curve are shown in Figure 6.5(b) for all the samples. The oxidation of carbon fabric was very rapid (~ within 40 min) and it oxidized completely at 650 ^{o}C. In the case of LSI composite, the weight gain was seen after 20 min of oxidation with increase in temperature. The liner oxidation process was continuous up to 650 ^{o}C beyond which weight loss was observed after 60min of oxidation due to the oxidation of a few exposed uncoated C_f/C preform. The reason for weight gain after 60 min of oxidation can be attributed to the oxidation

of free Si and SiC. The CVD SiC coated hybrid composite tube showed no significant weight change with the onset of oxidation time. Figure 6.5(b) reveals that the oxidation rate of CVD SiC coated hybrid composite is negligible compared to carbon fabric and LSI composite even at high temperatures. The high-temperature stability of CVD SiC coated composites at temperatures as high as 1450 ^{o}C can be seen from the TGA graph shown in Figure 6.5.

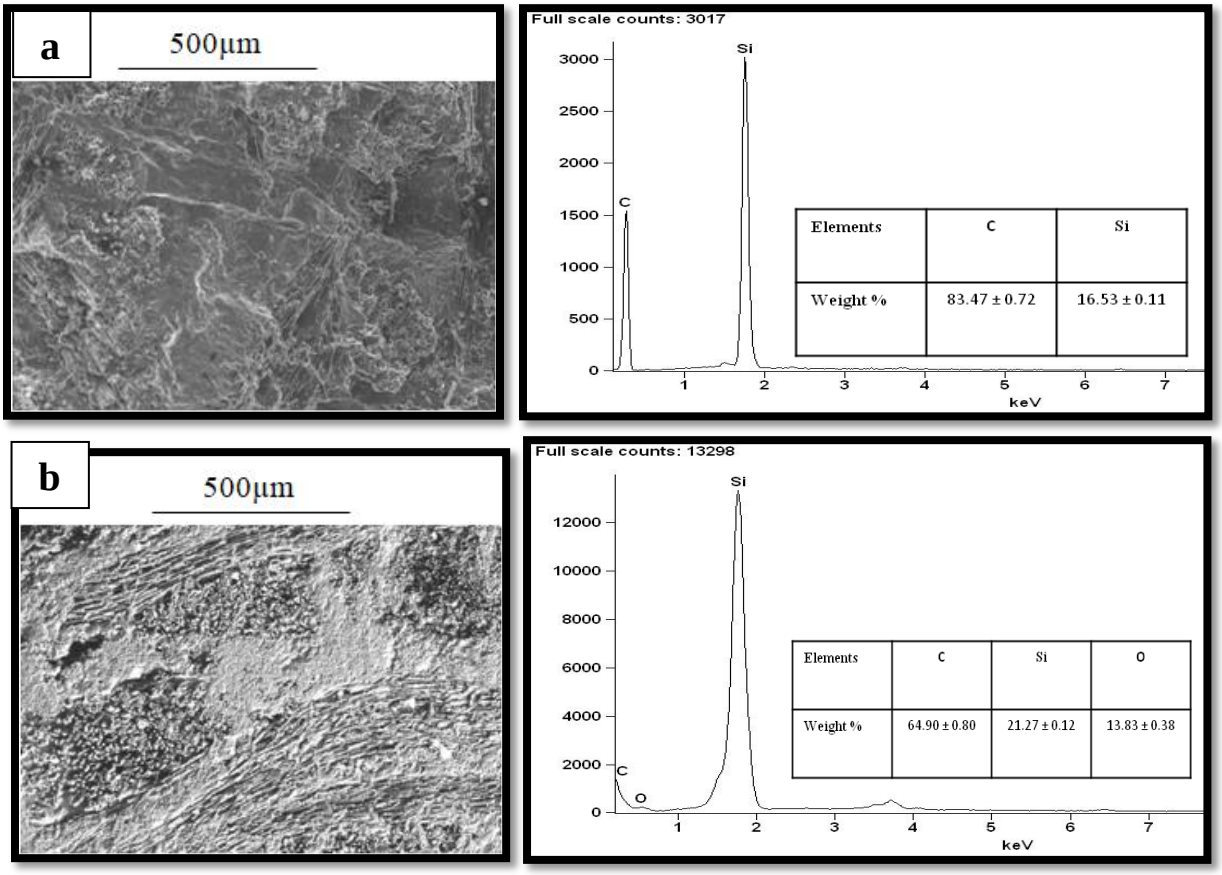

Figure 6.4: SEM-EDS analysis of LSI C_f/C-SiC composite a) before and b) after TG test.

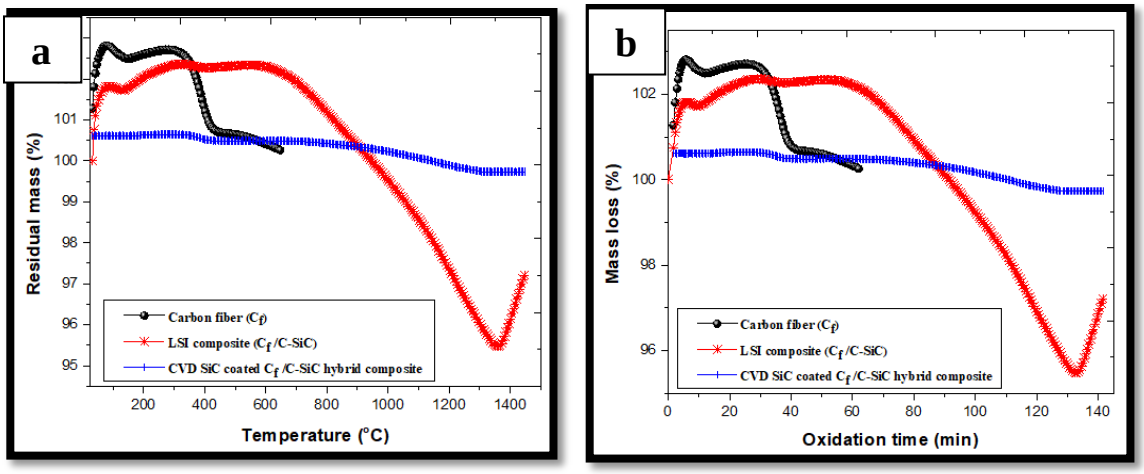

Figure 6.5: Thermogravimetric analysis of mass change in samples with respect to a) temperature b) oxidation time.

6.2 Conclusions

1. Sintered SiC(CNFs) composite tubes braided with different carbon fabric and weaving patterns were infiltrated with liquid silicon.
2. The infiltrated tubes were further coated with SiC by CVD technique to fabricate SiC coated C_f/C-SiC hybrid composite tubes.
3. SEM-EDS line scan of SiC coated hybrid composite has shown stoichiometric distribution of Si and C on SiC coating. The formation of oxide layer (SiO_2) on the surface of CVD SiC coated hybrid composite and LSI composite was observed after the TG test. The EDS elemental analysis revealed the presence of elemental oxygen which was more in the case of bare LSI composite compared to SiC coating.
4. The overall residual mass of TG analysis was found to be 24 % and 0.7 % respectively for LSI and SiC coated hybrid composite samples.
5. The oxidation of CVD SiC coated SYG braided hybrid composites showed minimal mass change and oxidation as revealed by TG and XRD analysis, due to the formation of dense CVD layer on the surface which restricts to form only a thin layer of SiO_2 on the surface during the high-temperature heating process.
6. Hence, the CVD coated liquid Si infiltrated C_f/C-SiC hybrid composite tubes can be explored for high-temperature load-bearing applications because of the vastly improved mechanical and oxidation properties.

6.3 References:

[1] Alberto Ortona, Thomas Fend, Hyun Woo Yu, Kati Raju, and Dang Hyok Yoon: *J. Eur. Ceram. Soc.*, 2014, vol. 34, pp. 1131–38.

[2] Uwe Schulz, Oriane Bernardi, Andrea Ebach-Stahl, Robert Vassen, and Doris Sebold: *Surf. Coatings Technol.*, 2008, vol. 2003, pp. 160–70.

[3] Paul Gabbott: *Principles and Applications of Thermal Analysis*, John Wiley & Sons, 2008, pp. 119–163.

[4] T. C. Vaimakis, *Thermogravimetry (TG) or thermogravimetric analysis (TGA)*, Chemistry department, Univeristy of Ioannina, Greece, 2013.

[5] Antonio Vinci, Luca Zoli, Elena Landi, and Diletta Sciti: *Corros. Sci.*, 2017, vol. 123, pp. 129–38.

[6] J W Hinze and H C Graham: *J. Electrochem. Soc.*, 1976, vol. 123, pp. 1066–73.

[7] Yung-Jen Lin and Lee-Jen Chen: *Ceram. Int.*, 2000, vol. 26, pp. 593–98.

[8] Takayuki Narushima, Takashi Goto, and Toshio Hirai: *J. Am. Ceram. Soc.*, 1989, vol. 72, pp. 1386–90.

[9] E. Ramberg, G. CrucianiK. E. Spear, R. E Tressler: *J. Am. Ceram. Soc.*, 1996, vol. 76(11), pp. 2897–2911.

CHAPTER 7

Surface properties evaluation of SiC-based composites using high speed nanoindentation technique

7.0 Introduction

In the present study, an advanced high-speed nano-indentation technique was employed to analyze the combined benefit of the particulate and continuous carbon fibers' reinforcing effect on SiC matrix. The properties of CVD SiC coated SiC based composite tube samples were evaluated using conventional processes as well as nano-indentation technique to compare the properties at different length scales. Attempts have been made to correlate the structure-property relations of complex multi-phase of SiC composites employing high-speed nano-indentation mapping as well as XRD, Digital optical, SEM and TEM analysis. The critical analysis of the structure-property correlation at the micrometer length scale helps in designing complex structures of fiber-containing SiC-based composites for applications in the fields of defense, nuclear, aerospace etc.

7.1 Results and Discussions

The crystal structure analysis of CVD coated SiC-based hybrid composite samples was studied individually with X-ray diffraction patterns is described in section 7.1.1. The microstructure and mechanical properties correlation with nano-indentation maps is explained in section 7.1.2. A comparative study on the properties of the samples with conventional tests and high-speed nano-indentation test results were discussed in section 7.1.3.

7.1.1 *XRD phases of the samples*

XRD pattern of monolithic SiC and SiC-CNFs composite with intense peaks at 34.22 ^{o}, 35.77 ^{o}, 38.27 ^{o}, 41.51 ^{o}, 60.13 ^{o}, 71.88 ^{o} and 73.46 ^{o} in Figure 7.1(a, b) correspond to α-SiC in the form of 6H polytype (ICDD File no.01-075-8314). The CVD SiC coating reports the reflection peaks at 35.6 ^{o}, 59.9 ^{o}, 71.8 ^{o} and 75.5 ^{o} corresponding to cubic SiC (ICDD File no. 04-008-4949) as shown in Figure 7.1(c). The XRD analysis of SiC hybrid composite has shown the corresponding 2θ value and diffraction planes of the phases represent 6H-SiC, in Figure 7.1(d).

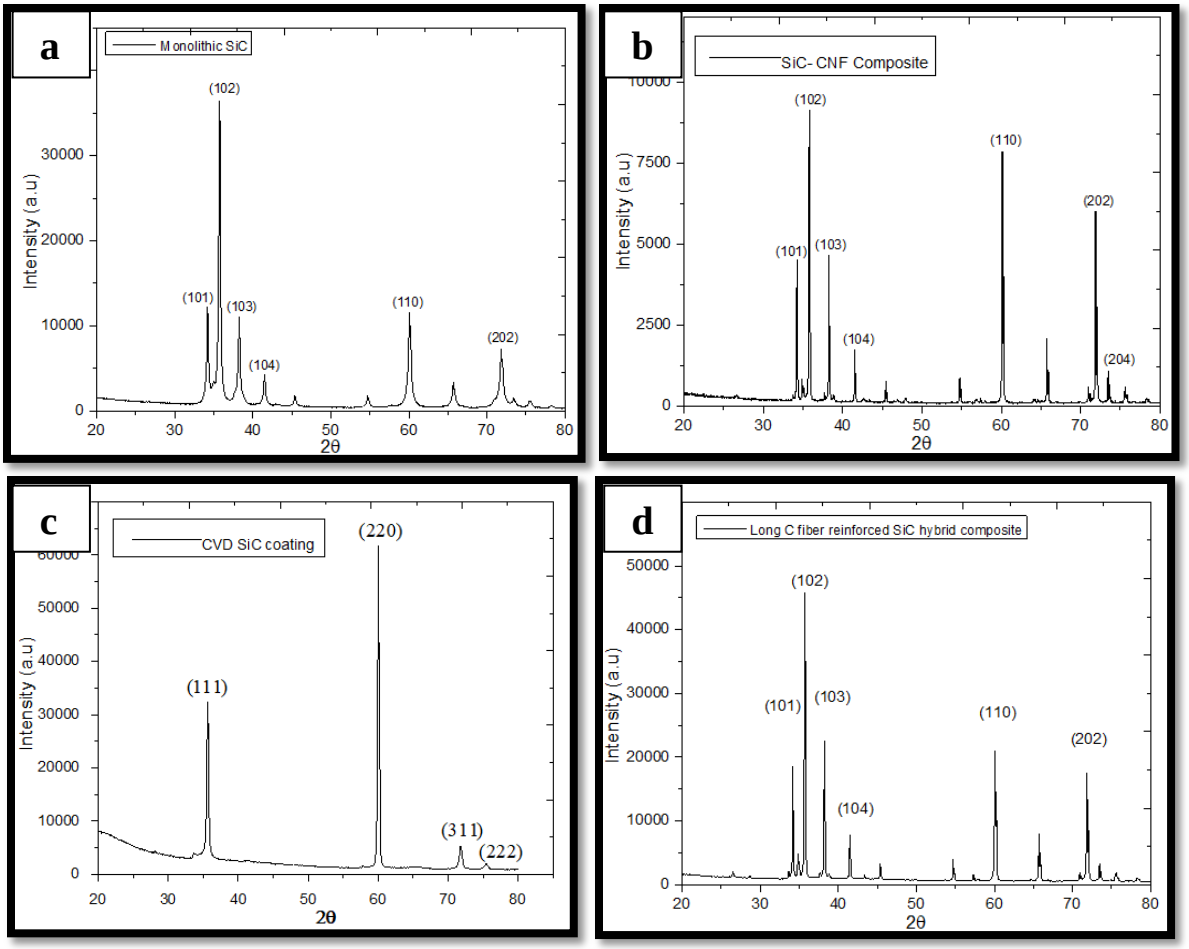

Figure 7.1: XRD phase analysis of a) monolithic SiC b) SiC-CNFs composite c) CVD SiC coating d) long C fibers reinforced SiC hybrid composite.

7.1.2 *Microstructure-property correlation*

The mechanical property maps (hardness (H) and elastic modulus (E)) obtained from the high-speed nano-indentation test and respective microstructure are correlated in this section to understand phase level properties.

The high-speed nano-indentation maps with different colors indicate the varied range of E or H values, and this feature may be due to the change in grain orientation, presence of multi phases, loose particles, pores, agglomerates or evolution of new phases. Although there is ambiguity about the variation of mechanical properties when indenter lands on any of the features specified

above, in the present study, the Berkovich indenter with indent spacing 1.5 μm provides reasons for the structure-property correlation at the micrometer length scale [1].

A. *Monolithic SiC:*

The in-house processed monolithic SiC sample showed equiaxed grain structure for which the indentation maps are shown in Figure 7.2(a). This grain structure can be attributed to the grain growth-inhibiting action of sintering additives (carbon and boron) during the sintering process. The soft and hard phase present in the sample with variation in hardness ranging from 15-35 GPa is shown in Figure 7.2(b). The difference of the elastic modulus ranging from 250-600 GPa of the phases, is as shown in modulus map Figure 7.2(c). The sintered polycrystalline SiC sample being anisotropic, such range in variation of properties can be expected, in addition to which few specific grains were noted to be having higher hardness (> 35 GPa) and higher modulus values (> 500GPa), as shown in Figure 7.2. The softer phases have hardness and elastic modulus in the range of 10-20 GPa and 250-350 GPa, respectively. The average hardness and elastic modulus of the monolithic SiC sample obtained from mapping were observed to be 29.67 GPa and 473.68 GPa, respectively.

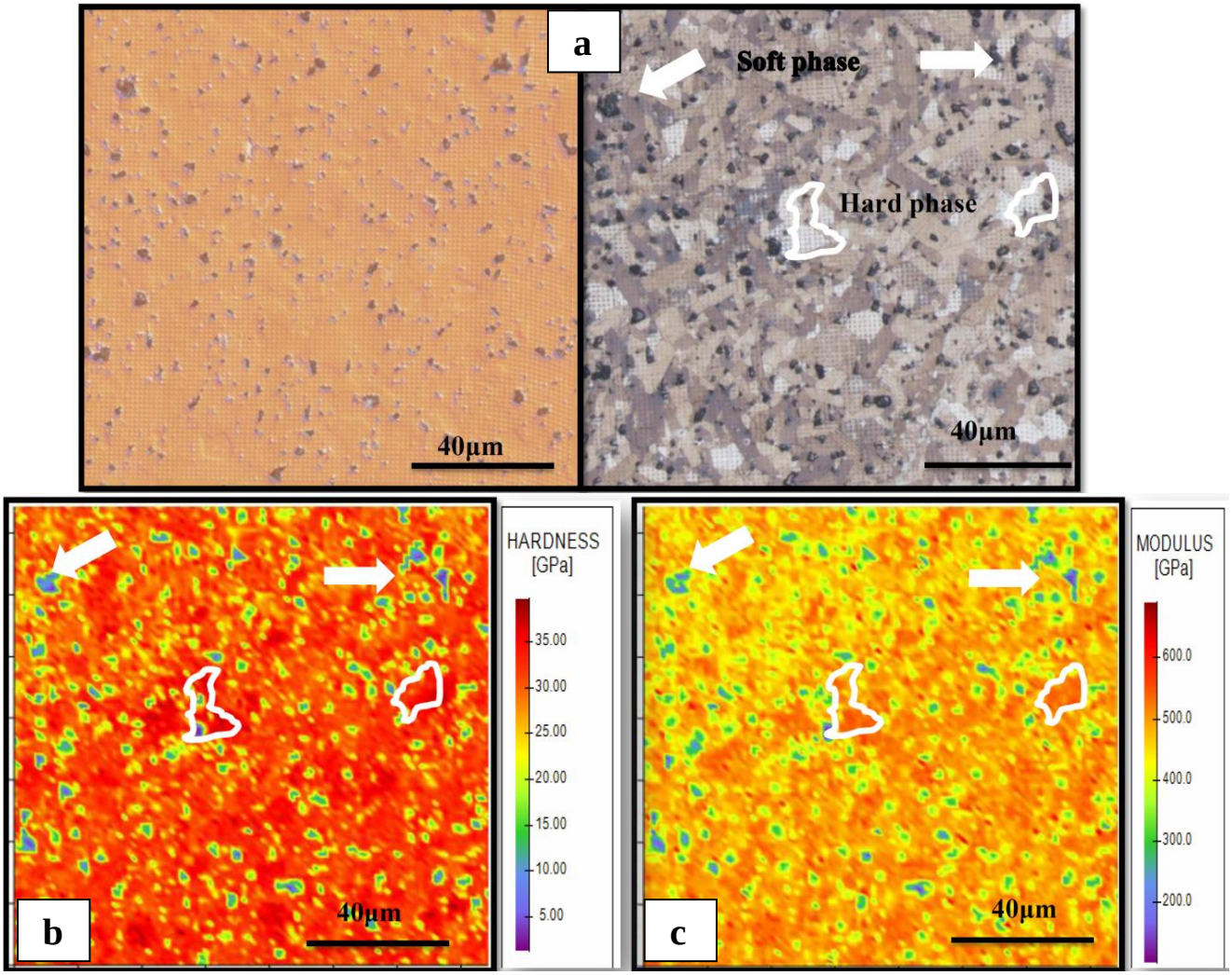

Figure 7.2: High-speed nanoindentation of monolithic SiC a) digital optical image map, b) hardness map and c) modulus map.

B. ***CVD SiC coating:***

CVD SiC coating was characterized by a homogenous matrix consisting of elongated columnar grains as evident from the microstructure and the indentation maps in Figure 7.3. The directionality in the properties (E & H) of the coating with respect to the arrangement of elongated grains may be seen from Figure 7.3(b, c). The directional growth of the cubic crystalline structure of SiC coating was also determined from XRD analysis (Figure 7.1(c)). The variation in the hardness and elastic modulus of the coating was observed to be in the range of 30-40 GPa and 500-600 GPa, respectively. When compared to monolithic SiC, the variation in the properties was very low due to the directionality of dense columnar grain structure. The

advantage of the columnar grain structure is that it reduces the stress build-up within the coating and provides high directional properties with uniform dense structure. This dense structure is an essential property for many thermal barrier coating and high-temperature creep resistant applications [2–4]. The overall average hardness and elastic modulus of CVD SiC coating maps were observed to be 33.06 GPa and 509.02 GPa, respectively.

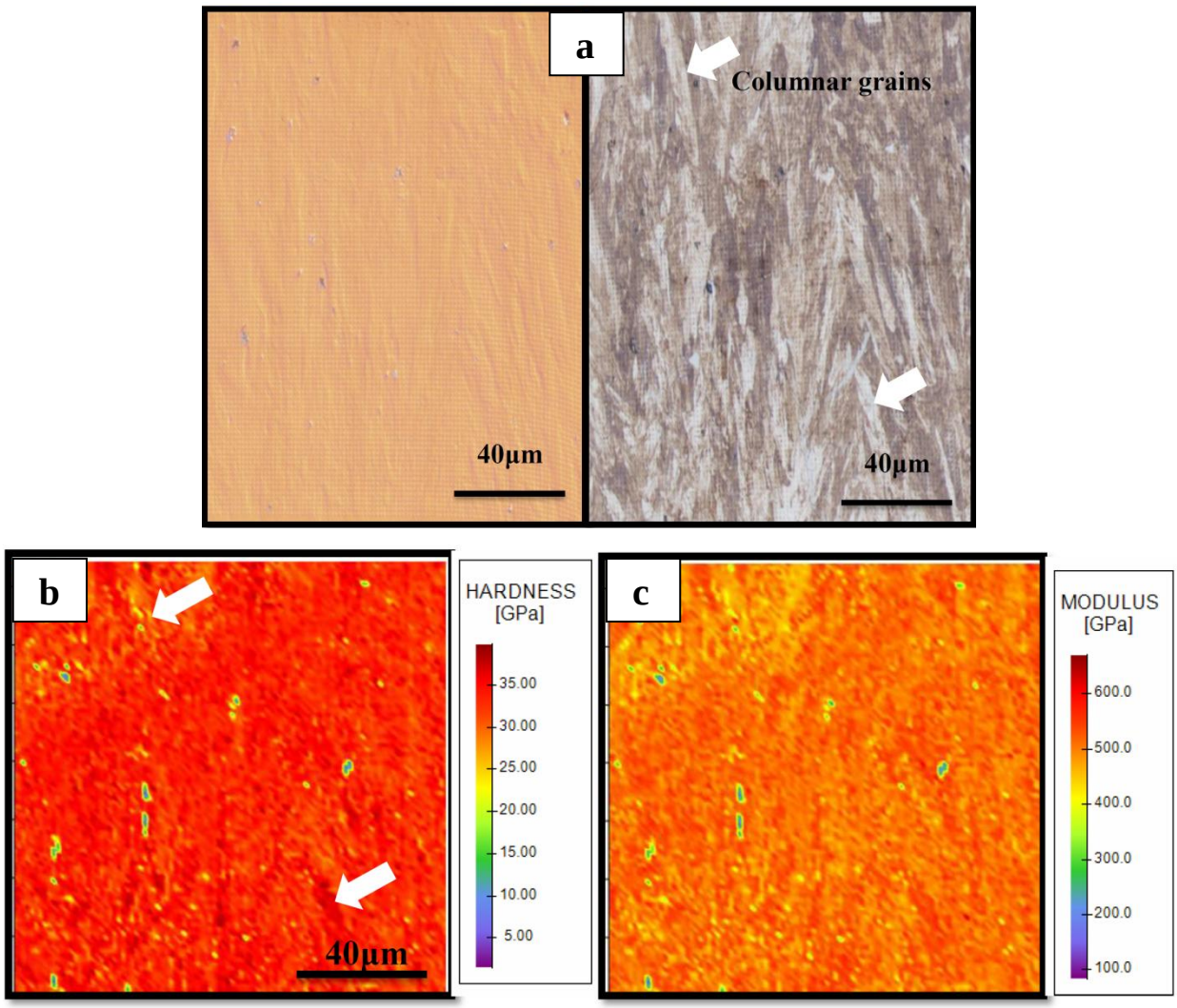

Figure 7.3: High-speed nanoindentation of CVD SiC coating a) optical image map, b) hardness map and c) modulus map.

C. *SiC-CNFs composite:*

The SiC-CNFs composite consists of SiC grains and CNFs phase in addition to many soft phases with an equiaxed grain structure in the maps representing the presence of secondary phases, and

unreacted loose carbon particles (incorporated as sintering aid) with occasional agglomerates, as marked in Figure 7.4(a). The dispersion of CNFs and the agglomeration of unreacted loose carbon particles in the SiC matrix are discussed in subsequent sections. SiC composite with CNFs dispersion has shown significant variation in properties compared to monolithic SiC and the CVD SiC coating, as shown in Figure 7.4(b, c). The change in the hardness and elastic modulus of the composite was observed to be in the range of 5-35 GPa, 150-600 GPa, respectively. The average hardness and elastic modulus of the SiC-CNFs composite sample obtained from mapping were 29.91 GPa and 472.99 GPa, respectively. The softer phases had hardness and elastic modulus in the range of 5-20 GPa and 150-350 GPa, respectively.

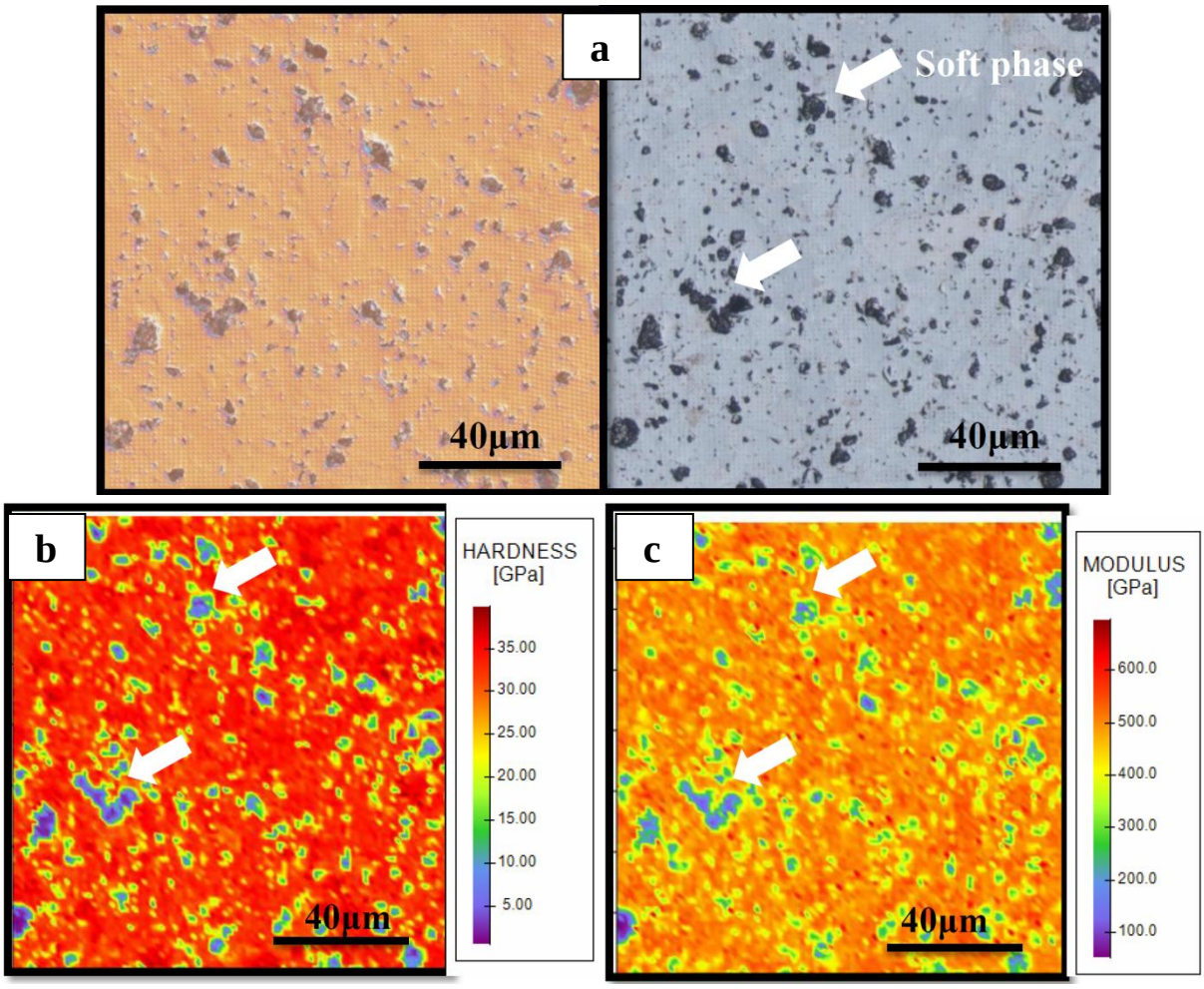

Figure 7.4: High-speed nanoindentation of SiC-CNFs composite a) optical image map, b) hardness map and c) modulus map.

D. *SiC hybrid composite:*

SiC hybrid composite has matrix material as SiC-CNFs composite in which long BN coated carbon fibers were reinforced continuously. As explained in the previous section, hybrid composite also shows weak phases in the hardness as well as elastic modulus map. The size of the weaker phases in the hybrid composite is slightly larger than the SiC-CNFs composite sample due to the presence of closed pores surrounded by unreacted free carbon particles adjacent to continuous carbon fibers reinforcement, as is clear from Figure 7.5(a). The variation in the hardness and elastic modulus of the composite was observed to be in the range of 5-35 GPa, 100-600 GPa, respectively, as shown in Figure 7.5(b, c). The average hardness and elastic modulus of the SiC hybrid composite sample obtained from mapping were observed to be 29.74 GPa and 472.05 GPa, respectively. The softer phases had hardness and elastic modulus in the range of 5-20 GPa and 100-350 GPa, respectively.

The weak bonding between the long C fibers and the composite matrix leads to the formation of loose carbon agglomerates [5]. High-resolution SEM-EDS analysis of such weaker spots in the map has shown carbon-rich region (from spectrum 2 and 3) which is indicated with arrows, as shown in Figure 7.5(d) and expected to be secondary phase dispersed region with free carbon particles, as specified above. The dispersion of secondary phases in the matrix can be seen from high magnification SEM and TEM analysis in the following sections. The overall composition of the sample is identified as having nearly stoichiometric SiC, which is clear from the EDS spectrum 1, shown in Figure 7.5(d) table.

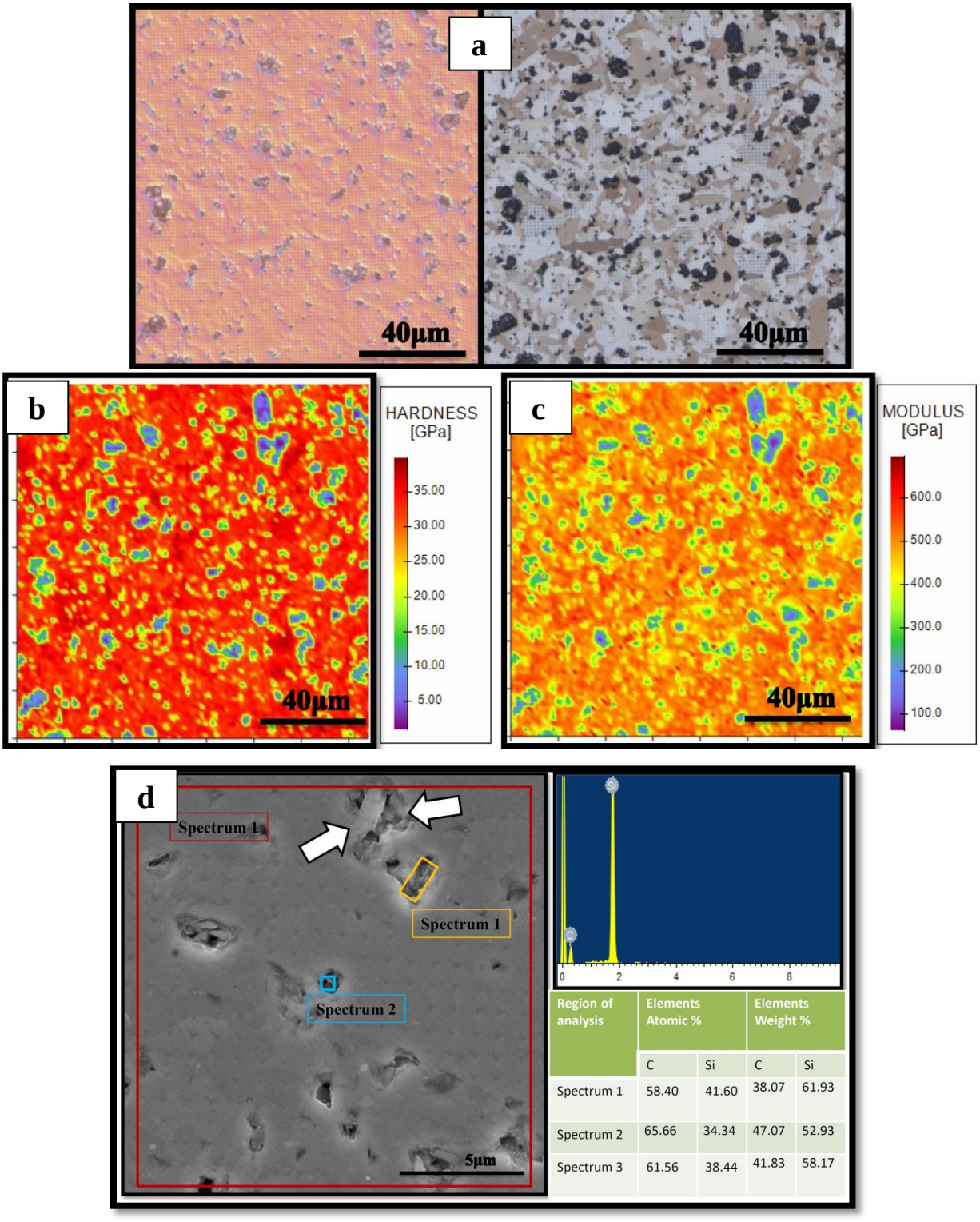

Region of analysis	Elements Atomic %		Elements Weight %	
	C	Si	C	Si
Spectrum 1	58.40	41.60	38.07	61.93
Spectrum 2	65.66	34.34	47.07	52.93
Spectrum 3	61.56	38.44	41.83	58.17

Figure 7.5: High-speed indentation of SiC hybrid composite a) optical image map b) hardness map, c) modulus maps and d) SEM-EDS analysis respectively.

The distribution of CNFs in the SiC matrix, as shown in the high-resolution TEM image Figure 7.6(a) is one of the primary reasons for significant variation in the hardness and modulus values of the composite, as discussed. However, it plays a vital role in optimizing the thermo-mechanical properties of the composite [6]. The cross-section of the sintered hybrid composite tube, as shown in Figure 7.6(b) (circled region), reveals the long C fiber distribution in the matrix, which is further illustrated at higher magnification in Figure 7.6(c).

It is apparent from Figure 7.6 (b, c) that the fibers are loosely bonded to the matrix, which helps avoid the micro and macro scale crack propagation in the matrix. Conversely, these loosely packed regions are accommodated with un-reacted free carbon, which was identified as weak regions in high-speed nano-indentation maps discussed in previous sections. The fracture surface of the hybrid tube reveals long fibre pull-outs, and the fiber bridging (marked with an arrow) is shown in Figure 7.6(d). Hence, it is expected that the weak bonding between the secondary phase material and the SiC matrix will enhance the fracture toughness of the composites by weakening the nearby grain boundaries. Further, the fibers also help in hindering grain growth.

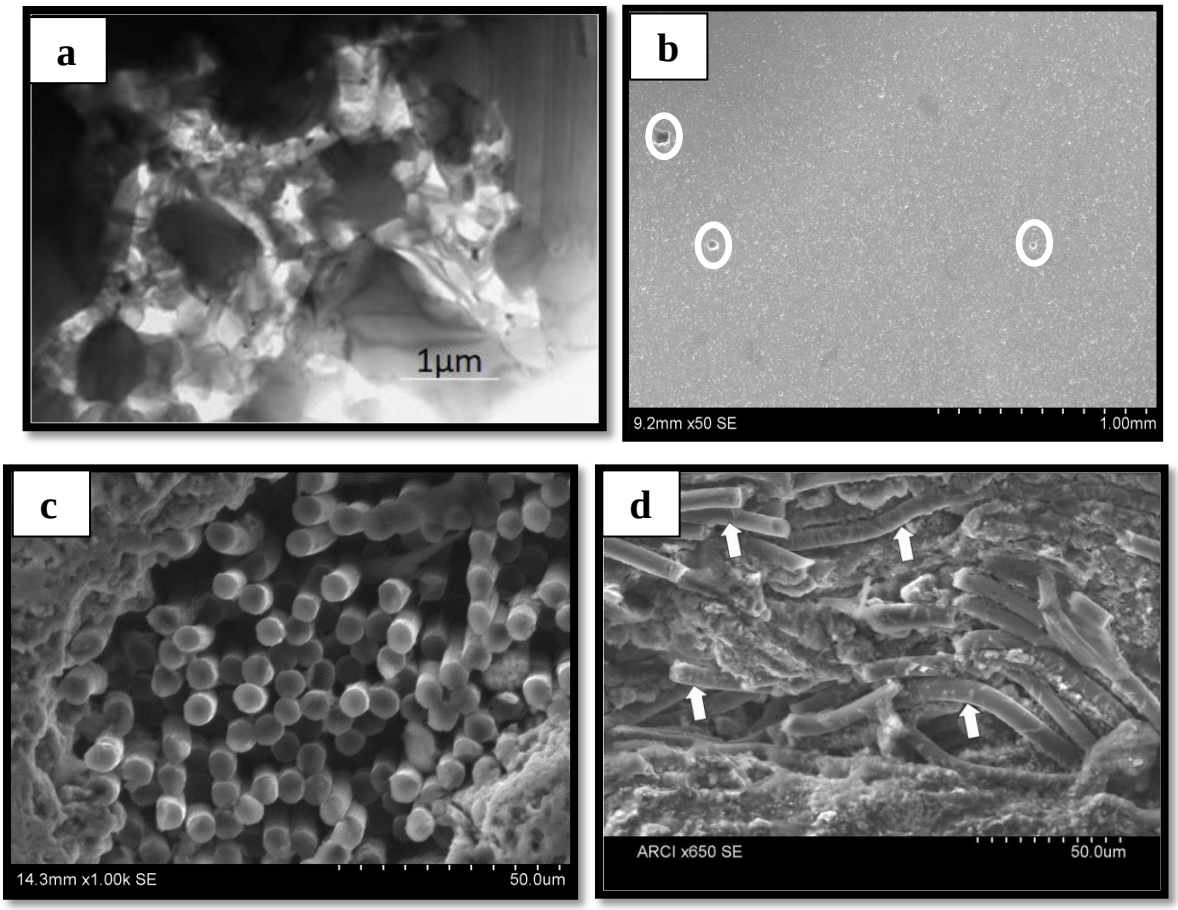

Figure 7.6: Hybrid composite a) TEM image of CNFs dispersion in the SiC matrix b) SEM cross-sectional image of long BN coated C fibers distribution c) high magnification image of (b) d) fracture surface of the hybrid composite tube.

7.1.3 *Averaged response comparison*

In the previous section, the structure-property correlation was presented to understand the effect of processing on the microstructure obtained. In this section, we present a comparison of the averaged properties for different samples.

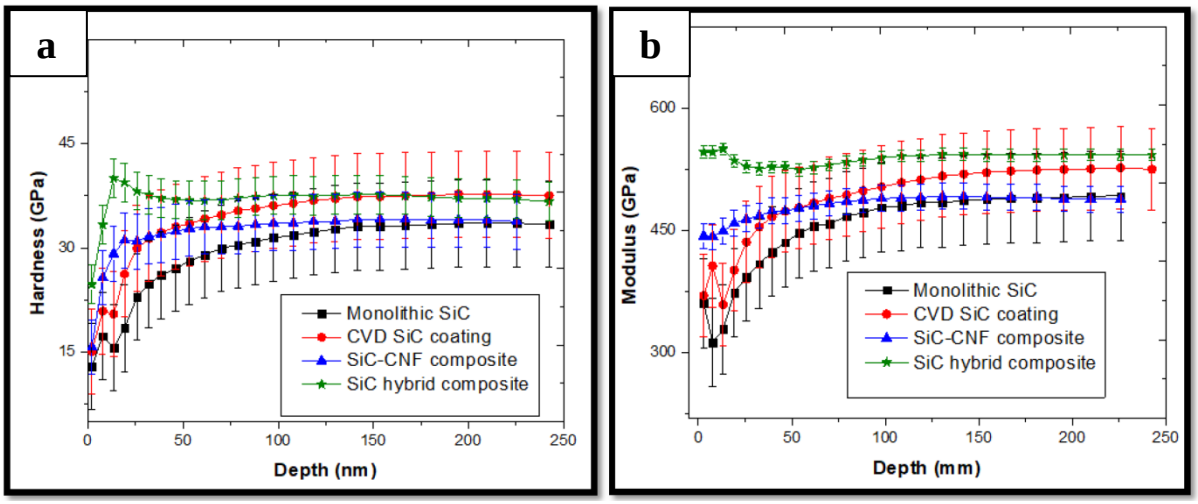

Figure 7.7: Conventional nanoindentation (CSM) test results, the average a) hardness b) modulus of the SiC samples.

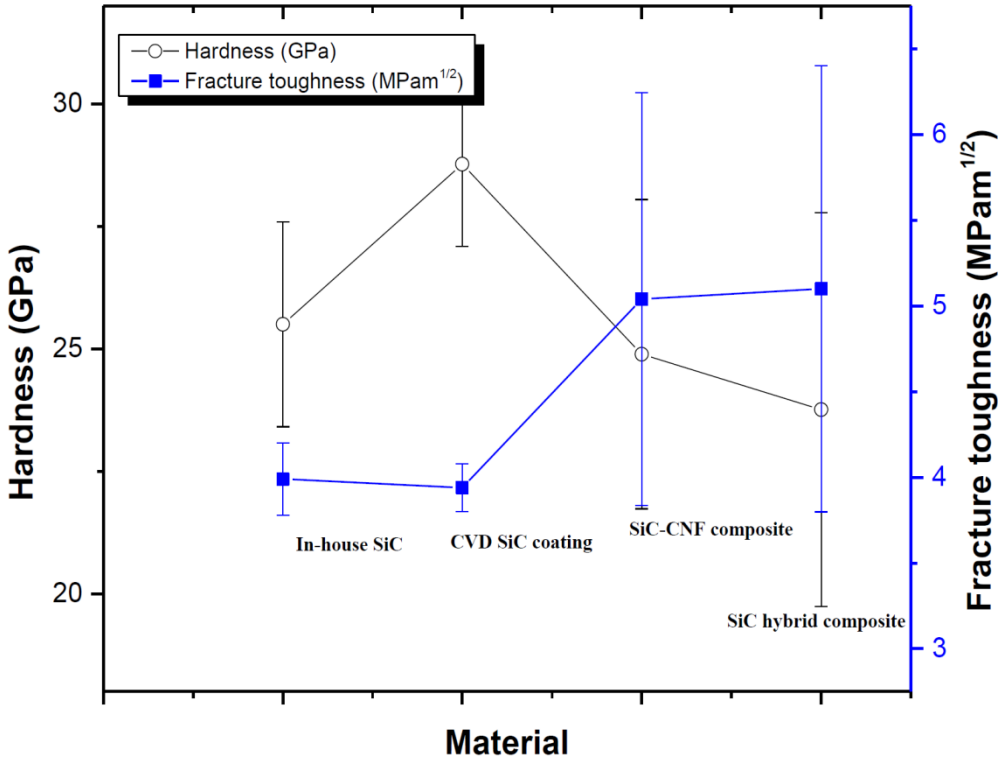

Figure 7.8: Average Vickers hardness and indentation fracture toughness of the SiC samples.

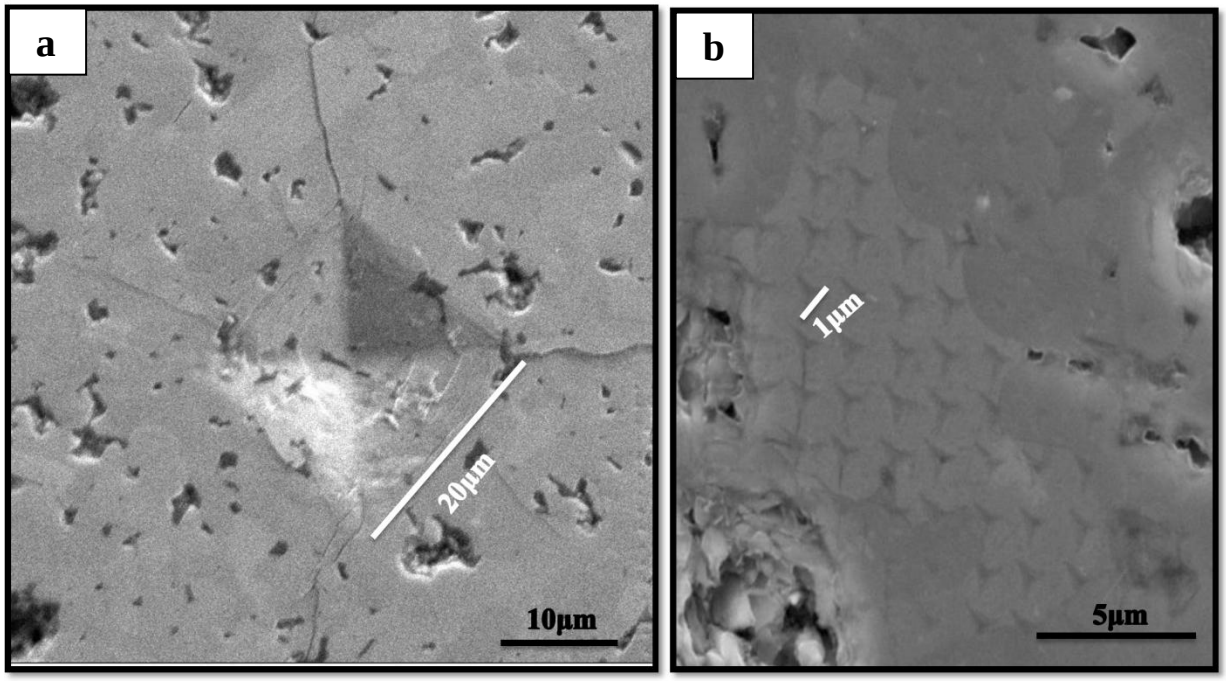

Figure 7.9: SEM image of a) square-based pyramid indent by Vickers test b)triangular based pyramid indent by high-speed nanoindentation test.

Table 7.1 summarizes the relative density, hardness, elastic modulus, and indentation fracture toughness of multi-phase hybrid composites determined from conventional methods (Vickers and CSM) and high-speed mapping data. CVD SiC coating was measured to have theoretical density with the highest hardness and elastic modulus among all the samples due to its uniform and dense columnar structure [7]. Conventional nano-indentation results of the hybrid composite show the highest hardness and modulus among all samples as shown in Figure 7.7, while Vickers hardness test results show the highest fracture toughness with small variation in hardness value as shown in Figure 7.8.

In Vickers hardness test, the indents were larger in size and the total area of contact was considered while measuring the properties, whereas in nano-indentation test the projected contact area was calculated from the penetration depth of the indent, which is the reason for variation in the values of the results as discussed and the differences (size and shape) were as shown in Figure 7.9 (a, b). High-speed nano-indentation mapping analysis was carried out keeping in mind the variation in properties at each indent with respect to the depth of penetration and the total

average of thousands of indents placed very close to each other. Due to close indentation maps, the small variation in properties was measured accurately and the interface properties between the fiber-matrix and surface coating-substrate matrix were visualized through micron range maps. However, the conventional nano-indentation (CSM) and Vickers test analysis results were the average values of some indents.

The improvement in the fracture toughness can be attributed to fibers bridging and fiber pullouts in the hybrid composites, as explained earlier (Figure 7.6(c)). High-speed nano-indentation mapping results of hybrid composite was shown to retain the base matrix (SiC-CNFs composite) properties with an additional advantage of improved fracture toughness as shown in Table 7.1, also evident from XRD analysis (Figure 7.1(d)).

Table 7.1: Physical and mechanical properties of the CVD SiC coated SiC composite samples.

Sample	**Relative Density (%)**	**Vickers Hardness (GPa)**	**Indentation fracture toughness ($MPam^{1/2}$)**	**Nanoindentation**			
				Elastic modulus (GPa)		**Hardness (GPa)**	
				CSM	**MAPPING**	**CSM**	**MAPPING**
Monolithic SiC	99.06	25.50 ± 2.09	3.99 ± 0.21	491.23 ± 20.39	473.68 ± 67.09	33.59 ± 2.05	29.67 ± 5.92
CVD SiC coating	99.60	28.77 ± 1.68	3.94 ± 0.14	524.58 ± 14.32	509.02 ± 35.86	37.60 ± 1.02	33.06 ± 3.06
SiC-CNFs composite	98.76	24.89 ± 3.16	5.04 ± 1.20	489.56 ± 19.32	472.99 ± 84.43	34.19 ± 1.87	29.91 ± 7.45
SiC hybrid composite	96.61	23.76 ± 4.02	5.10 ± 1.30	543.13 ± 9.55	472.05 ± 91.03	36.83 ± 1.71	29.74 ± 7.91

7.2 Conclusions

1. The monolithic α-SiC and SiC-CNFs composite powders were processed using advanced spray freeze granulation technique, and SiC-CNFs composite powder was used as a base matrix for the fabrication of SiC hybrid composite tubes.
2. The monolithic SiC, SiC-CNFs composite thin tubes (1-2 mm) and thick SiC hybrid composite tubes (10-12 mm) with systematic laying pattern of continuous C_f in SiC-CNFs matrix were shaped using cold isostatic pressing (CIP) and subsequently pressureless sintered and surface coated with β-SiC through CVD process.
3. Comparative evolution of mechanical properties of monolithic SiC, SiC-CNFs composites, CVD SiC coating, and SiC hybrid composite was studied using conventional processes (Vickers & CSM) and advanced high-speed nano-indentation mapping.
4. An excellent correlation between the microstructure and mechanical properties has been made with the help of massive data generated through high-speed nano-indentation mapping.
5. Uniform and dense columnar structured CVD SiC coating with the cubic phase showed superior mechanical properties (hardness and elastic modulus).
6. Hybrid composite processed with BN coated continuous carbon fibers, reinforced in SiC-CNFs matrix has shown improved fracture toughness while retaining other superior base matrix properties.
7. Hybrid composite with weak inter-phase bonding between continuous C fibers and the matrix helped to optimize the fracture toughness by restricting crack propagation through fiber pullouts.
8. The insight studies on the structure-property correlation with high-speed nano-indentation mapping at the micrometer length scale helped to design the complex structure of fiber-containing SiC-based composites for defence, nuclear and aerospace applications.

7.3 References:

[1] F. Solá and R. Bhatt: *Mater. Lett.*, 2015, vol. 159, pp. 395–98.

[2] Zhiying Hu, Dingheng Zheng, Rong Tu, Meijun Yang, Qizhong Li, Mingxu Han, Song Zhang, Lianmeng Zhang, and Takashi Goto: *Materials (Basel).*, 2019, vol. 12, pp. 1–10.

[3] I. K. Igumenov and A. N. Aksenov: *Therm. Eng.* , 2017, vol. 64, pp. 865–73.

[4] J. R. Vargas Garcia and Takashi Goto: *Sci. Technol. Adv. Mater.*, 2003, vol. 4, pp. 397–402.

[5] D. Frazer, M. D. Abad, D. Krumwiede, C. A. Back, H. E. Khalifa, C. P. Deck, and P. Hosemann: *Compos. Part A Appl. Sci. Manuf.*, 2015, vol. 70, pp. 93–101.

[6] Mubina Shaik, Asit Kumar Khanra, and Bhaskar Prasad Saha: *Mater. Chem. Phys.*, 2018, vol. 220, pp. 225–32.

[7] Siti Aisyah Zawawi, Azrul Azlan Hamzah, Burhanuddin Yeop Majlis, and Faisal Mohd-Yasin: *Jpn. J. Appl. Phys.*, 2019, vol. 58, pp. 1–16.

CHAPTER 8

Summary, Future plan of the work, Implications and List of Publications

8.0 Summary

- Earlier studies reported in the literature have explained the influence of secondary phase (carbon fibers) addition on the properties of SiC based composites. In this regard a detailed study was carried out in the present work, with the incorporation of different types of reinforcement in in-house fabricated SiC based composites by adopting various processing techniques.

- Fabrication of SiC based composites through various powder processing routes such as rotary evaporation, conventional route, advanced freeze granulation etc. was carried out. Surface modification of CNFs and spray freeze granulation process were used to produce well-dispersed spherical SiC – CNFs composite powder.

- A systematic study was carried out to optimize the process parameters of SiC-CNFs composites using Taguchi approach. The material properties of the composites were optimized through design of experiments to optimize parameters like sintering temperature, heating rate, holding time using different CNFs compositions for the experimental design method with an L_9 (3^4) orthogonal array. The surface treated CNFs and BN coated long C fibers incorporated SiC-based hybrid composite tubes of various dimensions were fabricated using CIP and pressureless sintering process.

- Highly dense green tubes produced out of surface modified 1 wt % CNFs composite spherical granules could achieve 98.5 % theoretical density and exhibited 25.62 GPa, 464.79 MPa and 5.14 $MPam^{1/2}$ of hardness, strength and fracture toughness values respectively, which are highest amongst all the other composites. The thermal conductivity value of 1 wt % CNFs containing composite was measured from room temperature to 1000 °C and found to be more than the monolithic SiC samples, which can be attributed to the strong bond between high thermal conductive CNFs with SiC matrix and high angle grain boundaries with less phonon scattering as evident from the HR-TEM & EBSD analysis. Highly dense CVD-SiC coating was employed on SiC tubes to form uniformly distributed stoichiometric coating with improved physical and mechanical properties as revealed by SEM & EDAX analysis.

- The sintered SiC-CNFs composite tubes were wrapped with long carbon fiber (C_f) of different braiding patterns for LSI. The surface properties of the sintered and LSI C_f/SiC hybrid composite

tubes (C_f/SiC-SiC(CNFs)) were further enhanced by coating with SiC by adopting chemical vapour deposition technique.

- The qualitative and quantitative phase analysis of BN-C_f, SiC-CNFs matrix and SiC based hybrid composite samples was analyzed by X-ray diffraction (XRD), selected area electron diffraction (SEAD), SEM, FTIR and Rietveld refinement using MAUD software. In addition, influence of new secondary phase evolved (B_4C), CNFs dispersion and long C_f reinforcement on optimization of physical and mechanical properties of the SiC hybrid composite were studied.

- The physical and mechanical properties of CVD SiC coated SiC-CNFs composites have been measured. The effect of variables on the properties of the composites was studied from the signal to noise ratio (S/N), analysis of variance (ANOVA), and interaction plots.

- The enhancement of oxidation resistance of LSI hybrid composite tubes by CVD SiC coating was also studied. The oxidation behavior of bare C_f, C_f/SiC composite and CVD- SiC coated C_f/SiC composite was examined separately using TGA under air from room temperature to 1350 ^oC. The overall residual mass of TG analysis was found to be 24 % and 0.7 % respectively for LSI and SiC coated hybrid composite samples. The oxidation of CVD SiC coated SYG braided hybrid composites has shown minimal mass change and oxidation as revealed by TG and XRD analysis due to the dense CVD layer on the surface which restricts the formation of SiO_2 on the surface during the high-temperature heating process.

- An advanced high-speed nanoindentation technique was employed to analyze the combined benefit of the particulate and continuous fiber reinforcing effect of secondary phase in SiC matrix. Mechanical properties and high speed mapping of the indented regions of CVD coated composite were investigated at different loading and holding time under ambient conditions. Further, XRD, SEM and TEM analysis were employed to characterize the microstructure of individual composites constituents and CVD coating. An excellent correlation between the microstructure and mechanical properties was made with the help of massive data generated through high-speed nanoindentation mapping. Uniform and dense columnar structured CVD SiC coating with the cubic phase showed superior mechanical properties (hardness and elastic modulus). The SiC-based hybrid composite processed with BN coated continuous carbon fibers reinforced in the SiC-CNFs matrix has shown improved fracture toughness while maintaining

other superior base matrix properties. Hybrid composite with the weak inter-phase bonding between the continuous C fibers and the matrix has helped to optimize the fracture toughness by restricting the crack propagation through fiber pullouts and fiber bridging.

8.1 Future scope of the work and Implications

Although the present study has helped in developing adequate understanding of the influence of reinforcements and processing method on properties of SiC based composites; a few areas emerged during the course of the present study, which demand further investigations for reasons given below.

The possible plan of work for the future based on the summary drawn from the present work is as follows :

Investigations of the impact of high temperature on the mechanical properties of processed SiC based composite such as modulus of rupture (MoR), Blast pressure, creep rupture tests, and radiation studies are planned.

- Looking into the possibility of processing of continuous SiC fiber reinforced SiC based composites and its characterization.
- The optimized processing parameter values and the role of the physical phenomena (e.g., solid state diffusion, crack initiation and propagation) using Taguchi stastical design and analysis.
- Interpretation of XRD, SEM and TEM analysis of SiC based composites processed in the present work.
- Elemental analysis of CVD-SiC coating and the SiC based composites using sophisticated techniques.
- Apart from the high temperature applications of SiC composites in nuclear, aerospace, defence and automobile applications, research in SiC based composite for other applications like solar, solid-state batteries, thermo-electronics, sea water desalination, etc., are also being contemplated.

- Attempts to compare properties of SiC-based composites sintered via SPS, Hot Press, etc., are in the pipeline too.
- Fabrication of SiC based composite using other processing techniques like, Electrophoretic deposition, CVI, PIP etc., is another viable area of research.
- Study of various protective coating materials and techniques for continuous fibers. The detailed chemistry, kinetics of the coating processes.
- Simulation and Modeling of properties of the SiC composites will be another interesting area of research for better understanding of industrial scale complex systems analysis.

8.2 List of Publications

International Journal Publications

1) ***Shaik Mubina***, *Asit Kumar Khanra, Bhaskar Prasad Saha,* "**Processing of sintered and CVD coated SiC/CNFs thin composite tubes**" *Materials Chemistry and Physics 220 (2018) 225–232.*
   DOI: 10.1016/j.matchemphys.2018.08.086
2) ***Shaik Mubina***, *Asit Kumar Khanra, Bhaskar Prasad Saha* "**Optimization of processing parameters, physical and mechanical properties of SiC – CNF composites using Taguchi approach**" *Materials Today: Proceedings 18 (2019) 5300–5308.*
   DOI: 10.1016/j.matpr.2019.07.554
3) ***Shaik Mubina***, *Asit Kumar Khanra, Bhaskar Prasad Saha* "**Enhancement of oxidation resistance of CVD SiC coated C_f/C-SiC hybrid composite tubes processed through Si-infiltration**" *Journal of Alloys and Compounds,* 826 (2020), 154107, 1–*10.*
   DOI: 10.1016/j.jallcom.2020.154107.
4) ***Shaik Mubina***, *P Sudharshan Phani, Asit Kumar Khanra, Bhaskar Prasad Saha* "**A nanoindentation based study on the effect of nanofibers on the mechanical properties of carbon fibers dispersed SiC composites**" Journal of Composite Interfaces, 2020, 1–19.
   DOI:10.1080/09276440.2020.1780555.

5) ***Shaik Mubina***, *M. Ilaiyaraja, Asit Kumar Khanra, Bhaskar Prasad Saha* "**Fabrication, microstructure analysis of continuous C fibers reinforced SiC based hybrid composite tubes through CIP and pressureless sintering**" Journal of Materials and Manufacturing Process, 2020, 1–9.
DOI: 10.1080/10426914.2020.1832685.

Conference attended

1. 8th International Congress on Ceramics, (ICC8, 2021), South Korea.
2. 84th Annual session of Indian Ceramic Society and National conference on Propelling Innovations in Glass and Ceramics for Atmanirbhar Bharat, 2020, India.
3. International Conference on Advances in Minerals, Metals, Materials, Manufacturing and Modelling (ICAM5-2019), India.
4. 9th International Conference on Materials Processing and Characterization (ICMPC-2019), India.
5. Sixth International Conference on Recent Advances in Composite Materials (ICRACM-2019), India.
6. International Conference on Engineering Materials, Metallurgy and Manufacturing (ICMMM-2018), India.
7. International Conference on Ceramics, Glass and Refractories - Emerging Innovations (Indian Ceramic Society, 2016), India.

Mubina Shaik

Senior Research Fellow

LinkedIn Link

Contact

E-mail: mubina.iiit@gmail.com

Phone: +91-8885-218-047

Address: 2-6, Vemuru, Guntur, Andhra Pradesh. India - 522261

Areas of Interest

- Powder Metallurgy
- Materials Fabrication
- Composites
- Ceramic Coatings

Professional Affiliations

- Indian Ceramic Society -- Life Member

Profile

- +05 years of research experience
- Advanced spray freeze granulation powder processing of ceramic based composites
- Fabrication and characterization of SiC-based composite tubes through cold isostatic pressing and sintering
- Liquid silicon infiltration and Chemical vapor deposition processes

Education

National Institute of Technology (NIT) Warangal (2016-Present)
PhD (Metallurgical and Materials Engg)
Thesis Submitted

RGUKT University (2010-2014)
B. Tech (Metallurgical and Materials Engg)
CGPA – 8.21/10
Distinction

Experience

Senior Research Fellow 2015 - Present
International Advanced Research Centre (ARCI) - Hyderabad

- Powder processing and optimization of processing parameters of SiC- based composites
- Taguchi design and experimental analysis
- Surface treatment secondary phase reinforcement
- Novel processing techniques to fabricate continuous fibers reinforced SiC-based composites tubes
- Optimization of physical, thermo-mechanical and high-temperature oxidation resistance properties SiC based composites

Publications

(1) Mubina Shaik, M. Ilaiayaraja, Asit Kumar Khanra, Bhaskar Prasad Saha, "Fabrication and microstructure analysis of continuous C fibers reinforced SiC-CNFs hybrid composite tubes", *J. Materials and Manufacturing processes*, 36 (3) 1–10 (2020), DOI: 10.1080/10426914.2020.1832685. Impact factor: **4.61**

(2) Mubina Shaik, P. Sudharshan Phani, Asit Kumar Khanra, Bhaskar Prasad Saha, "A nanoindentation based study to evaluate the effect of carbon nanofibers on the mechanical properties of SiC composites", *Journal of Composite Interfaces*, 1–18 (2020), DOI: 10.1080/09276440.2020.1780555. Impact factor: **2.95**

(3) Mubina Shaik, Asit Kumar Khanra, Bhaskar Prasad Saha, "Enhancement of oxidation resistance of CVD SiC coated C_f/SiC- SiC(CNF) hybrid composites processed through Si-infiltration", *Journal of Alloys and Compounds*, 826 1–10 (2020), DOI: 10.1016/j.jallcom.2020.154107. Impact factor: **5.31**

(4) Mubina Shaik, Asit Kumar Khanra, Bhaskar Prasad Saha, "Processing of sintered and CVD coated SiC/CNFs thin composite tubes", *Materials Chemistry and Physics*, 220 225–232 (2018), DOI: 10.1016/j.matchemphys.2018.08.086. Impact factor: **4.09**

(5) Mubina Shaik, Asit Kumar Khanra, Bhaskar Prasad Saha, "Optimization of processing parameters, physical and mechanical properties of SiC – CNF composites using Taguchi approach", *Materials Today Proceedings*, 18 (7) 5300–5308 (2019), DOI: 10.1016/j.matpr.2019.07.554.

Technical Expertise

- Powder processing routes (Conventional drying, spray drying, Rotary drying & Advanced spray freeze drying etc.), Surface treatment or Functionalization of fibers
- Cold iso-static press (CIP), Pressureless sintering furnace
- Si-infiltration (LSI), Chemical Vapour Deposition (CVD)

Programming & computation skills

- C, Python, Java
- SQL, DBMS
- Abacus, Catia

Characterization Tools

- **Topography Analysis:** Scanning Electron Microscope, Digital Optical Microscopy (Hands on)
- **Mechanical & Thermal Testing:** Vickers, Universal testing machine, High-speed Nano Indentation and Laser flash (Hands on)
- **Spectroscopy Analysis:** UV-Vis Spectroscopy, Electro Impedance Spectroscopy, Infrared Spectroscopy (Hands on)
- **Other Analysis Techniques**: Transmission Electron Microscopy (TEM), X-Ray Diffraction (XRD), Thermogravimetric analysis (TGA-DSC)

Conference attended

1. 8th International Congress on Ceramics, (ICC8, 2021), South Korea.
2. 84th Annual session of Indian Ceramic Society and National conference on Propelling Innovations in Glass and Ceramics for Atmanirbhar Bharat, 2020, India.
3. International Conference on Advances in Minerals, Metals, Materials, Manufacturing and Modelling (ICAM5-2019), India.
4. 9th International Conference on Materials Processing and Characterization (ICMPC-2019), India.
5. Sixth International Conference on Recent Advances in Composite Materials (ICRACM-2019), India.
6. International Conference on Engineering Materials, Metallurgy and Manufacturing (ICMMM-2018), India.
7. International Conference on Ceramics, Glass and Refractories - Emerging Innovations (Indian Ceramic Society, 2016), India

Awards & Fellowships

- Best paper award at International conference on Engineering Materials, Metallurgy and Manufacturing (ICEMMM2018).
- University Branch Topper in B.Tech for 2014 - Gold medalist.

Languages

- English, Hindi – Fluent
- Telugu – Native
- Korean, Spanish, Arabic – Intermediate Fluency

References

1. **Dr. Bhaskar Prasad Saha**

   Scientist-F & Team Leader

   Center for Non Oxide Ceramics, ARCI- Hyderabad, India

   Email: bpsaha@arci.res.in / Ph no: +91 9885901318

2. **Dr. Asit Kumar Khanra**

   Associate Professor & HOD,

   Department of Metallurgical & Materials Engineering,

   National Institute of Technology Warangal, India

   Email: asit_iitkgp@yahoo.com / Ph no: +91 9701578514

3. **Mr. A Ashok Kumar**

   Assistant Professor,

   Department of Metallurgical & Materials Engineering

   Rajiv Gandhi University of Knowledge Technologies, Basar, India

   Email: ashokiiitbas@rgukt.in / Ph no: +919949811238